

FORCED CONVECTION NUCLEATE BOILING DATA FOR LOW  
HEAT FLUX DENSITIES TO WATER CONTAINING  
A VOLATILE ADDITIVE

By

MAHMOUD HOOD SABET

Bachelor of Science  
University of Alexandria  
Alexandria, Egypt  
1949

Master of Science  
University of Alexandria  
Alexandria, Egypt  
1953

Master of Science  
University of Rhode Island  
Kingston, Rhode Island  
1957


Submitted to the Faculty of the Graduate School  
of the Oklahoma State University  
in partial fulfillment of the requirements  
for the degree of  
DOCTOR OF PHILOSOPHY  
May, 1962

Thesis  
11/20  
S1155  
cap. 2

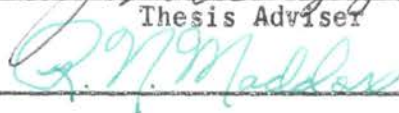
NOV 13 1962

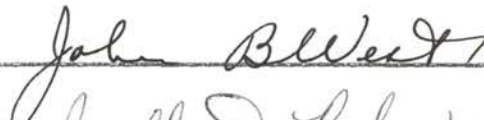
FORCED CONVECTION NUCLEATE BOILING DATA FOR LOW  
HEAT FLUX DENSITIES TO WATER CONTAINING  
A VOLATILE ADDITIVE

Thesis Approved:

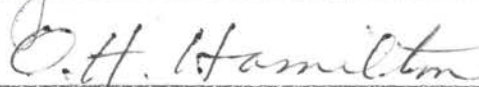


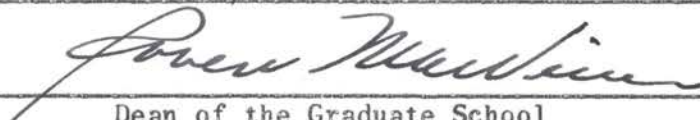
Thesis Adviser











Dean of the Graduate School

505229

## ACKNOWLEDGEMENT

This work was supported by the National Science Foundation which provided the funds necessary for the modification of the heat transfer loop in addition to the financial assistance of which the author was the grateful recipient.

The author gratefully acknowledges the guidance and assistance of Dr. James H. Boggs, during the course of this investigation and throughout the author's graduate program.

The author also wishes to express his thanks to the contributive suggestions and efforts of: Dr. J. B. West, Dr. R. N. Maddox, Dr. O. H. Hamilton, Dr. R. R. June, Prof. B. S. Davenport, Dr. J. D. Parker, J. A. McCandless, and G. M. Cooper.

The numerous calculations for the reduction and correlation of the experimental data were made possible through the kind assistance of the personnel of the Oklahoma State University Computing Center, and the Aerospace Division of Boeing Airplane Company, Seattle.

Gratitude is certainly due the author's wife, Ellie, for her patience and understanding during the course of this project, and for her assistance in typing this thesis which is dedicated to her.

## TABLE OF CONTENTS

Chapter	Page
I. INTRODUCTION . . . . .	1
II. SUMMARY OF PREVIOUS INVESTIGATIONS . . . . .	4
III. APPARATUS AND PROCEDURE . . . . .	12
IV. REDUCTION AND CORRELATION OF EXPERIMENTAL DATA . . . . .	29
V. EXPERIMENTAL DATA . . . . .	50
VI. ANALYSIS OF THE EXPERIMENTAL RESULTS . . . . .	62
VII. ANALYSIS OF EXPERIMENTAL ERRORS . . . . .	73
VIII. CONCLUSIONS AND RECOMMENDATIONS . . . . .	75
BIBLIOGRAPHY . . . . .	78
APPENDICES . . . . .	82
A. Inside Wall Temperatures . . . . .	83
B. Properties of the Mixtures and the Pure Components . . . . .	89
C. Thermocouple Calibration . . . . .	103
D. Orifice Calibration . . . . .	108
E. Properties of AISI Type 304 Stainless Steel . . . . .	110
F. Reproducibility of Data . . . . .	112
G. Degassing Experiment . . . . .	116
H. Moyno Pump Characteristics . . . . .	119
I. Nomenclature . . . . .	121

## LIST OF TABLES

Table	Page
I. References for Pure Liquids in Nucleate Boiling . . . . .	4
II. Variables for Experimental Data . . . . .	51
III. Experimental Data . . . . .	52
IV. Experimentally Determined Values of the Constant C in Forster-Greif Correlation for Water, Methanol and n-Butanol Mixtures . . . . .	69
A-I. Comparison of Heat Conduction Equation Solutions . . . . .	88
B-I. Critical Constants of Pure Components . . . . .	94
B-II. Experimentally Determined Mixture Properties . . . . .	95
B-III. Derivatives of Vapor-Pressure Curve for Water . . . . .	100
B-IV. Thermodynamic Equilibrium of the Mixtures . . . . .	102
C-I. Thermocouple Wire Correction . . . . .	104
D-I. Orifice Calibration Data . . . . .	108
F-I. Reproduction Data . . . . .	114

## LIST OF FIGURES

Figure	Page
1. The Data of Bonilla and Perry for Ethanol-water Mixtures . .	8
2. The Data of Van Wijk et al. for MEK-water Mixtures . . . . .	9
3. The Data of Leppert et al. for Methanol-water Mixtures . . .	10
4. The Data of Leppert et al. for Isopropanol-Water Mixtures. .	10
5. Schematic Diagram of Test Facility . . . . .	13
6. Test Section and Attachments . . . . .	16
7. Thermocouple Attachments . . . . .	17
8. Thermal Guard . . . . .	18
9. Instrumentation and Control Identification . . . . .	26
10. Heat Flux Calculation . . . . .	31
11. Representative Temperature Profiles . . . . .	34
12. Nucleate Boiling Data of Water . . . . .	38
13. Effect of Concentration of Methanol on the Superheat at Constant Heat Flux (P = 50 psia) . . . . .	41
14. Effect of Concentration of Methanol on the Superheat at Constant Heat Flux (P = 100 psia) . . . . .	41
15. Effect of Concentration of Methanol on the Superheat at Constant Heat Flux (P = 150 psia) . . . . .	42
16. Effect of Pressure on the Superheat for the Methanol Mixtures at Constant Heat Flux . . . . .	42
17. Effect of MEK Concentration on the Superheat at Constant Heat Flux (P = 50 psia) . . . . .	43
18. Effect of MEK Concentration on the Superheat at Constant Heat Flux (P = 100 psia) . . . . .	43

Figure	Page
19. Effect of MEK Concentration on the Superheat at Constant Heat Flux (P = 150 psia) . . . . .	44
20. Effect of Pressure on the Superheat for the MEK Mixtures at Constant Heat Flux . . . . .	44
21. Effect of Concentration of n-Butanol on the Superheat at Constant Heat Flux (P = 50 psia) . . . . .	45
22. Effect of Concentration of n-Butanol on the Superheat at Constant Heat Flux (P = 100 psia) . . . . .	45
23. Effect of Concentration of n-Butanol on the Superheat at Constant Heat Flux (P = 150 psia) . . . . .	46
24. Effect of Pressure on the Superheat for the n-Butanol Mixtures at Constant Heat Flux . . . . .	46
25. Effect of Mass Velocity on $\Delta T_1$ for the Methanol Mixtures. . . . .	47
26. Effect of Mass Velocity on $\Delta T_1$ for the MEK Mixtures . . . . .	47
27. Effect of Mass Velocity on $\Delta T_1$ for the n-Butanol Mixtures . . . . .	47
28. Correlation of the Methanol Mixtures Data for the Fully Developed Nucleate Boiling Region . . . . .	48
29. Correlation of the n-Butanol Mixtures Data for the Fully Developed Nucleate Boiling Region . . . . .	49
30. Temperature Profiles of Some Water Data . . . . .	63
31. Temperature Profiles of Water and Some Mixtures . . . . .	64
32. Pressure-Superheat Relationship for Water and Methanol Mixtures . . . . .	67
33. The Transition Region for Water and Some Mixtures . . . . .	72
34. Haselden and Peters Data for N <sub>2</sub> and O <sub>2</sub> . . . . .	72
A-1. Segment of Heated Tube . . . . .	84
B-1. Density of Water . . . . .	90
B-2. Thermal Conductivity of Water . . . . .	91
B-3. Specific Heat of Water . . . . .	92
B-4. Vapor Pressure of Pure Components . . . . .	93



Figure	Page
B-5. Fluidity of Pure Components . . . . .	96
B-6. Surface Tension of Pure Components . . . . .	99
C-1. Corrections for Surface Thermocouples . . . . .	106
C-2. Temperature Profile Correction for Some Runs . . . . .	107
D-1. Orifice Calibration . . . . .	109
F-1. Reproduction . . . . .	115
G-1. Degassing Experiment . . . . .	117
H-1. Moyno Pump Characteristics . . . . .	120

LIST OF PLATES

Plate	Page
I. View of Test Section with Insulation . . . . .	19
II. View of Test Section Showing the Pressure Taps . . . . .	19
III. Close-up of Boiling Region of the Test Section . . . . .	20
IV. Test Section Showing Bare Tube with Thermocouples and the Pressure Taps . . . . .	20
V. Transformers . . . . .	23
VI. Rear View of Test Apparatus . . . . .	23
VII. View of Control Panel . . . . .	25

## CHAPTER I

### INTRODUCTION

Particular emphasis has been placed on the study of nucleate (local) boiling heat transfer to liquids in recent years. This is due to its importance as a very efficient mode of heat dissipation in a number of high performance heat transfer applications. Nuclear reactors, electronic power-tube cooling coils, and rocket engine cooling jackets are examples of application where the high heat generation can be dissipated efficiently through this type of heat transfer. Water received most of the attention as a media to study this mode of heat transfer because of its availability, and its desirable characteristics as a coolant. Recently, attention has been focused on cryogenic (low temperature) liquids and on rocket fuels because of their importance in the varying and expanding space applications.

It is impossible to understand and explain the different phenomena associated with nucleate boiling without a comprehensive study of the theory of bubble growth in particular, and bubble dynamics in general. Considerable strides toward this goal have been made in the past ten years. As a consequence, four different models of heat transfer during nucleate boiling have been postulated as possible mechanisms through which the high heat flux densities in nucleate boiling could be explained. One of these mechanisms, together with the correlation equation based on it, was suggested by Forster and Greif (10), and proved to this writer to be particularly attractive. This correlation equation

showed promising agreement with experiment since its publication in 1959. A discussion of the various mechanisms of nucleate boiling proposed so far may be found in reference (10).

Aside from the differences in saturation temperatures between the various fluids, the most important property affecting the behavior of a liquid in nucleate boiling is the surface tension. This property, together with other adhesive and cohesive forces, determines the value of the contact angle between a vapor bubble and the heating surface, which in turn controls the volume of an average bubble as it breaks away from the surface. The study of the behavior of water containing a volatile additive like alcohol is then important insofar as it uncovers the dependency of the relationship between the heat flux and the superheat on the contact angle. Adding a small amount of volatile additive to water has the effect of reducing the surface tension of water appreciably without causing any appreciable change in the other properties of water.

Although some work has been done on the study of the behavior of liquid mixtures in pool boiling (11) (12) (13), very little has been done on forced convection nucleate boiling heat transfer to binary liquid mixtures. Leppert et al. (14), in their experiment on forced convection heat transfer to water containing a volatile additive, reported an increase of the heat transfer coefficient with some mixtures over that of pure water. Their data were at small mass velocities, at low pressures, and for cross-flow.

The purpose of this investigation was to continue the study of such mixtures at higher pressures and higher mass velocities for flow in a tube.

The range of variables covered in this investigation was:

System Pressure: 50 to 250 psia

Heat Flux: 60,000 to 260,000 Btu/hr-ft<sup>2</sup>

Mass Velocity: 190 to 400 lb<sub>m</sub>/ft<sup>2</sup>-sec

The concentrations of the additives used were:

Methyl alcohol: 1.02%, 2.04% and 3.06% by weight.

Methyl Ethyl Ketone: 1.00%, 2.03% and 3.00% by weight.

n-Butyl alcohol: 1.00%, 2.07% and 3.12% by weight.

## CHAPTER II

### SUMMARY OF PREVIOUS INVESTIGATIONS

In this chapter the previous work in nucleate boiling which has a bearing on the present investigation will be outlined. This includes both pure fluids and mixtures and correlation of their experimental data during nucleate boiling, as well as the recent work published on bubble dynamics.

#### Pure Fluids

Experimental work on nucleate boiling of pure fluids has been conducted by many investigators on a variety of liquids, at pressures ranging from subatmospheric to 2465 psia, and at mass velocities up to  $2000 \text{ lb}_m/\text{ft}^2\text{-sec}$ . The following is a list of some references dealing with pure liquids in nucleate boiling:

TABLE I  
REFERENCES FOR PURE LIQUIDS IN NUCLEATE BOILING

---

Water	(1)	(2)	(3)	(4)	(5)	(28)	(29)
Alcohols	(27)	(28)	(31)				
Aniline	(31)						
Mercury	(21)						
Liquid H <sub>2</sub>	(33)						
Liquid N <sub>2</sub> & O <sub>2</sub>	(32)						
Potassium Carbonate	(28)						
Carbon Tetrachloride	(28)						

## Correlations

Three methods of correlating the heat transfer data of nucleate boiling of liquids appeared in the literature during the last ten years.

Rohsenow (9) in 1952 gave the following equation:

$$\frac{c \cdot \Delta T_1}{L \cdot P_F^{1.7}} = F_{sf} \left[ \frac{\bar{q}}{\mu \cdot L} \sqrt{\frac{g_c \sigma}{g(\rho_L - \rho_V)}} \right]^{0.33}$$

where the coefficient  $F_{sf}$  is dependent on the heating-surface-fluid combination. All properties of the fluid in this equation are to be evaluated at the saturation temperature.

In 1959, Forster and Greif (10), and S. Levy (34) published simultaneously two correlation equations based on different models of heat transfer during nucleate boiling.

Levy presented the following "generalized equation" for surface boiling

$$\bar{q} = \frac{1}{B_L} \cdot \frac{k c \rho_L^2 \Delta T_1^3}{\sigma T_s (\rho_L - \rho_V)}$$

where the coefficient  $B_L$ , "determined empirically, was found to be a function only of the product  $\rho_V L$ ."

The Forster-Greif correlation, and the model for heat transfer during nucleate boiling which the authors suggested, are described in Chapter IV.

## Bubble Dynamics

Without considering the important factors which affect bubble formation, it is impossible to understand the different phenomena associated with boiling.

The degree of superheat necessary for a bubble to be initiated is controlled by the physical condition of the heating surface and by the surface tension of the fluid. Bubbles form only at favorite spots on the heating surface, and as the heat flux increases, the number of these nucleation centers increases. In contrast, the number of bubbles in each column issuing per second does not change as fast by an increase in the heat flux. M. Jacob (35) reports that a linear relation exists between the heat flux and the number of the bubble columns visible, and that "for every increase of the heat flux by  $700 \text{ Btu/hr-ft}^2$ , one more column was formed on a polished horizontal surface."

The study of the growth of a vapor bubble in a superheated layer received its due attention in recent years. Gunther and Kreith (30) studied the lifetime of a steam bubble and found it largely dependent on the heat flux. The degree of subcooling was found to control the maximum size of an average bubble.

The studies of Forster and Zuber (7) in the growth of a vapor bubble led to the establishment of "two distinct time domains" in the bubble's lifetime; "one is of the order of  $10^{-4}$  sec. during which the effect of the hydrodynamic forces may be an important factor in the growth, and another during which this effect is unimportant." A solution of the second domain of bubble lifetime was presented by the authors. The authors showed also in another paper (24) that "the product of bubble radius and radial velocity is constant, and independent of bubble radius."

The theoretical studies of Forster and Zuber (7) (24), of Plesset and Zwick (23), and of Griffith (22), agree very well with the experimental data of Dergarabedian (20) and of Ellion (19).

High speed photographic studies in boiling have been attempted by



Gunther (24), Gunther and Kreith (25) and by Siegel et al. (26) under conditions of reduced gravity.

### Fluid Mixtures

Heat transfer during nucleate pool boiling of binary mixtures has been investigated by Bonilla and Perry (4). They studied mixtures of ethanol-water, butanol-water, butanol-acetone, acetone-water, and butanol-ethanol. Their results for the ethanol-water mixtures are reproduced in Figure 1 where  $\log \bar{q}$  was plotted against  $\log \Delta T_1$ . The analysis of their data showed that the behavior of the binary mixtures in nucleate boiling "fell between the pure components in all cases."

Van Wijk et al. (2), studied the heat transfer during nucleate pool boiling of mixtures of water and MEK (Methyl-Ethyl-Ketone) at atmospheric pressure. Their results reproduced in Figure 2 indicate that the nucleate boiling heat transfer curves for the different water-MEK mixture studied fell between those of the pure components. The authors reported that "the size of the bubbles leaving the heating surface was definitely smaller for 4.2 % by weight MEK than with the other mixtures or with the pure components. It can be seen from Figure 2 that the value of the maximum nucleate boiling heat flux ( $\bar{q}_{max.}$ ) for some mixtures is considerably higher than that of the pure components, reaching a value of 2.5 times that of pure water for 4.2 % by weight of MEK.

Nucleate boiling heat transfer to water containing a volatile additive was investigated by Leppert et al. (5) for cross flow near atmospheric pressure and at small flow rates. Their results for isopropyl alcohol and methyl alcohol are reproduced in Figures 3 and 4. The authors reported that "with about one per cent isopropyl alcohol or two per cent

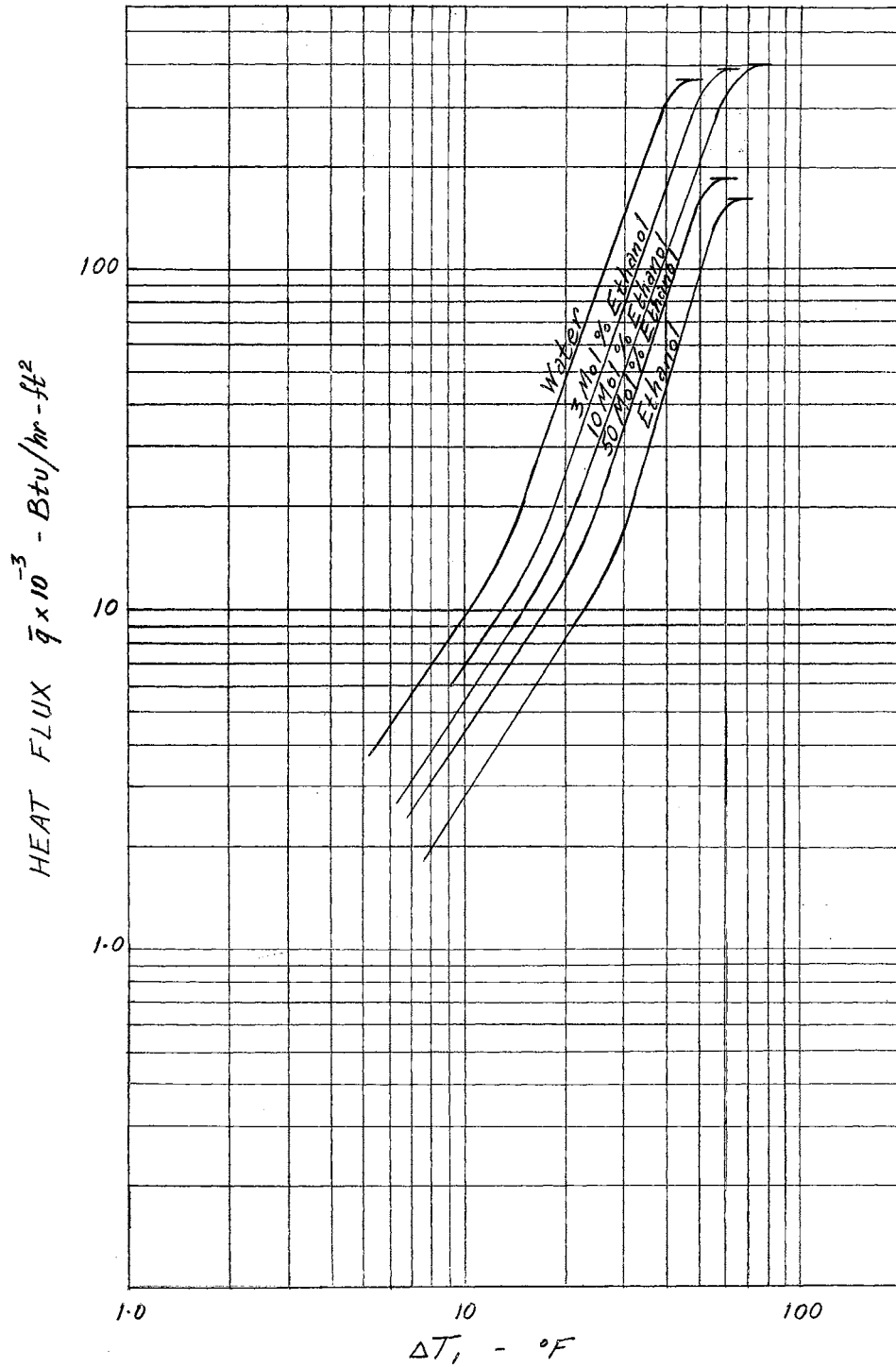


Figure 1. The Data of Bonilla and Perry for Ethanol-water Mixtures

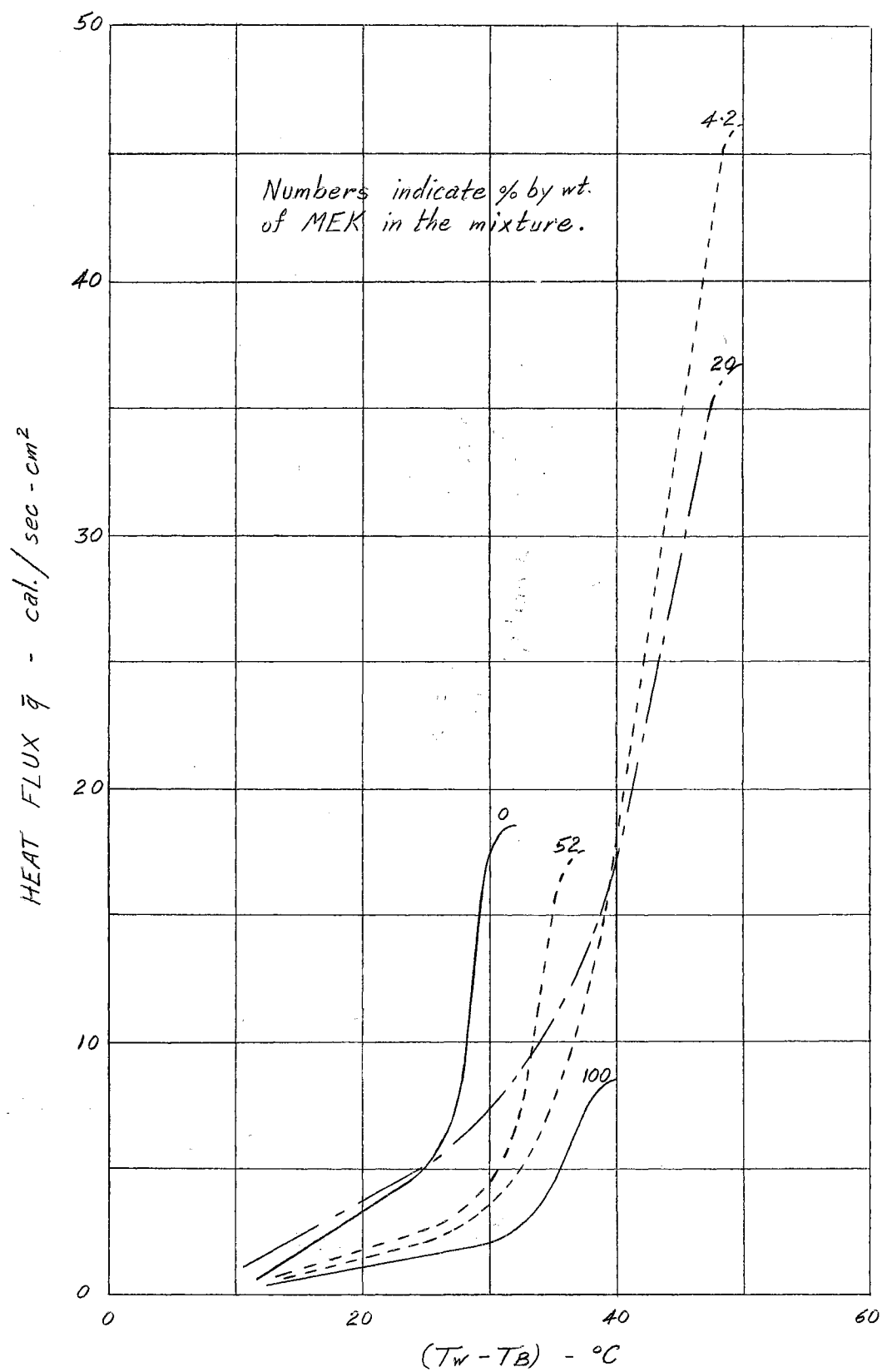


Figure 2. The Data of Van Wijk et al. for MEK-water Mixtures

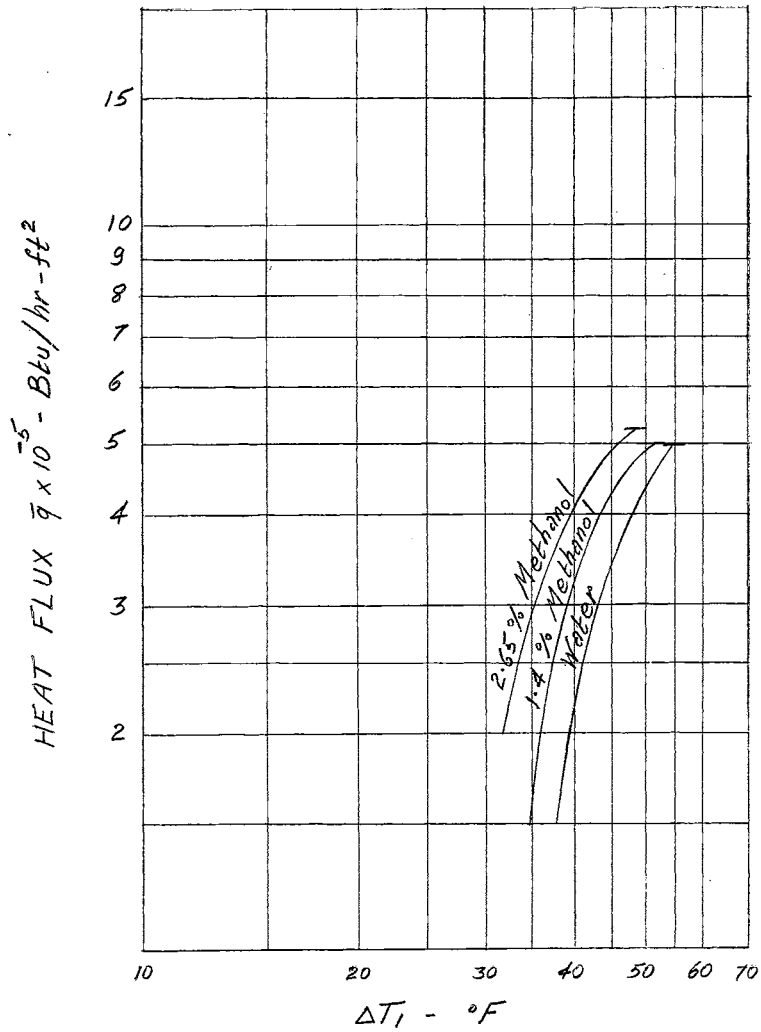


Figure 3. The Data of Leppert et al. for Methanol-water Mixtures

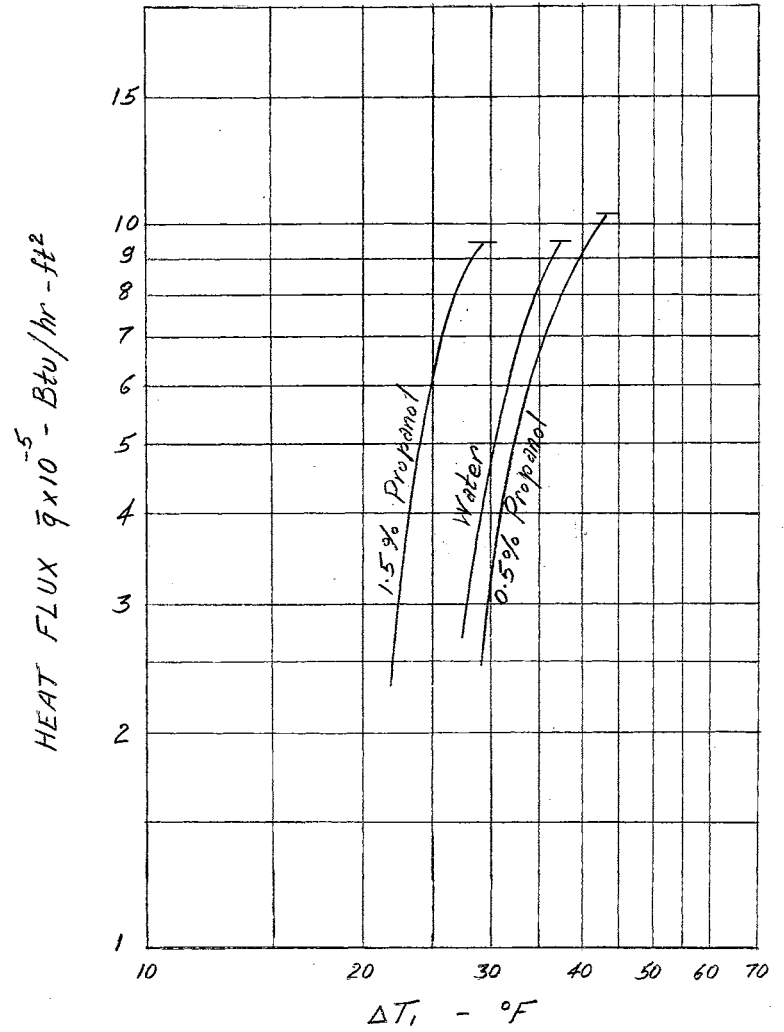


Figure 4. The Data of Leppert et al. for Isopropanol-water Mixtures

methyl alcohol by weight, the nucleate-boiling heat transfer coefficient is either unaltered or slightly improved, while the average and maximum bubble sizes are very notably reduced." The authors also predicted a decrease in the pressure drop during forced convection nucleate boiling of such mixtures based on the smaller bubble size observed.

## CHAPTER III

### APPARATUS AND PROCEDURE

#### Experimental Apparatus

The heat transfer loop used in this investigation was constructed in 1958 at the Mechanical Engineering Laboratory of Oklahoma State University under a grant from the Atomic Energy Commission. In this chapter a brief description of the loop will be presented, together with a description of the modifications done on it for the purpose of this investigation.

The original design of the apparatus is similar in principle to one used by Mumm (2), Leppert (15), and Reynolds (16), with the following outstanding changes:

1. The power available for the preheater was increased by 50 per cent.
2. Provision was made to take heat-transfer and pressure-drop data simultaneously.
3. A Moyno pump was used with a variable speed drive.

A schematic diagram of the heat transfer loop is shown in Figure 5. Modifications done on the apparatus for the purpose of this investigation comprise the following:

1. Method of thermocouple attachment to the test section.
2. Insulation of the test section and addition of a thermal guard

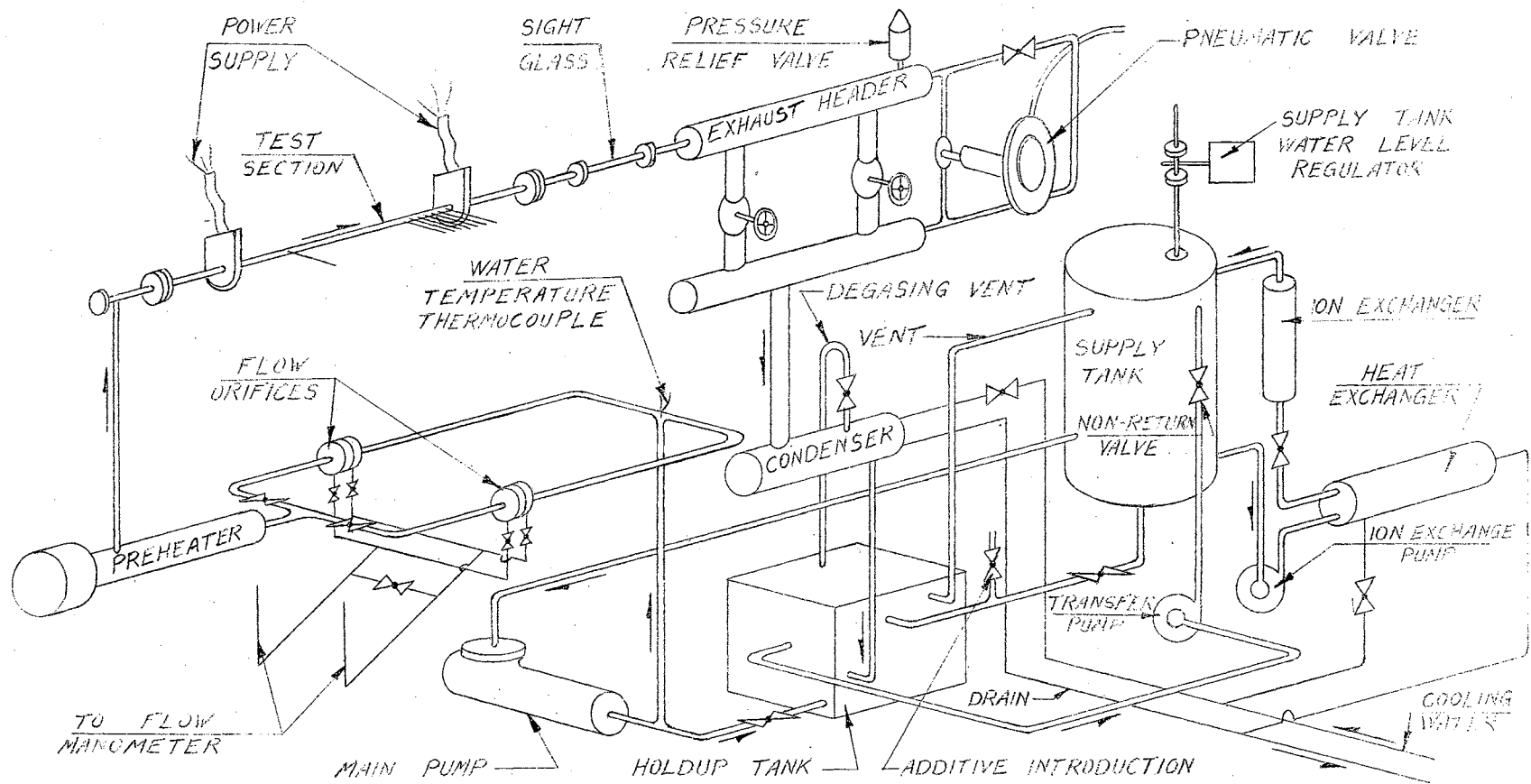


Figure 5. Schematic Diagram of Test Facility

which provided the surface thermocouples with an isothermal region.

3. Pressure control system.
4. Pressure tap connections to the manometers and piping system of the manometers.
5. Temperature reading instruments.
6. Piping system between the water supply tank and the holdup tank.
7. Provisions for degassing the system fluid.

### Flow Cycle

Starting from the holdup tank, the system fluid was transferred to the supply tank by the transfer pump (see Figure 5). A "Moyno" pump of the positive displacement type was used to circulate the system fluid under pressure through the loop. From the main circulating pump, the fluid was passed into a network of metering orifices and through the preheater where it was heated before it entered the test section.

The fluid was then allowed to boil in the test section by raising the test section wall temperature above the saturation temperature of the system fluid. Heating of the test section was achieved by electrical energy dissipation in the test section walls.

The boiling fluid was then passed through an exhaust header and into a shell and tube heat exchanger (condenser) where it was cooled down to the room temperature. From the condenser, the system fluid was allowed to return to the holdup tank.

### Test Section

Details of the test section and its attachments are shown in Figures



6, 7, 8, and Plates I, II, III, IV.

The test section material was AISI type 304 stainless steel with a 0.502 inch O.D. and a 0.399 inch I.D. The overall length of the test section was seven feet between the inlet and outlet flanges. The heated length between the electrical lugs was six feet. Seven iron-constantan 30-gauge thermocouple wires were attached to the test section in the boiling region (last two feet of test section). A sheet of mica 0.0065 inches thick was provided between the outer surface of the test section and the thermocouple junctions to insulate them electrically from the test section. The junctions were then clamped to the test section as shown in Figure 7. In addition to these seven thermocouples, another thermocouple was attached in the nonboiling region.

Thermal insulation was provided the test section by wrapping it with three layers of asbestos strips covered with a 1-inch thick layer of 85 per cent magnesia.

The thermal guard, Figure 8, surrounded the insulation in the boiling region and was heated by resistance wire coiled around the entire 2.25-foot length of the ceramic tube. A General Radio Company variac (115 V. input, 20A) was used to regulate the a.c. power to the resistance wire. Three thermocouple junctions were placed inside the ceramic tube and the tube was covered with a thick layer of asbestos to minimize the heat loss to the atmosphere from the resistance wire.

A Pyrex glass sight tube installed downstream of the test section allowed visual observation of the flow.

Other attachments to the test section which comprised the pressure taps, the voltage taps and the inlet and outlet thermocouple junctions are shown in Figure 6.

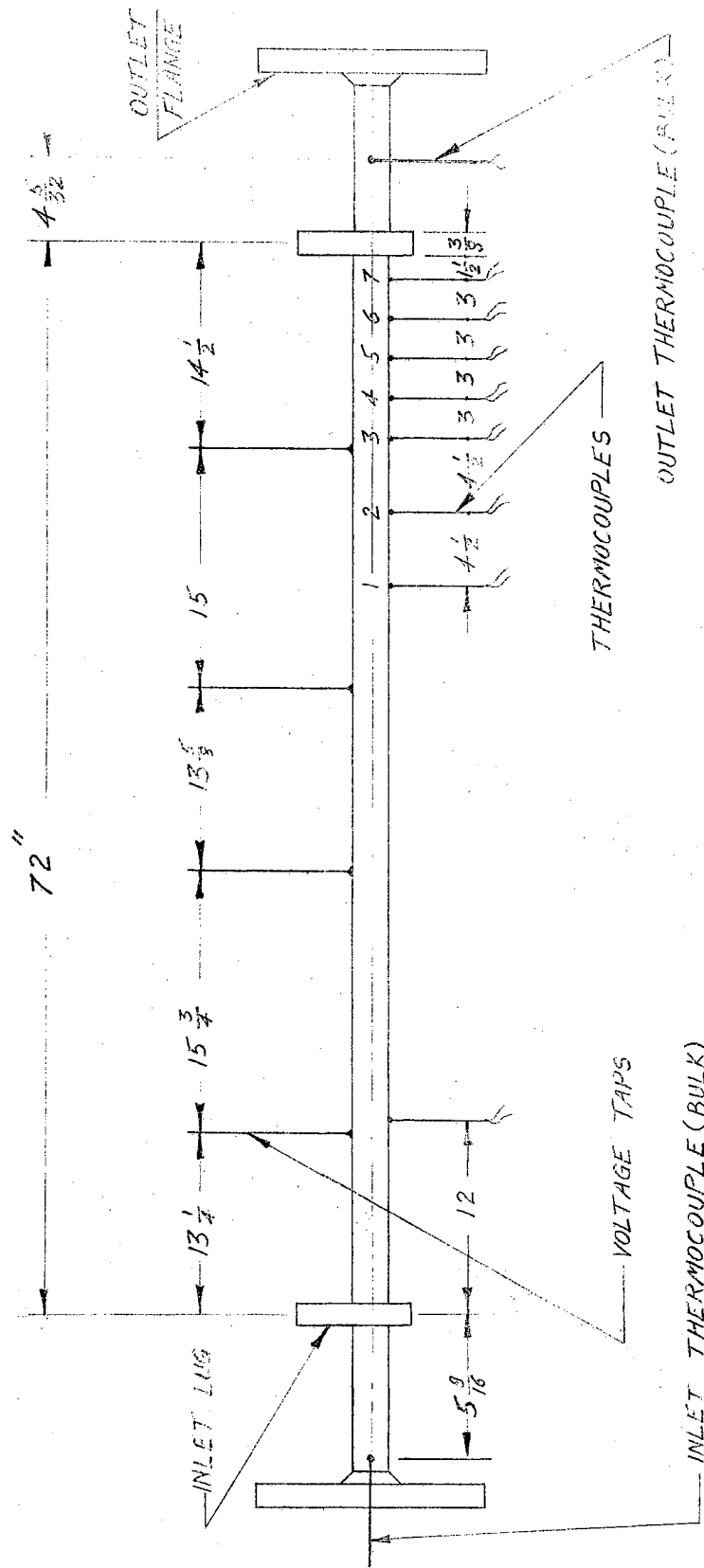


Figure 6. Test Section and Attachments

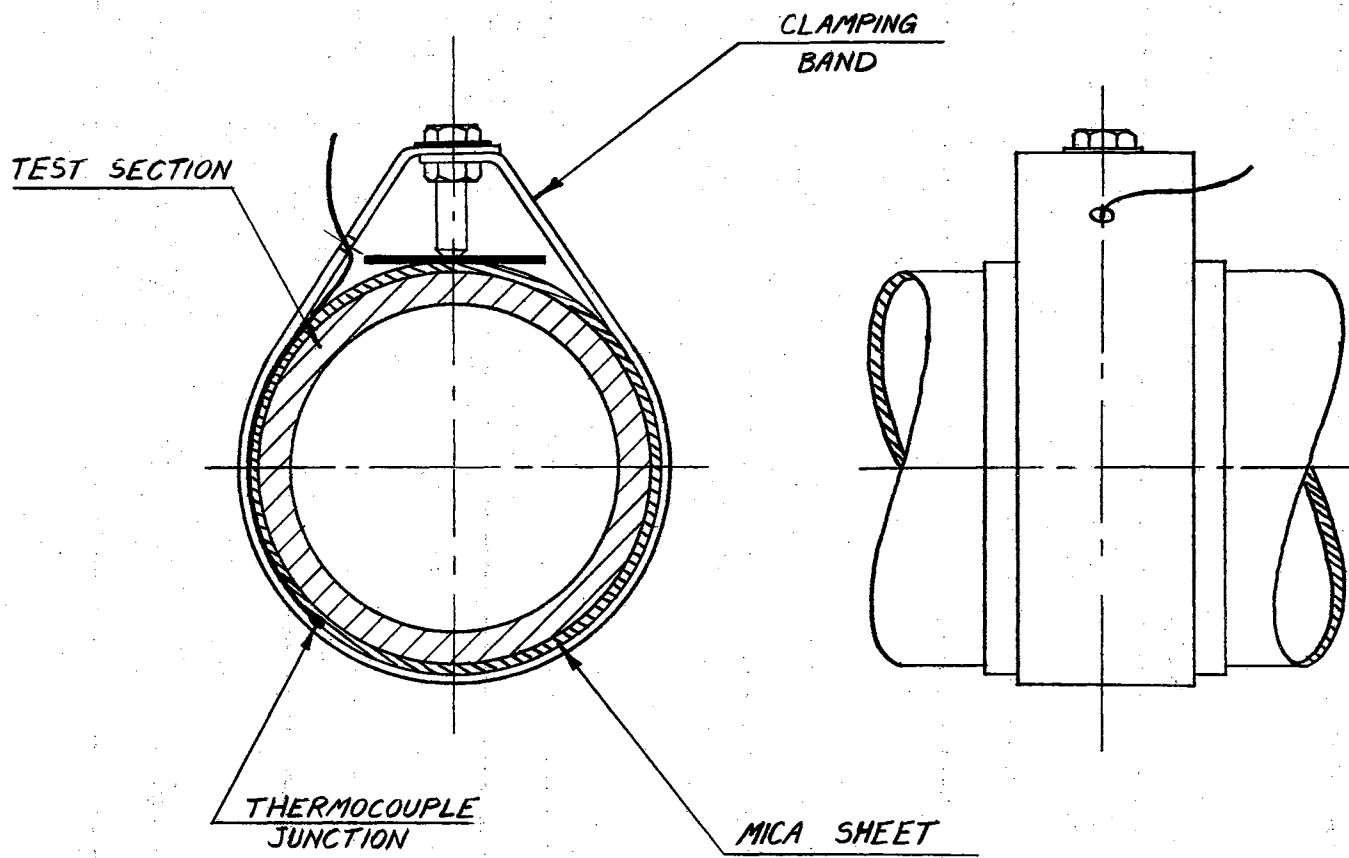


Figure 7. Thermocouple Attachments

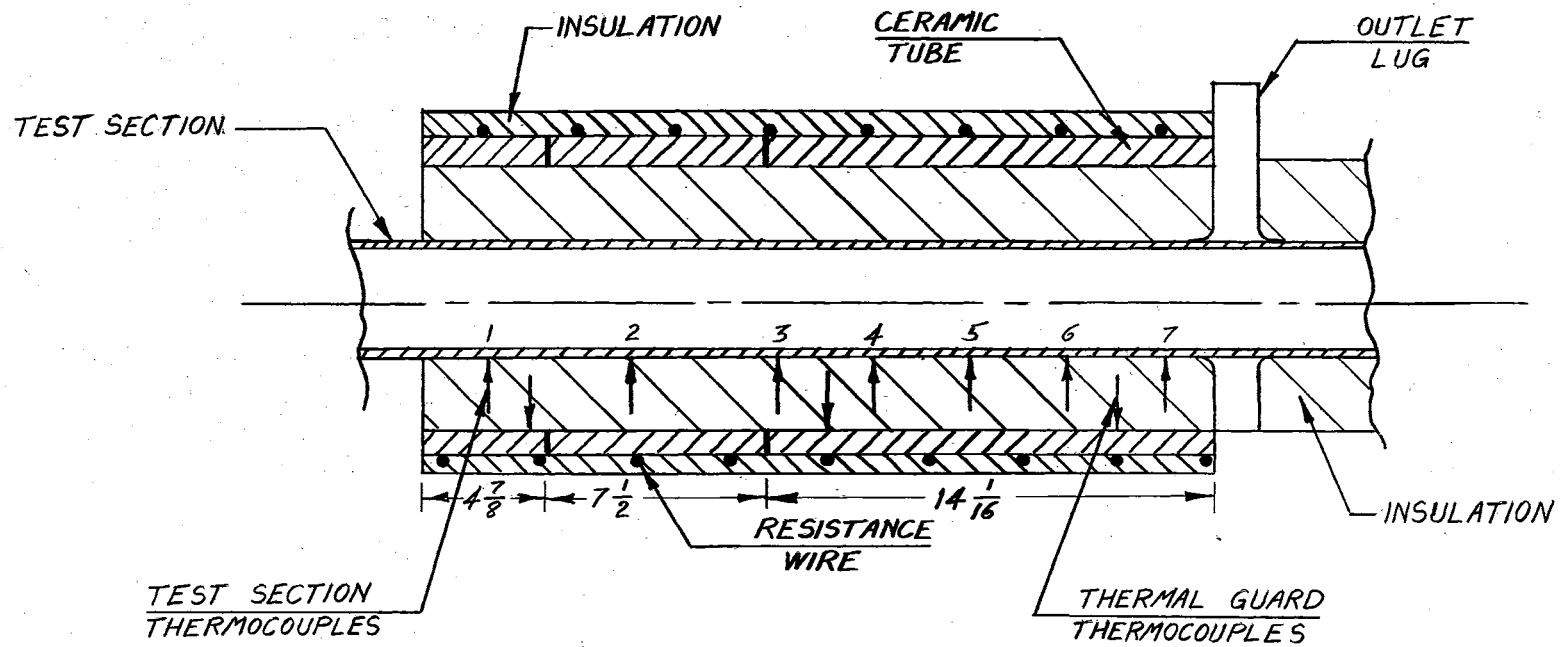
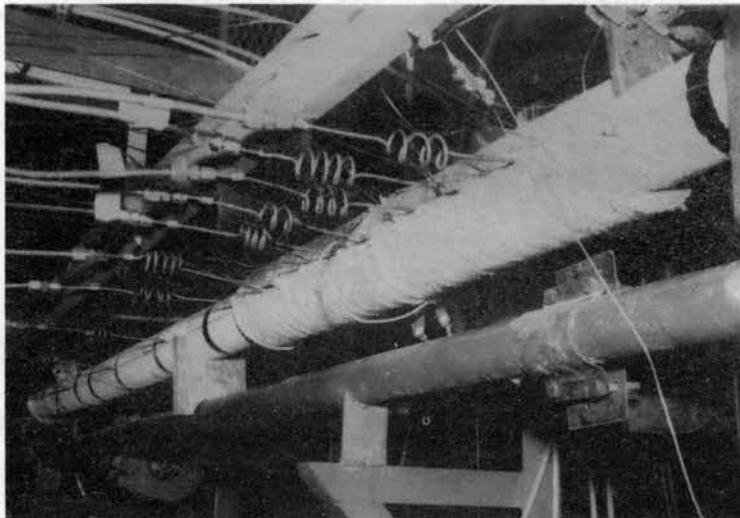


Figure 8. Thermal Guard

## PLATE I

View of Test Section with Insulation



## PLATE II

View of Test Section Showing the Pressure Taps

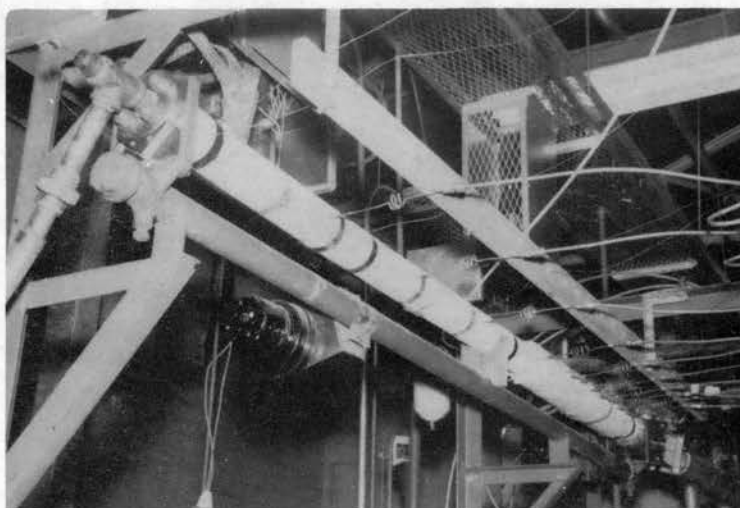


## PLATE III

Close-up of Boiling Region of Test Section

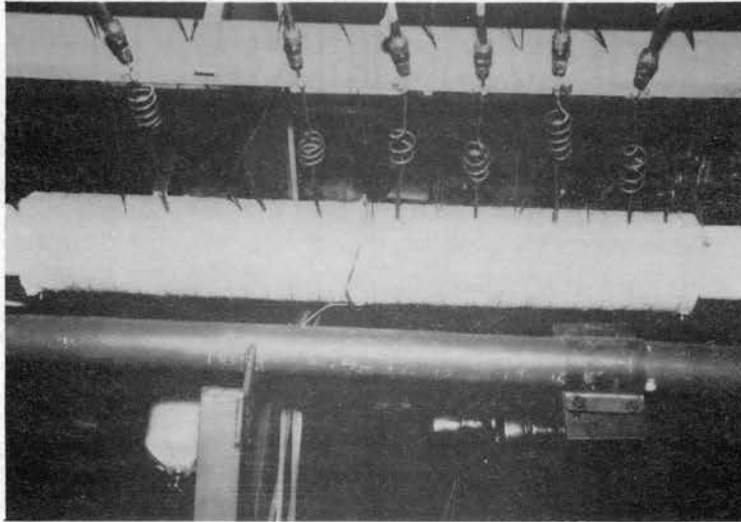
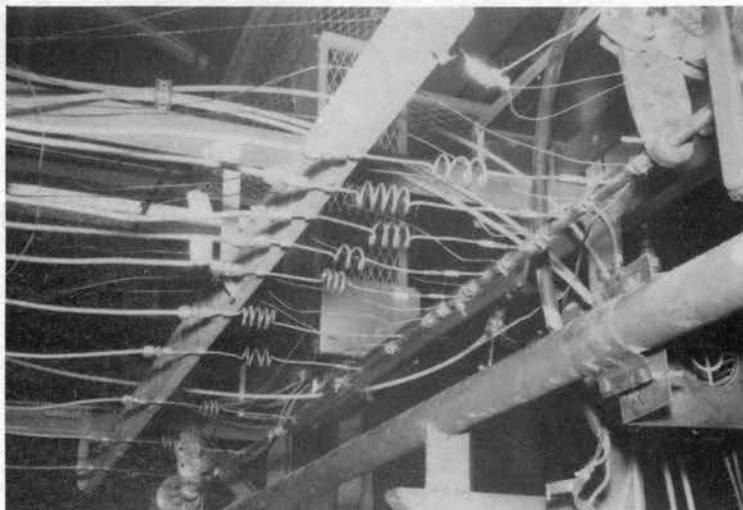


## PLATE IV

Test Section Showing Bare Tube with  
Thermocouples and Pressure Taps



## Components

The main pump was a stainless steel Robbins and Meyers "Moyno" pump, frame 6M, type SSQ, which was a six-stage progressing-cavity pump. The volumetric displacement of this pump was almost independent of the discharge pressure, as can be seen from Figure (H-1), Appendix (H).

The two auxiliary pumps, one for the ion exchanger and the other for the fluid transfer from the holdup tank to the supply tank, were identical Yeomans Brothers centrifugal pumps driven by 1/3 HP General Electric motors, and had cast-iron housings. The housings of these two pumps which were the main source of rust within the entire loop were carefully coated with a plastic (Epoxy Resin).

Rohm and Haas "Amberlite" resin was used with the ion exchanger to remove iron ions from the system fluid. The system fluid was continuously pumped from the supply tank through the column of the resin in the ion exchanger and returned to the supply tank.

Piping and fittings which came in contact with the system fluid were either stainless steel type 304 or non-ferrous metal.

The orifice plates used in conjunction with the flow-metering network were 0.353 inches and 0.453 inches in diameter. They were supplied by the Daniel Orifice Fitting Company. Only the smaller orifice was calibrated and used in this investigation. A valve mounted on the shell side of the heat exchanger allowed the discharge of air and vapor (but not any liquid) to the atmosphere. This valve was used for the degassing of the system fluid (see Appendix G).

For detailed description of the loop, see reference (17).

## Electrical Energy

Electrical energy was supplied to the test section by three Lincoln 400 "Fleetwelder Special" transformers connected in parallel. Output rating of each transformer is 400 amps at 40 volts. (See Plate V).

Preheating of the system fluid was accomplished with six Cromalox MT-201, 240 volt, 10,000 watt, two-element heaters. Six of the single heaters were connected through individual switches on the control panel, and six were connected by individual switches on the control panel and operated by a 45 KW Powerstat variable transformer supplied by the Superior Electric Company.

## Instrumentation and Control

The emf. of the thermocouples was measured by a Leeds and Northrup portable precision potentiometer, No. 8663. The ice point was used as the reference. The smallest division was 0.01 mv. which corresponded to about 0.33°F. The thermocouple leads were connected to a multi-position selector switch which was in turn connected to the potentiometer. For calibration of the thermocouples, see Appendix C.

A Two-mode TEL-O-SET pneumatic balance controller was used to control the system pressure. This was supplied by the Minneapolis-Honeywell Regulator Company. The signal from the pneumatic controller was transmitted to a valve located at the outlet of the exhaust manifold. This valve is shown in Plate (VI). System pressure was measured by a Heise calibrated gauge, 0-750 psi, 16-inch diameter dial, graduated in 1-psi increments.

Flow was measured by connecting the orifice flange pressure taps to



PLATE V

Transformers

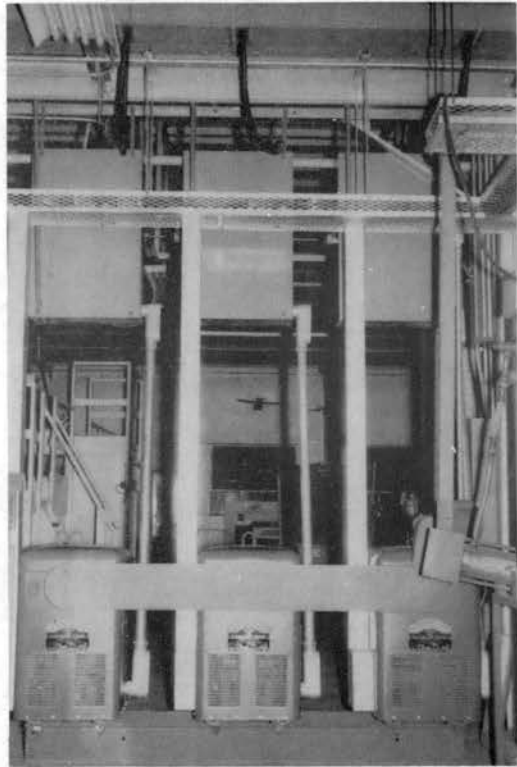
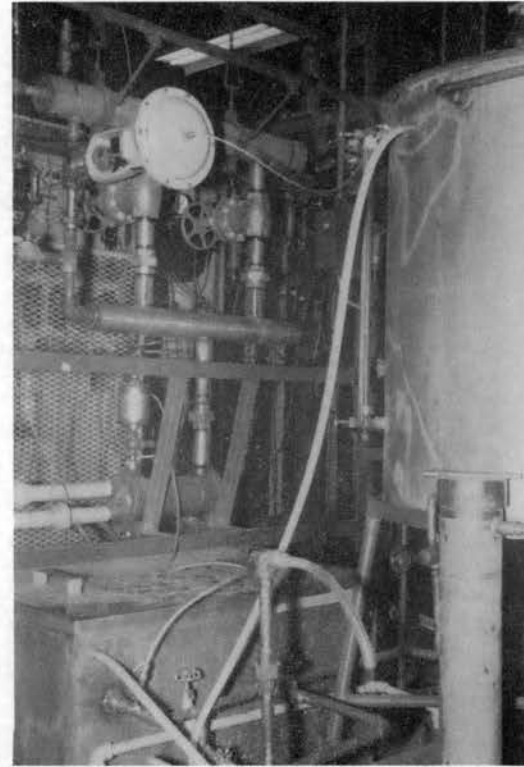


PLATE VI

Rear View of Test Apparatus



a Meriam, Model 30, flow manometer with a 60-inch scale graduated in inches and tenths of an inch. Meriam blue manometer fluid with specific gravity 1.75 was used. For orifice calibration see Appendix D.

Flow control was achieved with the Moyno pump and the associated drive system.

Power to the test section was measured with a single-phase General Electric P-3 wattmeter with a range of 0-200/400 watts and an accuracy of 0.2 per cent of full scale. Voltage drop along the test section was measured with a General Electric P-3 voltmeter with a range of 0-15/30 volts and an accuracy of 0.2 per cent of full scale. A General Electric JKR-2 current transformer with a ratio of 5:1500 was used to supply current to the wattmeter. A brown multipoint Electronik Strip Chart Recorder, type J, 0-600<sup>o</sup>F, was used to match the emf. of the test-section thermocouples with that of the guard heater thermocouples.

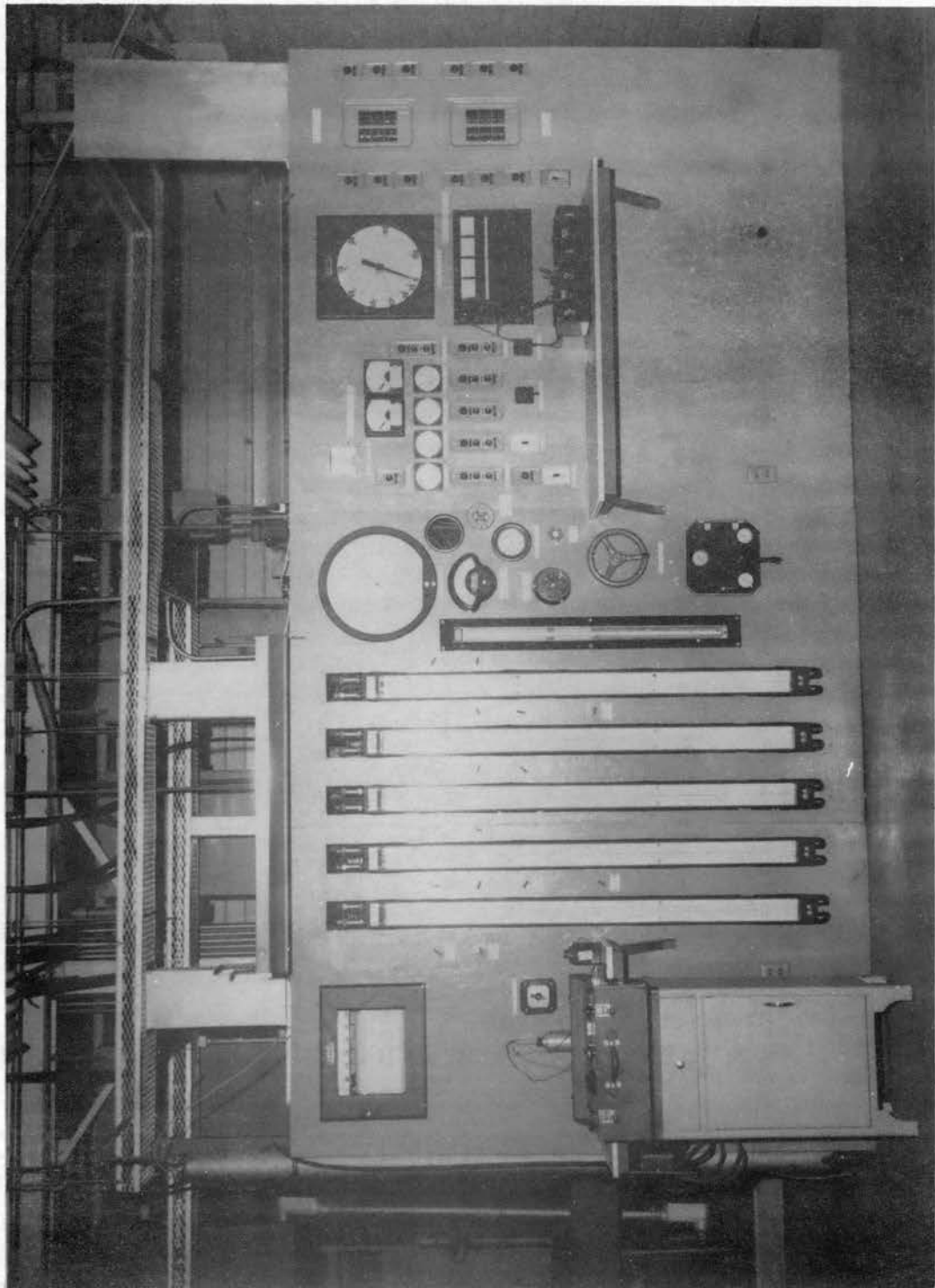
All instrumentation which was used to control the operation of the loop or to read the experimental data was mounted on the control panel shown in Plate (VII) and illustrated in Figure 9.

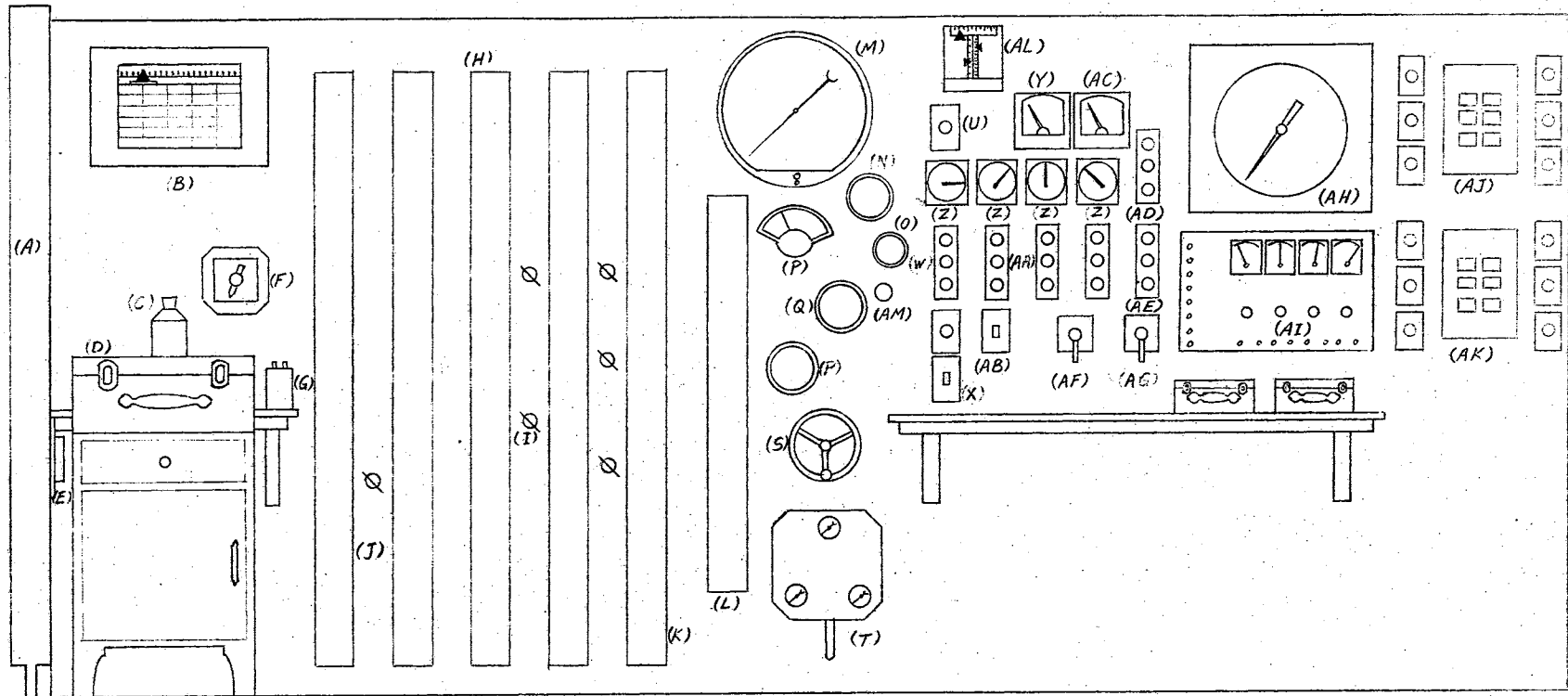
#### Procedure

All previous work in local boiling heat transfer has emphasized the importance of the effect of the heat transfer surface condition on the superheat, and thereby on the heat transfer coefficient. This was especially important in the present investigation, because changing surface conditions made it hard to compare data of the different mixtures used. Therefore a considerable effort and a number of precautions were taken throughout the experimental work to render a reproducible heat transfer surface. For details of the different steps taken to that end,

PLATE VII

View of Control Panel





- (A) MANOMETER BLEED COLUMN
- (B) TEMPERATURE RECORDER
- (C) DEWAR FLASK
- (D) POTENTIOMETER
- (E) VARIAC
- (F) THERMOCOUPLE SELECTOR
- (G) STANDARD CELL
- (H) CHECK VALVES
- (I) SHUTOFF VALVES
- (J) PRESSURE DROP MANOMETERS
- (K) FLOW MANOMETER
- (L) AUXILIARY MANOMETERS
- (M) PRECISION PRESSURE GAGE

- (N) OBSERVATION PORT
- (O) THROTTLE VALVE
- (P) MAIN PUMP SPEED INDICATOR
- (Q) SYSTEM PRESSURE GAGE
- (R) HOLDUP TANK TEMP INDICATOR
- (S) MAIN PUMP SPEED CONTROL
- (T) SYSTEM PRESSURE SENSOR
- (U) PANIC SWITCH
- (V) TOTAL CURRENT AMMETER
- (W) MAIN PUMP SWITCH
- (X) TRANSFER PUMP SWITCH
- (Y) TEST SECTION VOLTMETER
- (Z) TRANSFORMER AMMETER

- (AA) TRANSFORMER SWITCHES
- (AB) ION EXCH. PUMP SWITCH
- (AC) TEST SECTION WATTMETER
- (AD) DIRECT PREHEATER
- (AE) POWERSTAT PREHEATER
- (AF) TRANSFORMER POWER CONTROL
- (AG) PREHEATER POWERSTAT CONTROL
- (AH) CURRENT RECORDER
- (AI) PREHEATER INSTRUMENT PANEL
- (AJ) PREHEATER JUNCTION BOX
- (AK) POWERSTAT JUNCTION BOX
- (AL) PRESSURE CONTROL
- (AM) BYPASS VALVE

Figure 9. Instrumentation and Control Identification

reference should be made to Appendix F.

Before data was taken for a specific additive, the test section was cleaned, treated with a dilute solution of nitric acid, and flushed thoroughly with distilled water. The system was then filled with distilled water, and the flow started at a moderately high rate to allow degassing, which was achieved by venting the valve on top of the condenser to the atmosphere. Degassing, when the system contained mixtures rather than distilled water, was achieved by venting this valve to the hold-up tank so that no additive vapor would escape from the system. The system was allowed to degass at all times during the experimental runs.

During the degassing time (1 to  $1\frac{1}{2}$  hours), the thermal guard power was started and allowed to warm up. The flow manometer, and the pressure manometers were then bled to remove any air bubbles that were noticed to collect in the manometer tubes. These manometers were working on a system-fluid over manometer-fluid principle with a relative density of the manometer fluid of 0.75. The manometers were bled by distilled water from an outside source so that the system fluid, when it contained additives, would not contaminate the manometer fluid.

The system was then sealed and the additive introduced to the hold-up tank through an aspirator located in the return line between the supply tank and the hold-up tank. Sufficient time was allowed for the additive to mix with the distilled water and to flow in the test section. The additives were weighed before introduction to the known amount of distilled water in the system, so that the concentrations of these additives were about 1%, 2% or 3%.

A large diameter vent line connecting the hold-up tank and the supply tank above the fluid surface in both tanks was introduced. This kept the pressure in both tanks atmospheric when the transfer pump was

pumping the system fluid from the hold-up tank into the supply tank, and thus kept the vapor leak at the seals to a minimum.

When the loop was ready, the flow, the system pressure, and the test section power were adjusted at their predetermined values, and the system was then allowed to reach a steady state. About one half hour was sufficient time for this purpose. During that time, the thermal guard heater power was adjusted so that the outside temperature of the test section in the boiling region matched the temperature of the guard. Once the steady state was reached, the data were read twice, and recorded.

## CHAPTER IV

### REDUCTION AND CORRELATION OF EXPERIMENTAL DATA

#### Experimental Measurements

Experimental measurements for each run were comprised of the following:

1. The emf. of the outside wall thermocouples of the test section at seven different locations in the boiling region and in one location in the non-boiling region. See Figure 6.
2. Inlet and outlet bulk temperature of the fluid in the test section.
3. Temperature of the fluid before entering the preheater.
4. System pressure at the downstream end of the test section.
5. Pressure drop across the flow orifice.
6. Wattmeter reading of the electrical energy dissipation in the test section wall.
7. Ammeter reading of the a. c. current flowing in the test section wall.
8. Voltage drop at four different locations along the entire length of the test section.

All experimental data were read twice and averaged after the steady state was reached.

### Reduction of the Experimental Measurements

The thermocouple wires were calibrated, and it was found that an emf. correction of 0.049 mv. should be added to the emf. readings of all thermocouples. In addition, the seven surface thermocouples used to read the outside wall temperature of the test section were calibrated in place against the inlet bulk temperature thermocouple. For the calibration and correction of the thermocouples, see Appendix C.

The electrical energy dissipation in the boiling region of the test section was calculated according to the following example for Water Run #5.

Example: Wattmeter reading = 153

Ammeter reading = 79

The ammeter reading was the percentage of 1500 amps.; and since the ratio of the current transformer was 1:300,

The power input to test section  $P = 153 \times 300 \times 3.413$   
 $= 1.565 \times 10^6$  Btu/ hr., and

The test section current  $I = 0.79 \times 1500 = 1185$  amps.

This value of the test section current was checked for each run against the value calculated from the following equation

$$I = \sqrt{P/R}$$

where  $R =$  the electrical resistance of the test section between the center lines of the lugs.

In order to calculate the resistance of the test section  $R$ , Figure 10 and the following equation were used:

$$R = \frac{1}{\pi (r_0^2 - r_i^2)} \left[ \rho \frac{1}{2} (L - L_b) + \rho_b \times L_b \right]$$



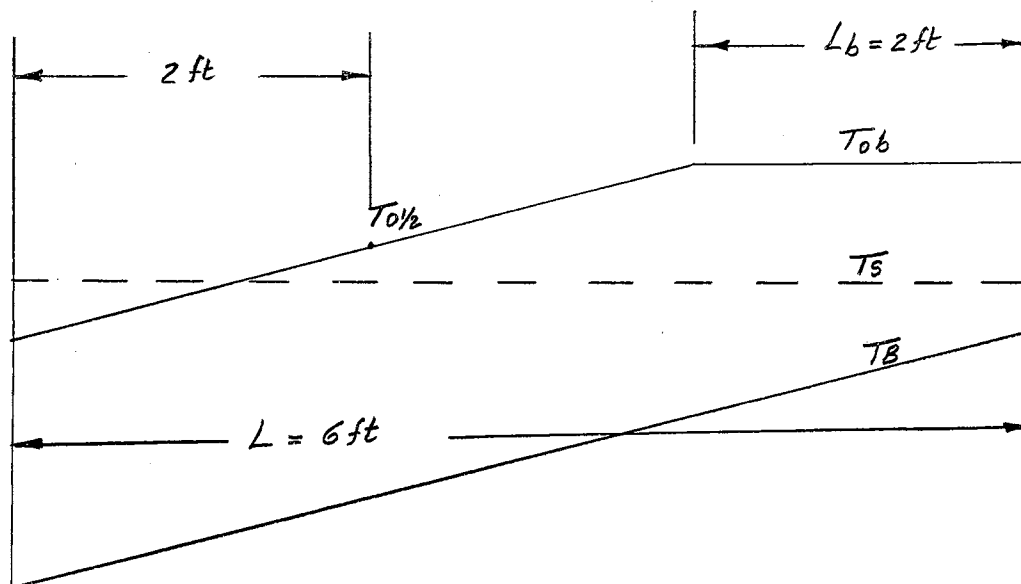


Figure 10. Heat Flux Calculation

Outside wall temperature in boiling region was

$$T_{ob} = 368.6 \text{ } ^\circ\text{F}$$

Mean outside temperature in non-boiling region was

$$T_{0\frac{1}{2}} = 313.2 \text{ } ^\circ\text{F}$$

Therefore  $\rho_{ob} = 2.808 \times 10^{-6} \text{ } \Omega \text{ - ft}$

$$\rho_{0\frac{1}{2}} = 2.733 \times 10^{-6} \text{ } \Omega \text{ - ft}$$

The resistance in the boiling region was

$$R_b = \frac{\rho_{ob} \times L_b}{\pi (r_o^2 - r_i^2)} = \frac{2.808 \times 10^{-6} \times 2}{5.062 \times 10^{-4}} = 1.110 \times 10^{-2} \text{ } \Omega$$

The resistance in the non-boiling region was

$$R_{nb} = \frac{\rho_{0\frac{1}{2}} (L - L_b)}{\pi (r_o^2 - r_i^2)} = \frac{2.733 \times 10^{-6} \times 4}{5.062 \times 10^{-4}} = 2.16 \times 10^{-2} \text{ } \Omega$$

Total resistance of test section was

$$R = 1.11 \times 10^{-2} + 2.16 \times 10^{-2} = 3.27 \times 10^{-2} \text{ } \Omega$$

$$I = \sqrt{P/R} = \sqrt{\frac{153 \times 300}{0.0327}} = 1185 \text{ Amps}$$

The values of the current checked as above, came within 0.6% of the measured values for all 160 runs.

Heat dissipation in boiling region was

$$\bar{q} = \frac{I^2 (R_b/2)}{A}$$

where A is the inside area of the test section/unit length

$$\bar{q} = \frac{(1185)^2 \times (1.11 \times 10^{-2}/2) \times 3.413}{\pi \times 0.03325} = 2.550 \times 10^{-5} \text{ Btu/hr-ft}^2$$

The average power dissipation in the test section was

$$\bar{q}_{\text{avg.}} = \frac{(1185)^2 \times (3.27 \times 10^{-2}/6) \times 3.413}{\pi \times 0.03325} = 2.500 \times 10^{-5} \text{ Btu/hr-ft}^2$$

In order to find the inside wall temperatures from the outside wall temperatures of the test section, a solution of the heat conduction equation, giving the temperature distribution inside the wall of an electrically heated tube, was required. The following Kreith-Summerfield solution (A-6a) was used.

$$\Delta T_w = \frac{m}{2} \left\{ \frac{\Delta x^2}{\Delta x} + \frac{\Delta x^3}{3r_o} + \left[ \frac{1}{4r_o^2} + \frac{m(\alpha + 3\beta + 4\alpha\beta\theta)}{12(1 + \alpha\theta)(1 + \beta\theta)} \right] \frac{\Delta x^4}{\Delta x} + \dots \right\}$$

A simplified solution was deduced and found helpful in rough calculations; this equation is

$$\Delta T_w = \frac{m}{2} \left[ r_o^2 \ln (r_o/r_i) - \frac{r_o^2 - r_i^2}{2} \right]$$

Both these solutions are derived in Appendix A.

The inside wall temperature at the seven different locations shown in Figure 6, in addition to the inlet and outlet bulk temperatures for each run, are listed in Table III.

The flow-measuring orifice was calibrated according to Appendix D.

#### Representative Temperature Profiles

In Figure 11, the inside wall temperature of the test section, and the bulk temperature of the fluid, are plotted against the test section length, measured from the center line of the downstream lug, for some experimental runs. These experimental runs are: Run # 10 for water, Run # 10 for 3.06 % methanol, Run # 10 for 3.00 % MEK, and Run # 10 for 3.12 % n-Butanol. The behavior of the temperature profile in the case of mixtures will be discussed in Chapter VI.

#### Forster-Greif Correlation

This correlation equation will be used to correlate some of the experimental data of this investigation; therefore a brief description of it, as well as of the mechanism of nucleate boiling, which the authors suggested, is in order.

Forster and Greif, in their recent paper (10), suggested a "vapor-liquid" exchange mechanism of heat transfer during subcooled nucleate boiling described in the following paragraph.

When surface boiling occurs, the bubbles, in growth and collapse, act as highly efficient piston pumps working at about 1000 cycles per second, which pump mechanically the hot liquid from the heating strip to the bulk and the cold liquid from the bulk to the heating surface.

Based on this mechanism of heat transfer during nucleate boiling, the authors also suggested the manner through which the mechanism remains unaffected by the degree of subcooling of the liquid bulk. They used Ellison's experimental data (19) on the effect of liquid temperature on bubble dynamics, in conjunction with the following equation (IV-1),

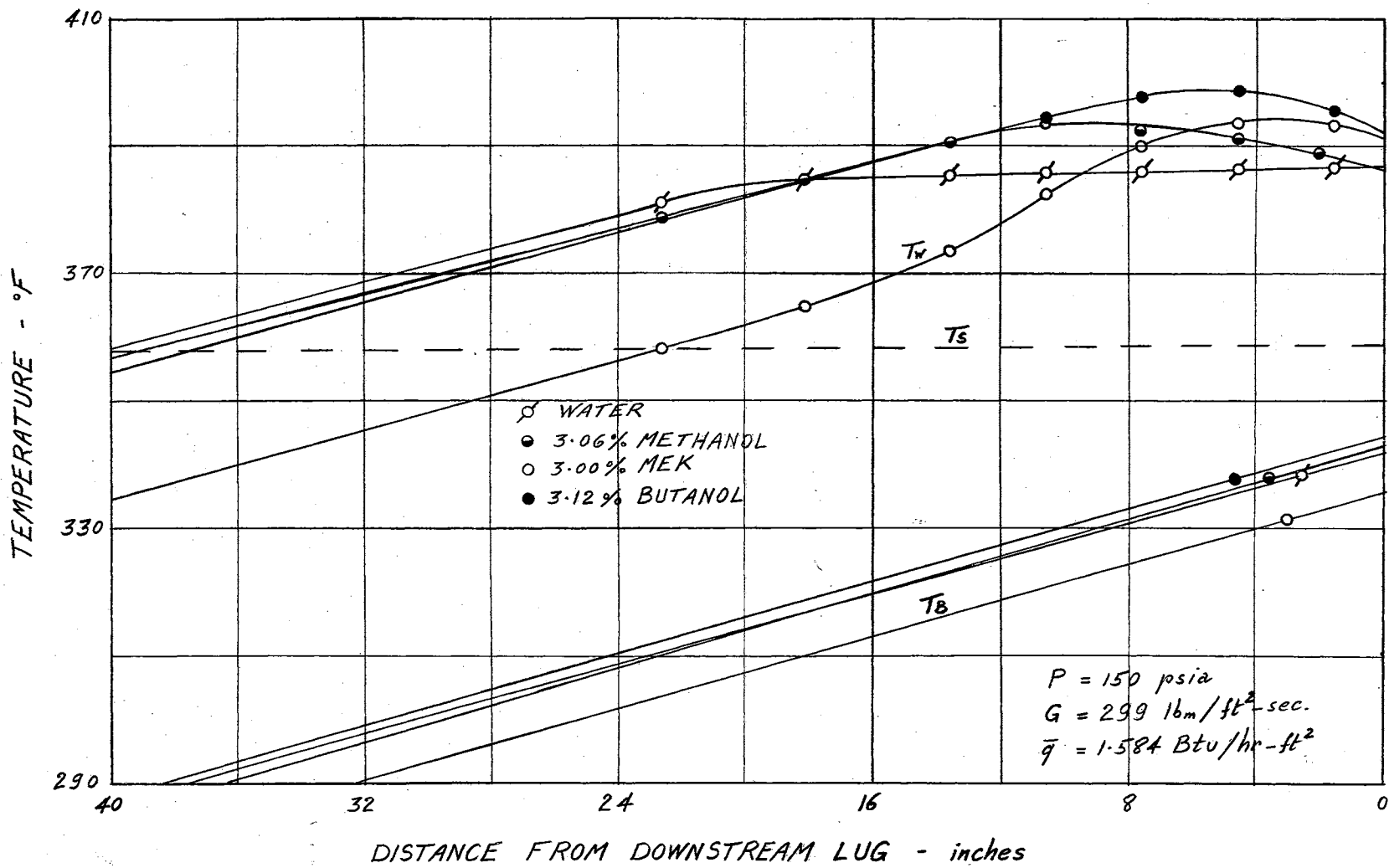


Figure 11. Representative Temperature Profiles

to show that the product  $(\Delta T_1 + \Delta T_2) R_{\max}^3 / \tau$  in this equation remains virtually constant while subcooling is changed by more than 400 per cent. This equation is

$$q \propto c \rho_L R_{\max}^3 (\Delta T_1 + \Delta T_2) \cdot \frac{1}{\tau} \quad (\text{IV-1})$$

where  $q$  = heat transfer by each bubble per second

$\tau$  = the period of growth-collapse cycle of a bubble

$R_{\max}$  = radius of the maximum size of an average bubble

The authors also argued that "once this highly effective mode of heat transfer is operative (yielding a heat flux 10 to 100 times that arising from eddy diffusion), the contribution stemming from convective heat transfer loses its importance."

In their correlation equation for nucleate boiling which they represented as correlation I, the authors defined three dimensionless groups in which the liquid properties are to be evaluated at the wall temperature. One of these is the PRANDTL group

$$\text{Pr} = \frac{\mu c}{k} \quad (\text{IV-2})$$

Another parameter which we shall call a REYNOLDS modulus is "representative of cycle frequencies and of the dynamics of bubble growth in general." This modulus can be defined as

$$\text{Re} = \frac{\rho_L}{\mu} A^2$$

where

$$A = B_1 \cdot \Delta P / \frac{dP}{dT}$$

The coefficient  $B_1$  have been previously calculated by the authors and was shown to be equal to

$$B_1 = \frac{c \rho_L}{L \rho_V} (\pi a)^{1/2}$$

$$= \frac{c \rho_L (\pi a)^{1/2} J}{T_s \frac{dP}{dT}}$$

where the Clausius-Clapeyron's equation was used for  $(L \rho_L)$ .

The Reynolds modulus, then, can be put in the form

$$Re = \frac{\pi c k}{\mu} \left( \frac{\rho_L J \Delta P}{T_s} \right)^2 \left( \frac{dP}{dT} \right)^{-4} \quad (IV-3)$$

where  $\Delta P$  is the excess pressure corresponding to the superheat  $\Delta T_1$ .

(7). This excess pressure is given in terms of the superheat  $\Delta T_1$  by

$$\Delta P = \frac{dP}{dT} \Delta T_1 + \frac{1}{2} \frac{d^2 P}{dT^2} \Delta T_1^2 + \dots \quad (IV-4)$$

The derivatives in equation (IV-4) are to be evaluated at the saturation temperature  $T_s$ . As a first approximation, the excess pressure  $\Delta P$  could be regarded as proportional to the superheat, where the factor of proportionality is the slope of the vapor-pressure curve at the saturation temperature  $T_s$ , i.e.:

$$\Delta P = \frac{dP}{dT} \Delta T_1 \quad (IV-4a)$$

The slope of the vapor-pressure curve can be evaluated by use of the Clausius-Clapeyron equation (see Appendix B).

The third dimensionless group introduced is a NUSSELT modulus "using the critical radius of a bubble ( $R_c = 2\sigma/\Delta P$ ) (38), as the characteristic length." This parameter is then defined by

$$Nu = \frac{2 \bar{q} \sigma}{k \Delta P \Delta T_1} \quad (IV-5)$$

Forster and Greif then represented their correlation equation in

the form

$$\text{Nu} = C \cdot \text{Re}^n \cdot \text{Pr}^{1/3}$$

or

$$\text{Nu} \cdot \text{Pr}^{-1/3} = C \text{Re}^n \quad (\text{IV-6})$$

They gave for the exponent  $n$  at low pressures the value of

$$n = \frac{1}{5}$$

They compared their correlation equation with the experimental data for water of Cichelli and Bonilla (27) and of Gunther and Kreith (30). This showed that for water

$$C = 7.0 \times 10^{-3}$$

#### Representation of the Experimental Data

The experimental data of this investigation are shown in Table III which lists the inside wall temperature of the test-section at seven different locations (see Figure 6), the inlet and outlet bulk temperatures, and the superheat  $\Delta T_1$  for each run. In case of the mixture runs, the superheat  $\Delta T_1$  reached a maximum value near the start of local boiling and then decreased downstream. The values of  $\Delta T_1$  for the mixture runs listed in Table III are the maximum values attained near the start of local boiling. For further discussion on  $\Delta T_1$  for the mixtures see Chapter VI. Table III also lists the values of the two parameters  $\text{Nu} \cdot \text{Pr}^{-1/3} \equiv Y$ , and  $\text{Re} \equiv X$  defined by equations (IV-3) and (IV-5).

The experimental data for water are shown in Figure 12 where the heat flux  $\bar{q}$  is plotted against the superheat  $\Delta T_1$  on a log-log graph for different pressures.

In order to compare the results of this investigation for water with other experimental data, the data of Gunther and Kreith (30) for water

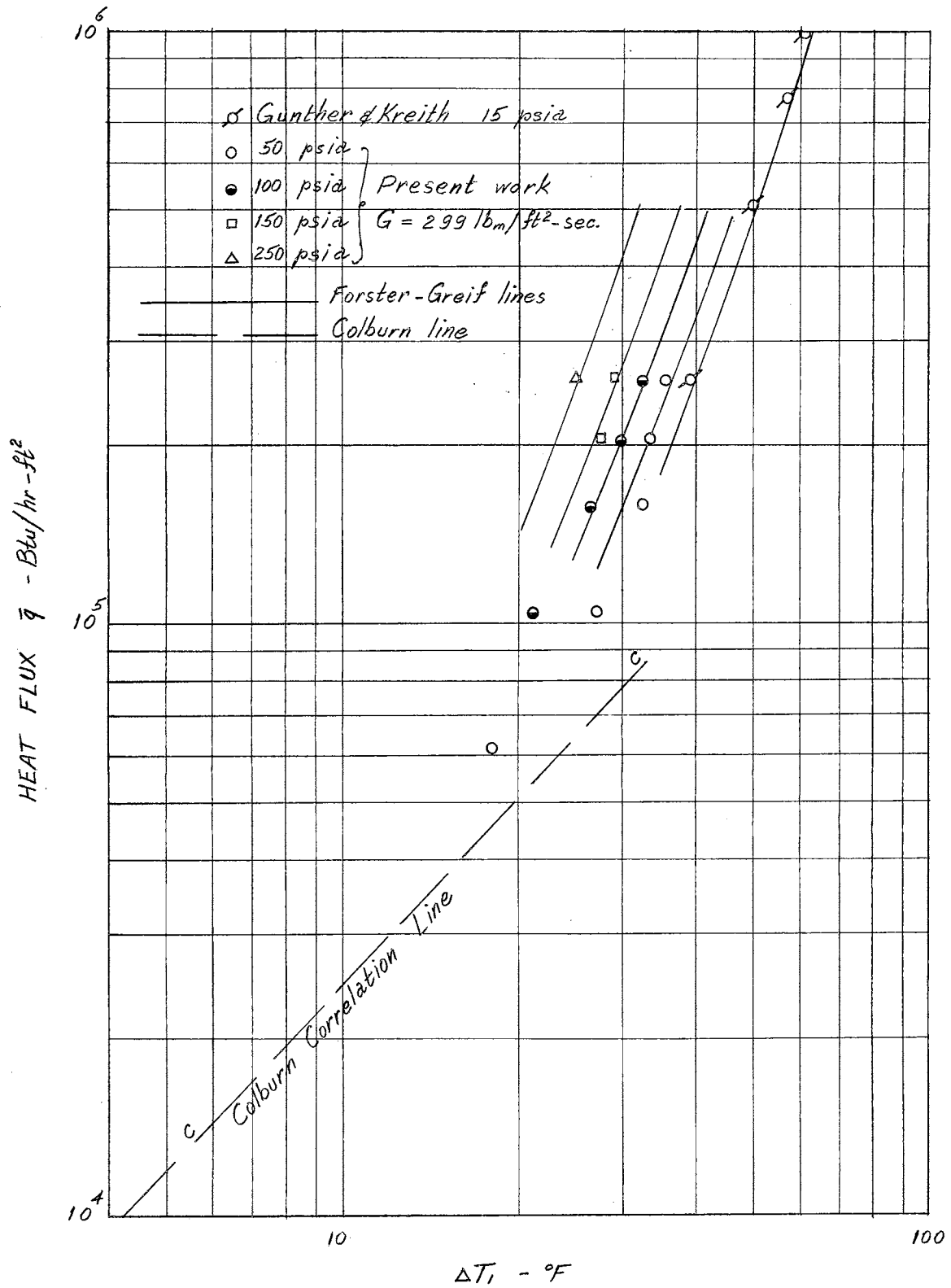


Figure 12. Nucleate Boiling Data of Water



at atmospheric pressure are reproduced in Figure 12.

At low values of the heat flux  $\bar{q}$ , the present data at 50 psia were compared to non-boiling heat transfer by including in Figure 12 the Colburn line c-c. This line represents the non-boiling heat transfer to saturated water at 50 psia, and was calculated from the equation

$$\bar{q} = 0.023 \Delta T_1 G C_B \left( \frac{\mu}{DG} \right)_F^{1/5} \left( \frac{k_F}{\mu C_B} \right)^{2/3}$$

where F indicates that the property is evaluated at the average film temperature

and B indicates that the property is evaluated at the bulk temperature.

Figures 13 through 24 show the effect of the concentration of the additives and the effect of the system pressure on the super-heat  $\Delta T_1$  at different heat flux levels for all the mixtures studied in this investigation. Figures 25 through 27 show the effect of the convective velocity (mass velocity) on the superheat  $\Delta T_1$ .

#### Correlation of the Experimental Data in the Fully Developed Nucleate Boiling Region

The experimental data in the fully developed nucleate boiling region for water, the Methanol mixtures and the n-Butanol mixtures were correlated by means of the Forster-Greif equation (IV-6). The four points representing the data at the highest heat flux used ( $2.57 \times 10^5$  Btu/hr-ft<sup>2</sup>) for four pressures were utilized for the correlation of each mixture. The parameters  $Nu \cdot Pr^{-1/3}$  and  $Re$  were calculated for each of these points as defined by equations (IV-3) and (IV-5), and plotted in Figure 28 for the Methonal mixtures and in Figure 29 for the n-Butanol mixtures. The

two parameters  $Nu \cdot Pr^{-1/3}$  and  $Re$  were also calculated for all other runs and listed in Table III. The same two parameters were calculated for the Gunther and Kreith data (30) and plotted in Figures 28 and 29 along with the data of the present investigation for water.

No attempt has been made to show a correlation for the data of the MEK mixtures which were believed to be all in the transition region (the region between non-boiling and the fully developed nucleate boiling regions). This may be seen also from Figure 2 which represents the results of Van Wijk et al. (2) on the MEK-water mixtures. The heat transfer line in Figure 2 for 4.2 % by weight MEK between the non-boiling and the nucleate boiling regions shows more curvature than that of either pure components. The heat flux range of the fully developed nucleate boiling region for 4.2 % by weight MEK is much higher than those for the pure components.

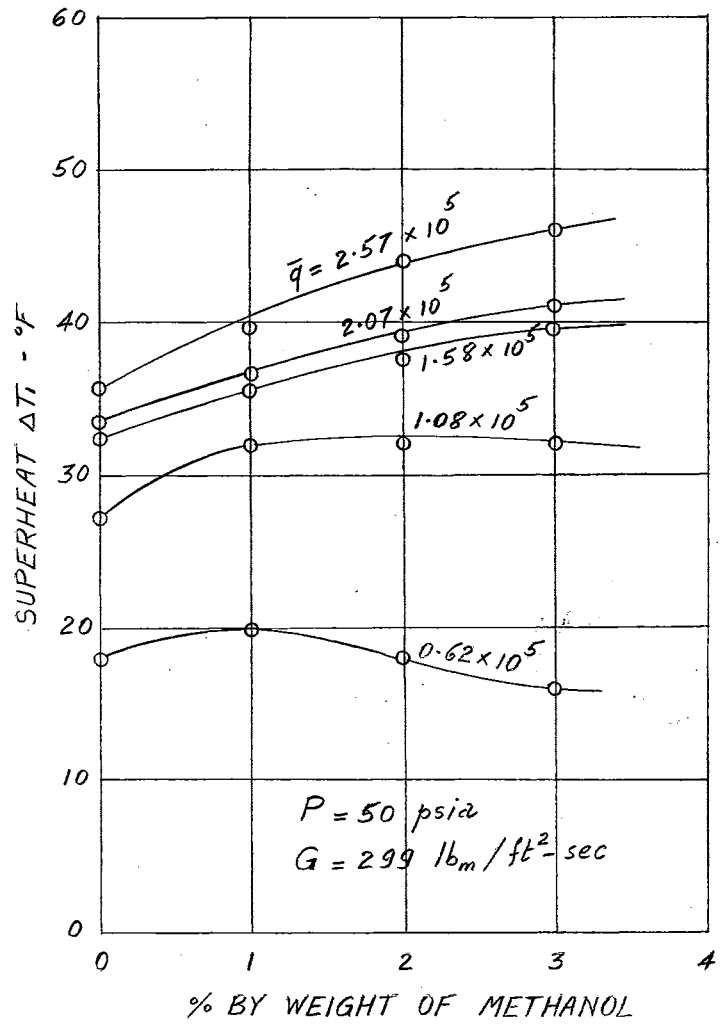


Figure 13. Effect of Concentration of Methanol on the Superheat at Constant Heat flux (P = 50 psia)

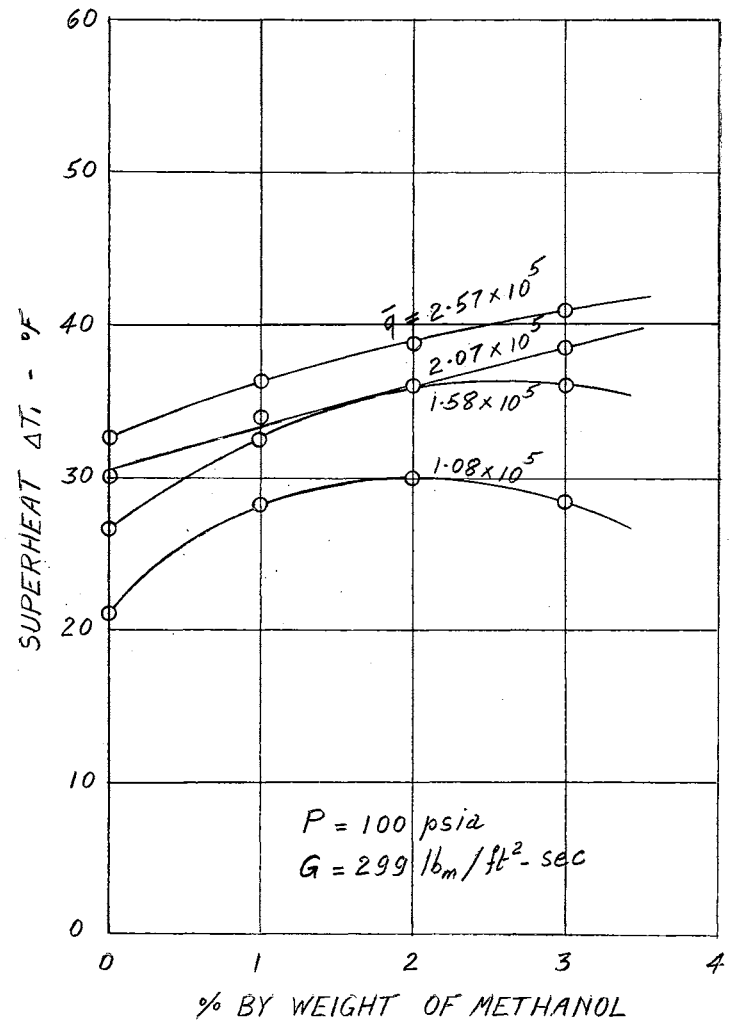


Figure 14. Effect of Concentration of Methanol on the Superheat at Constant Heat flux (P = 100 psia)

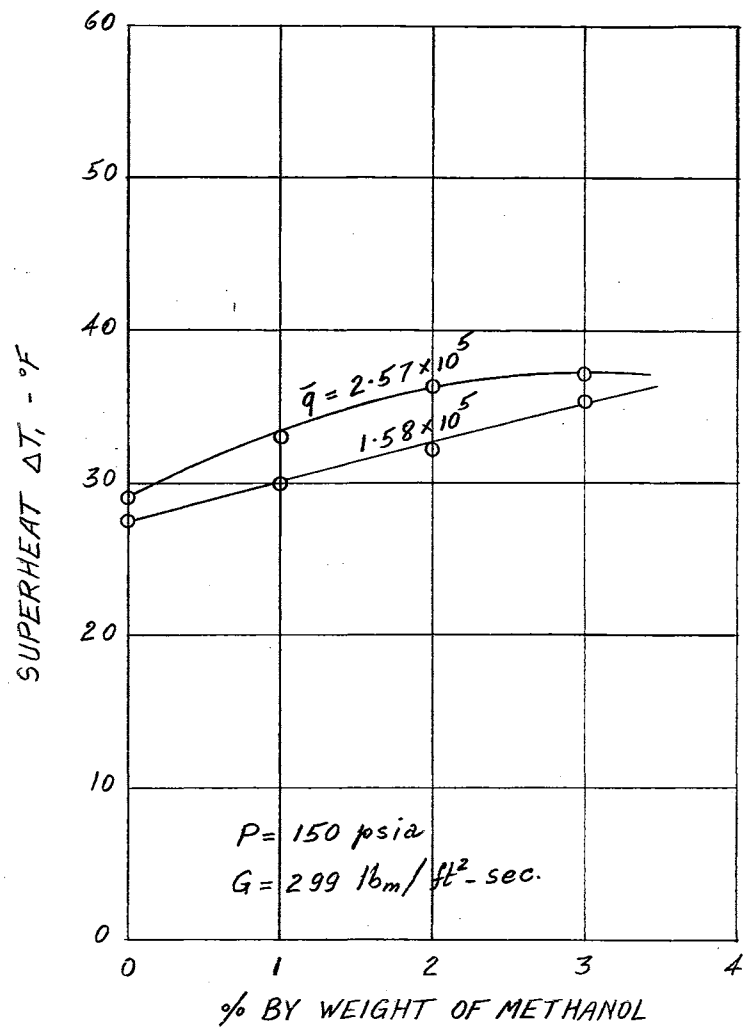


Figure 15. Effect of Concentration of Methanol on the Superheat at Constant Heat Flux ( $P = 150 \text{ psia}$ )

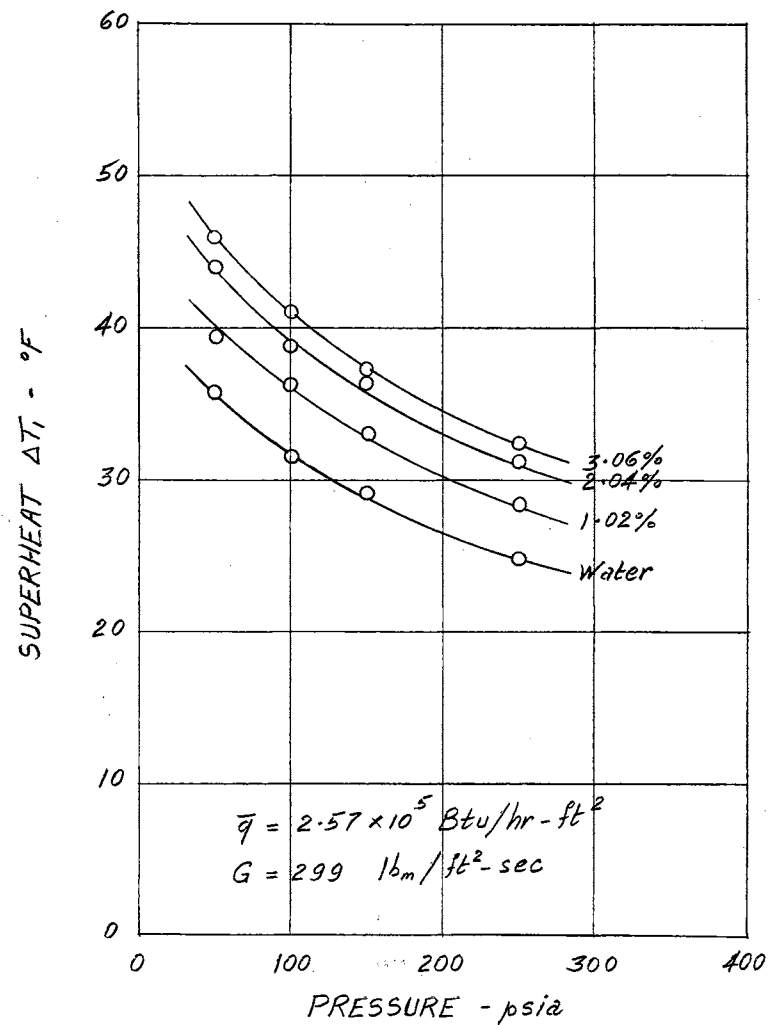


Figure 16. Effect of Pressure on the Superheat for the Methanol Mixtures at Constant Heat Flux

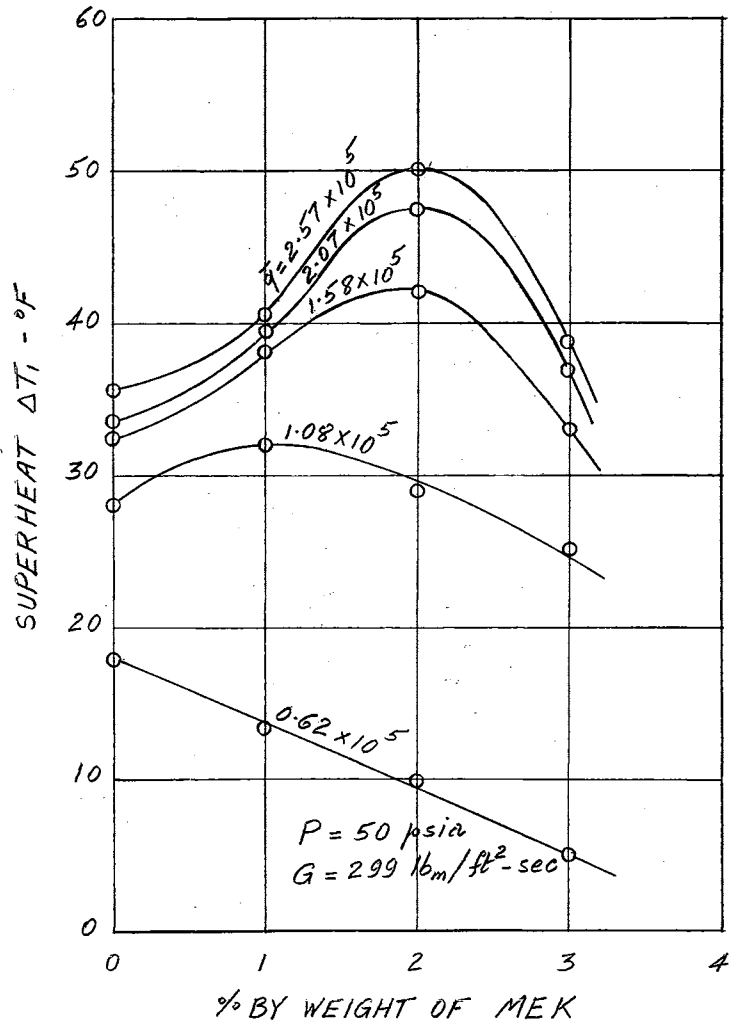


Figure 17. Effect of MEK Concentration on the Superheat at Constant Heat Flux ( $P = 50$  psia)

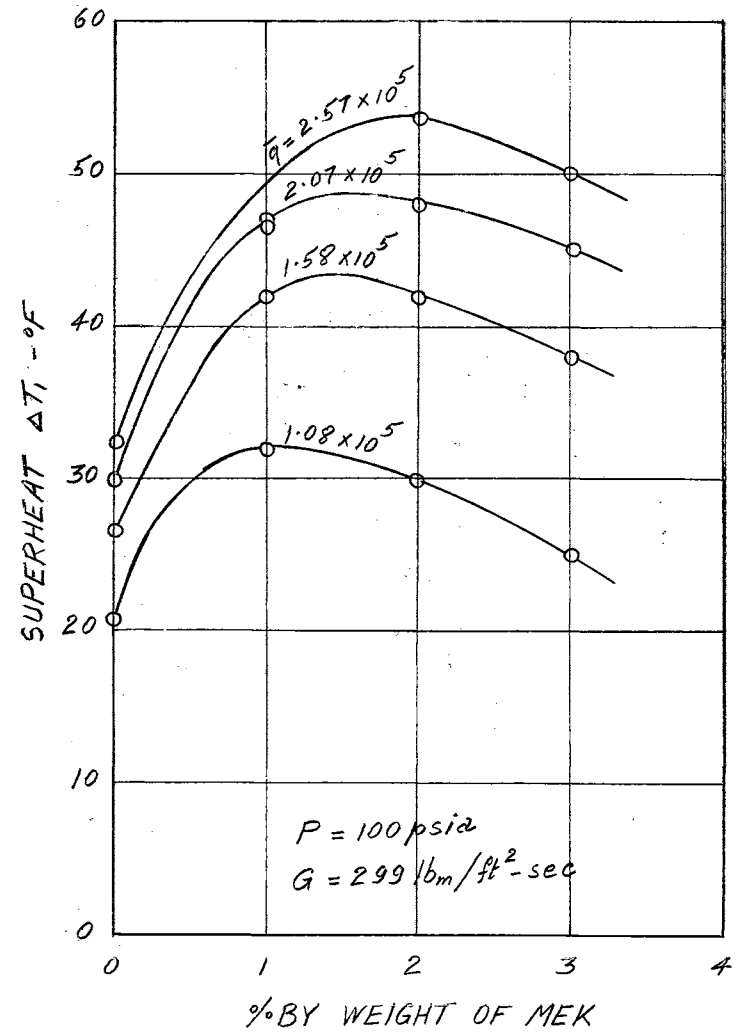


Figure 18. Effect of MEK Concentration on the Superheat at Constant Heat Flux ( $P = 100$  psia)

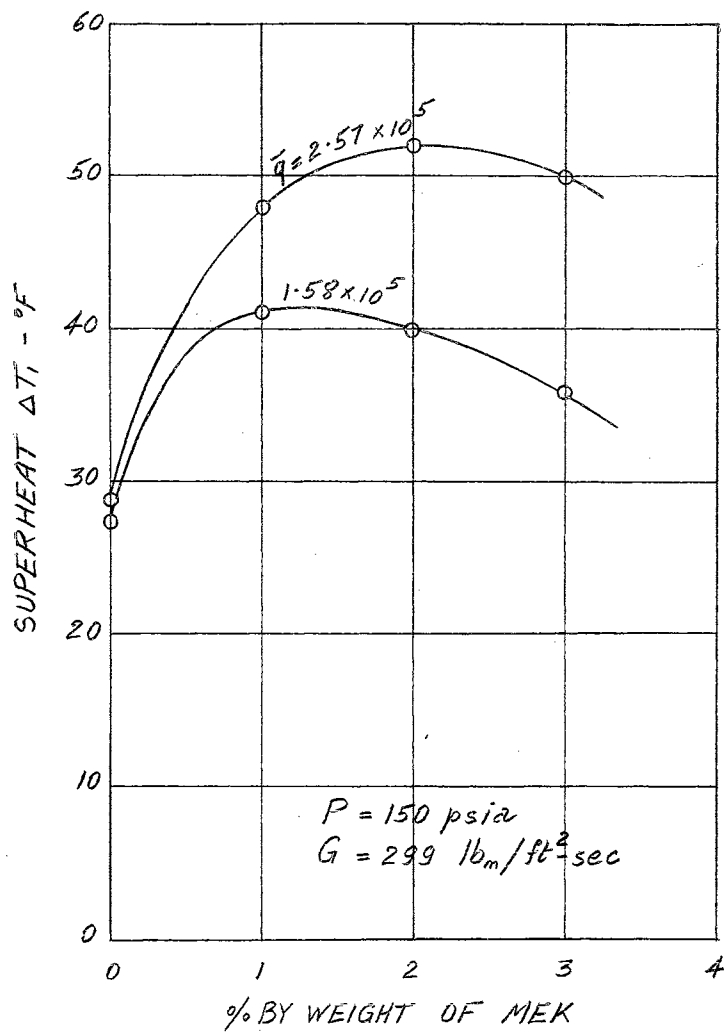


Figure 19. Effect of MEK Concentration on the Superheat at Constant Heat Flux (P = 150 psia)

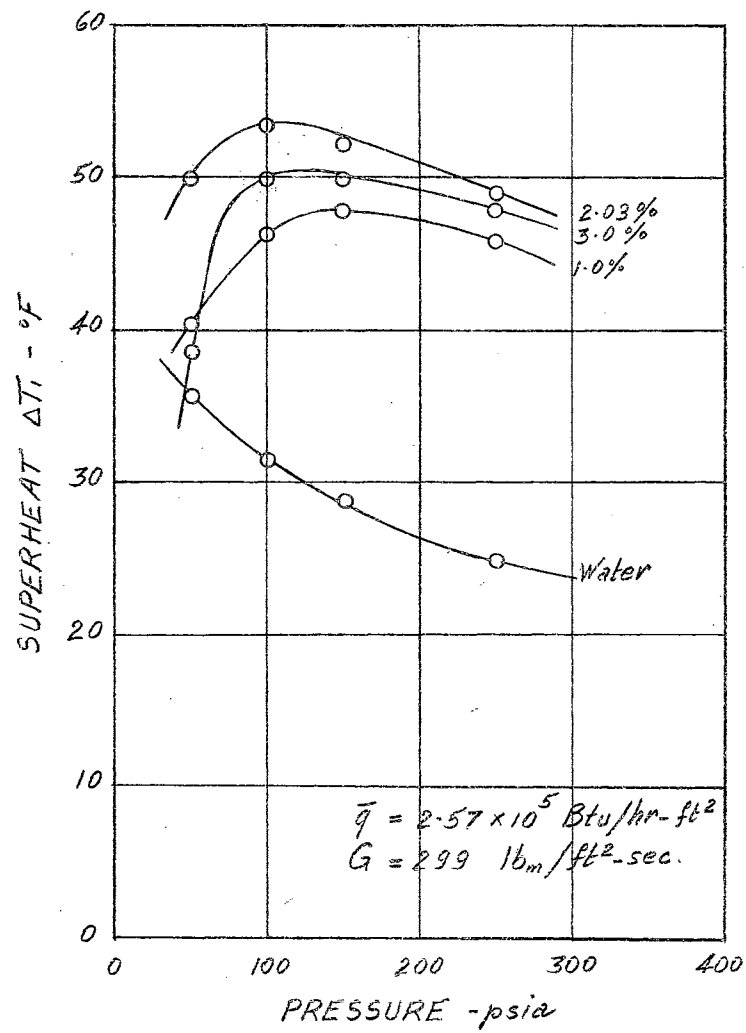


Figure 20. Effect of Pressure on the Superheat for the MEK Mixtures at Constant Heat Flux

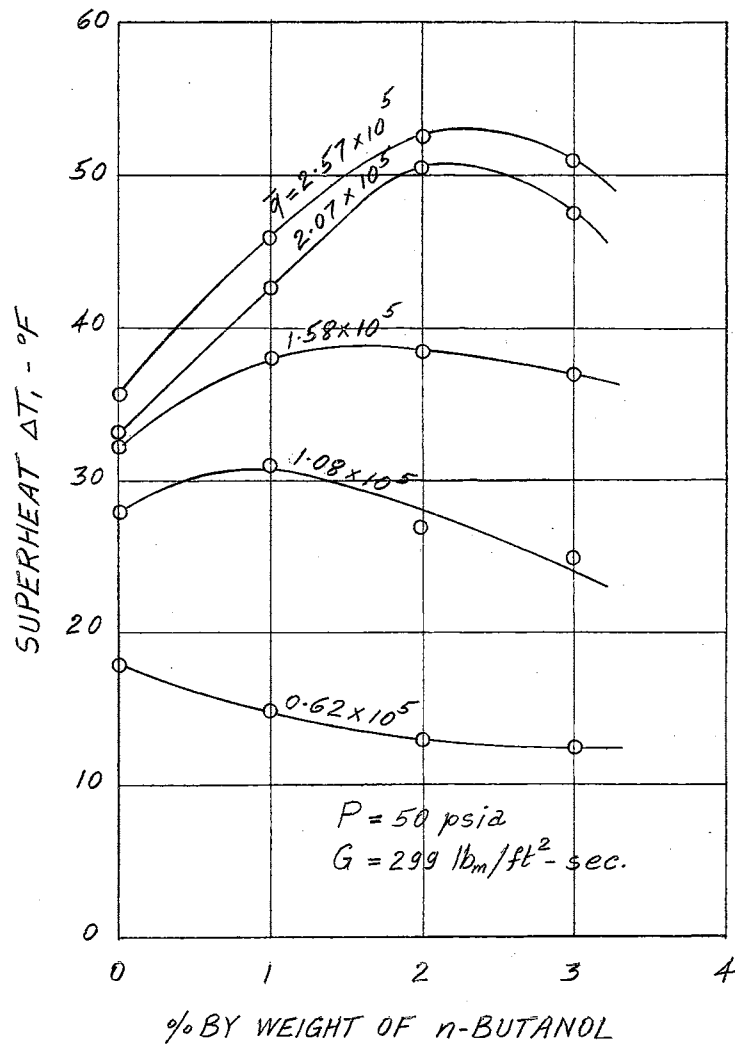


Figure 21. Effect of Concentration of n-Butanol on the Superheat at Constant Heat Flux ( $P = 50$  psia)

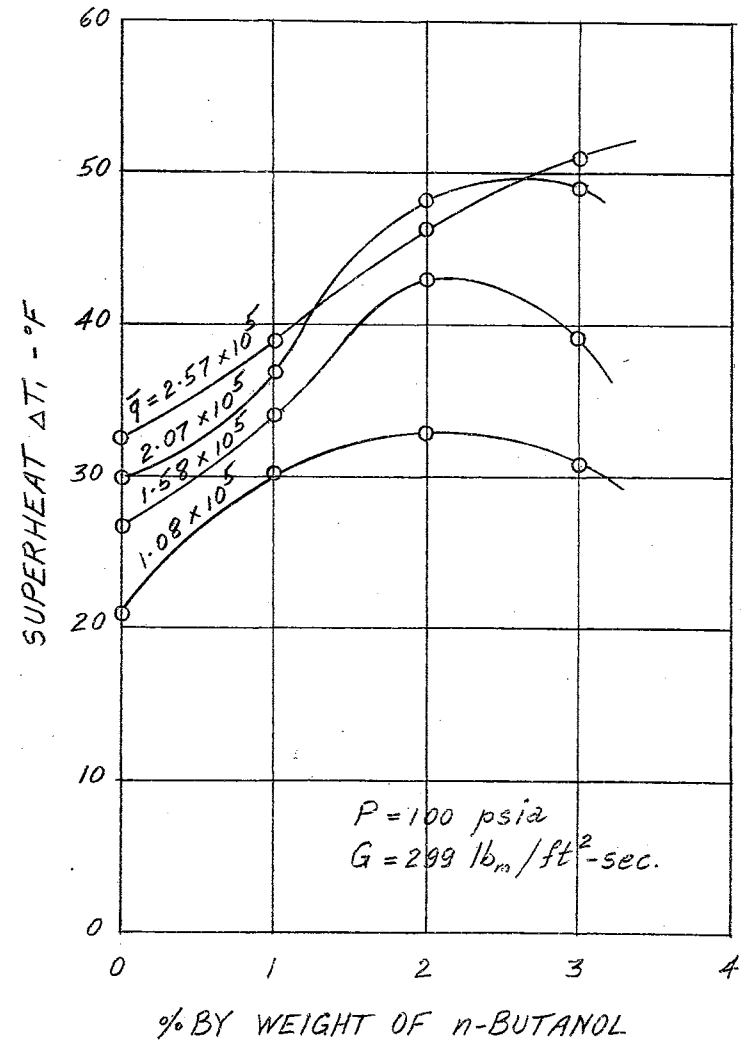


Figure 22. Effect of Concentration of n-Butanol on the Superheat at Constant Heat Flux ( $P = 100$  psia)

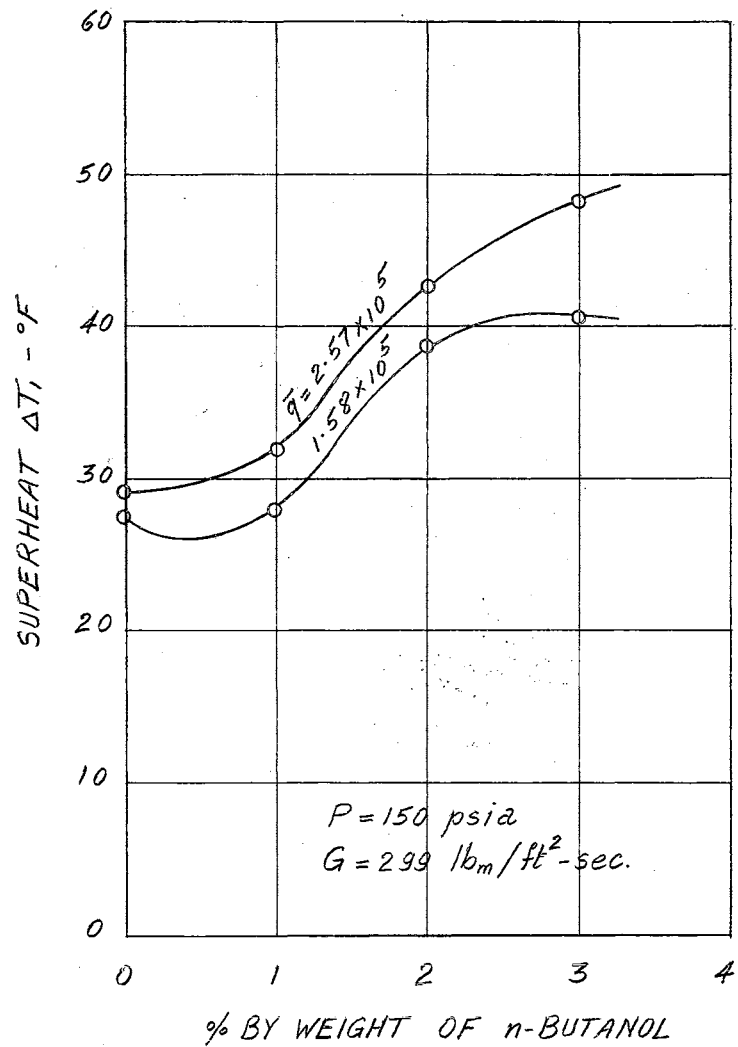


Figure 23. Effect of Concentration of n-Butanol on the Superheat at Constant Heat Flux ( $P = 150 \text{ psia}$ )

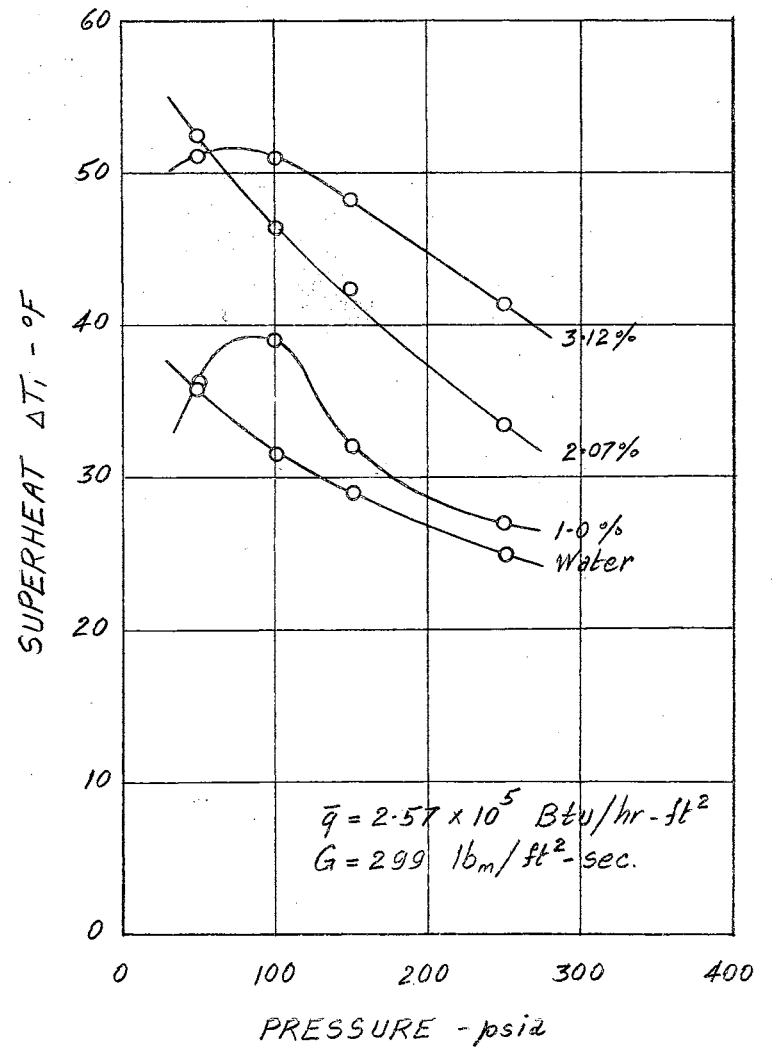


Figure 24. Effect of Pressure on the Superheat for the n-Butanol Mixtures at Constant Heat Flux



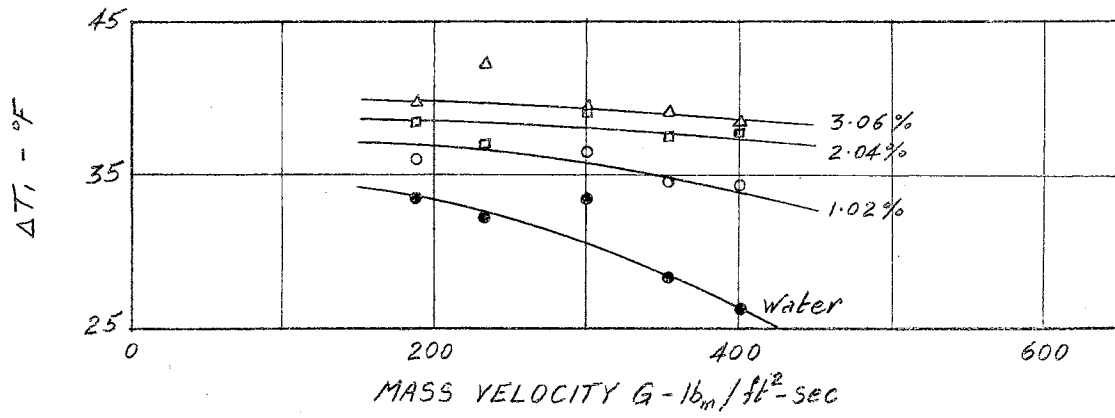


Figure 25. Effect of Mass Velocity on  $\Delta T_1$  for the Methanol Mixtures

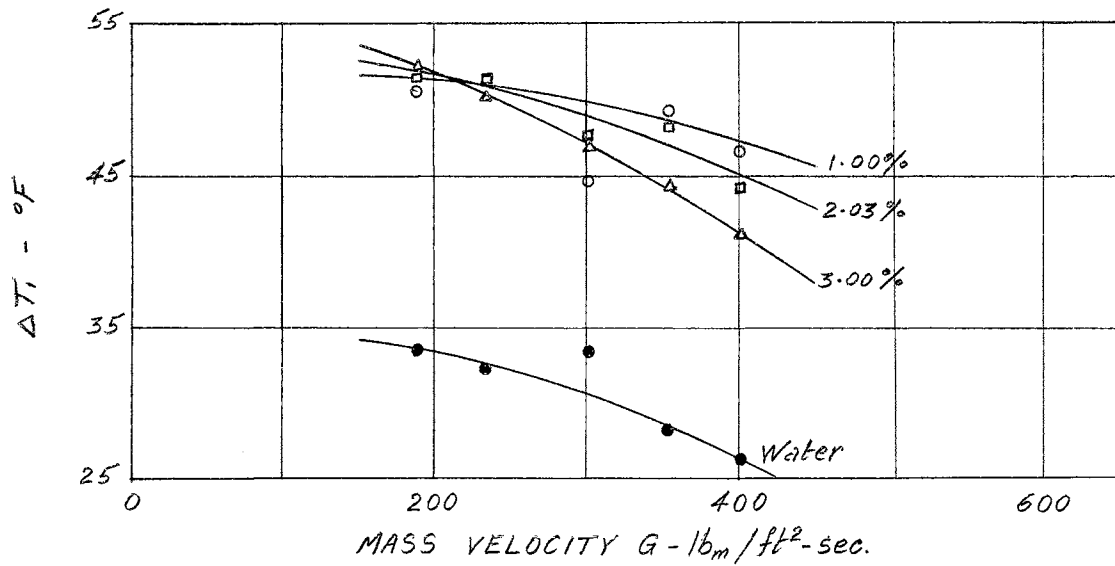


Figure 26. Effect of Mass Velocity on  $\Delta T_1$  for the MEK Mixtures

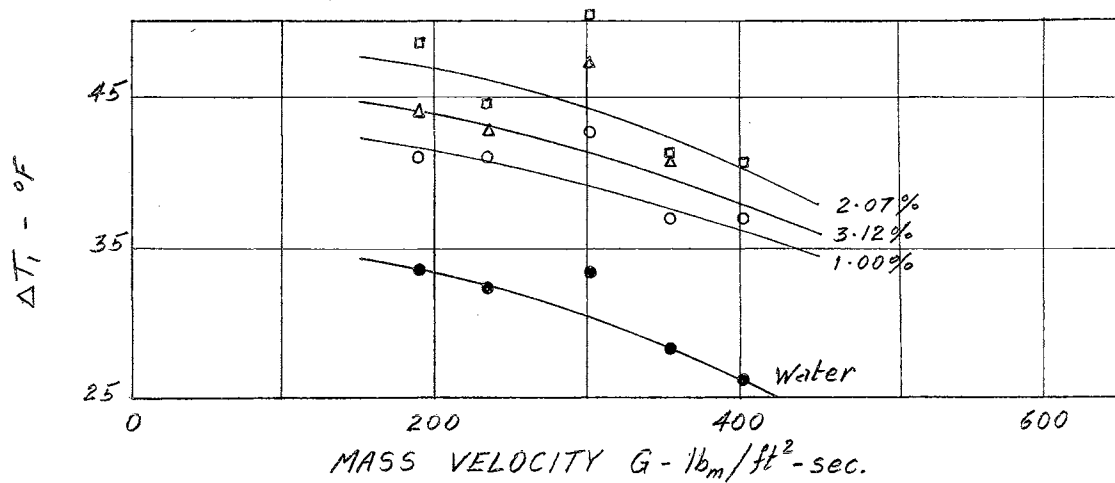


Figure 27. Effect of Mass Velocity on  $\Delta T_1$  for the n-Butanol Mixtures

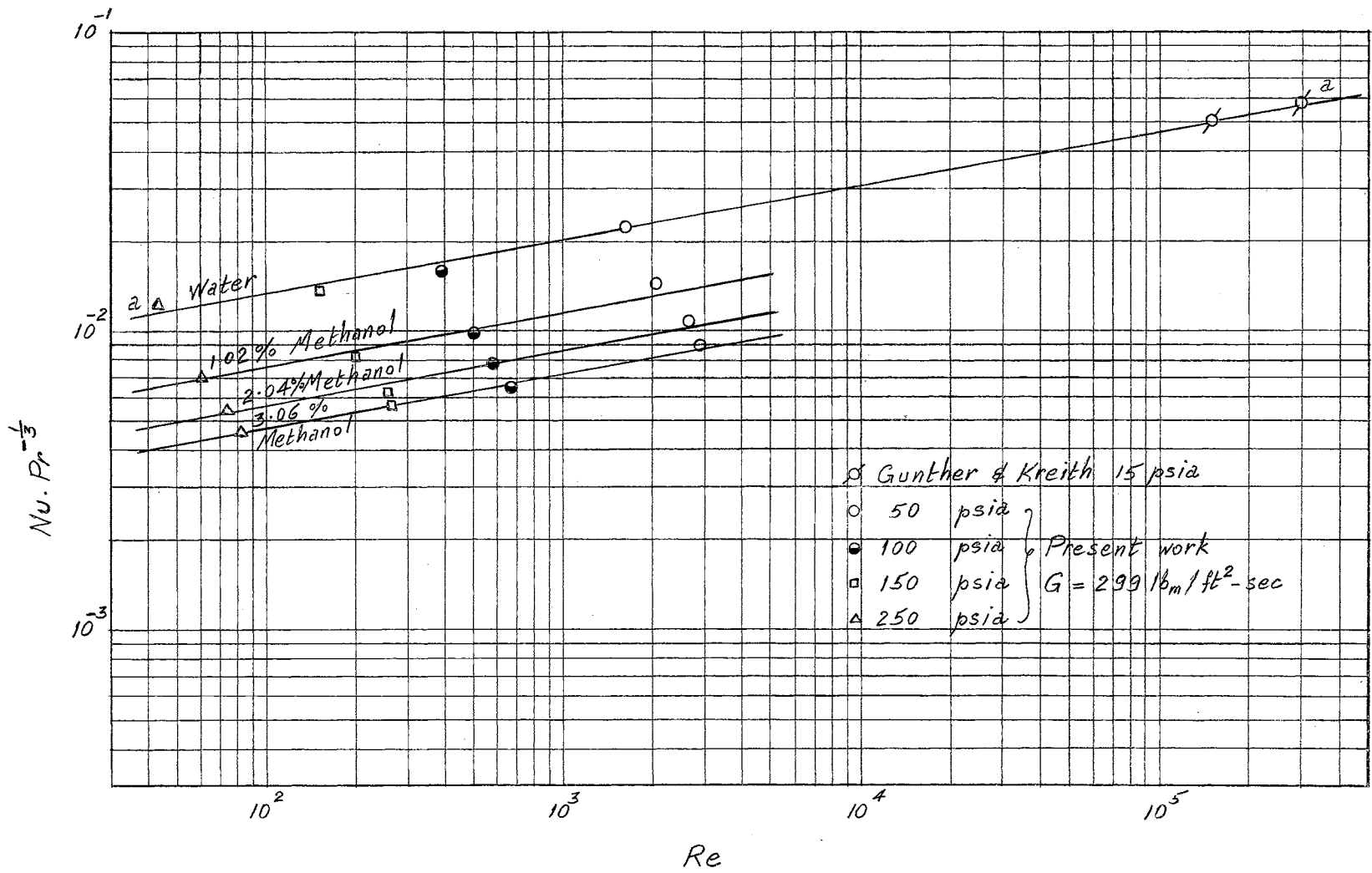


Figure 28. Correlation of the Methanol Mixtures Data for the Fully Developed Nucleate Boiling Region

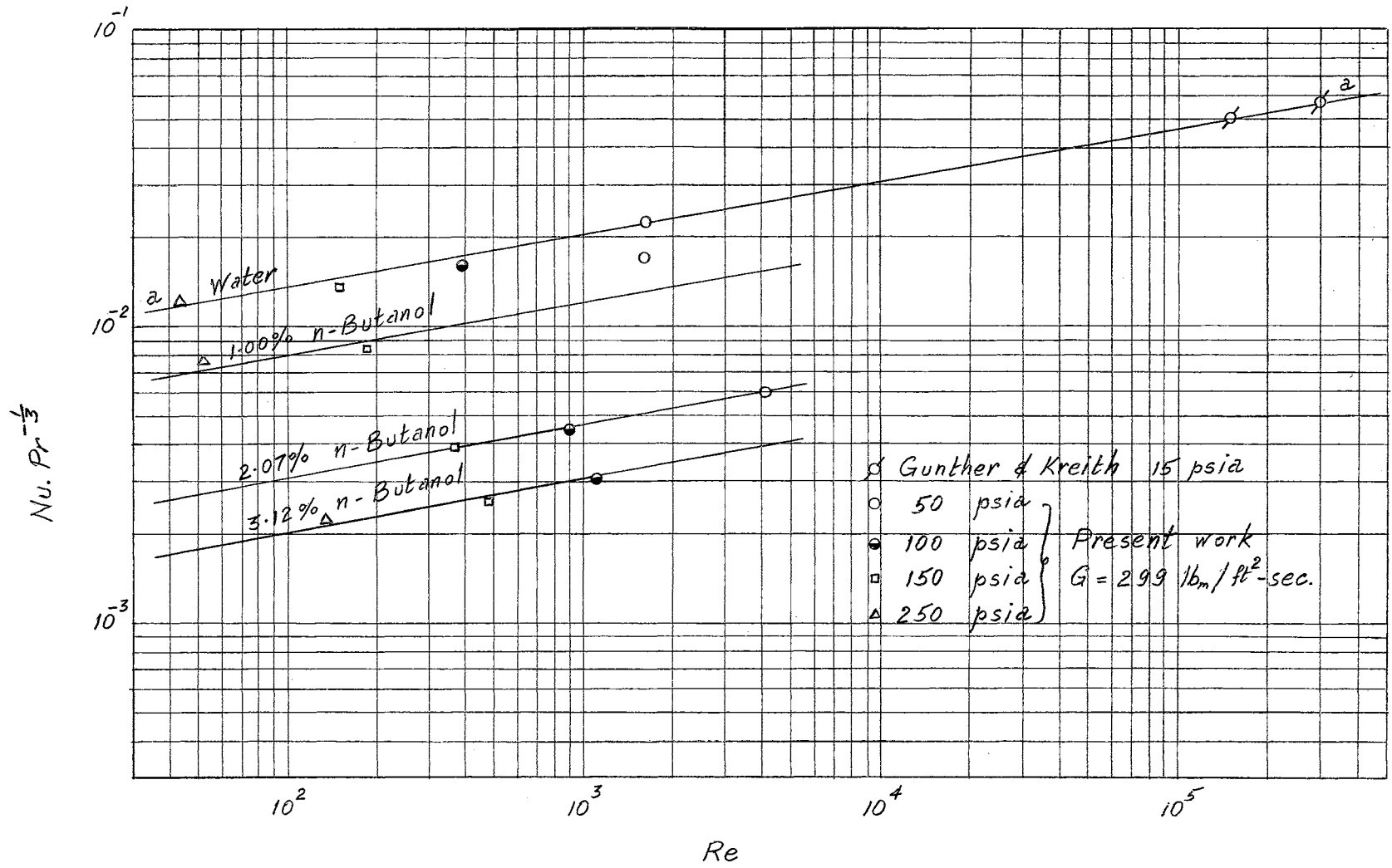


Figure 29. Correlation of the n-Butanol Mixtures Data for the Fully Developed Nucleate Boiling Region.

## CHAPTER V

### EXPERIMENTAL DATA

All the relevant experimental data are listed in Table II and Table III. The first column of each table contains the number of the run.

Runs of the different mixtures having the same numerical number as listed in the first column were conducted at the same system pressure  $P$ , the same mass velocity  $G$ , and the same heat flux  $\bar{q}$ . These are listed in Table II.

Table III lists the inlet and outlet bulk temperatures, the inside wall temperature of the test-section at seven different locations, and the superheat  $\Delta T_1$  for each run. In the case of the mixture runs  $\Delta T_1$  is the maximum value of the superheat attained just after the start of local boiling. For the locations of the different thermocouples along the test section, see Figure 6.

All temperatures are in degrees Fahrenheit.

Table III also lists, for each run, the following calculated parameters in the last two columns

$$X \equiv Re = \frac{\pi c K}{\mu} \cdot \left( \frac{J \rho_L \Delta P}{T_s} \right)^2 \cdot \left( \frac{dP}{dT} \right)^{-4}$$

$$Y \equiv Nu \cdot Pr^{-1/3} = \frac{2 \sigma \bar{q}}{k \Delta P \Delta T_1} \cdot \left( \frac{\mu c}{k} \right)^{-1/3}$$

TABLE II  
VARIABLES FOR EXPERIMENTAL DATA

Run Number	P psia	$G$ $\text{lb}_m/\text{ft}^2\text{-sec.}$	$\bar{q} \times 10^{-5}$ $\text{Btu/hr-ft}^2$
1	50	299	0.620
2	50	299	1.057
3	50	299	1.584
4	50	299	2.075
5	50	299	2.572
6	100	299	1.057
7	100	299	1.584
8	100	299	2.075
9	100	299	2.572
10	150	299	1.584
11	150	299	2.572
12	250	299	2.572
13	100	188	2.075
14	100	232	2.075
15	100	353	2.075
16	100	401	2.075

TABLE III  
Water

#	Bulk Temp.		Inside Wall Temperature							$\Delta T_i$	X	Y
	Inlet	Outlet	1	2	3	4	5	6	7			
1	233.9	273.5	291.9	294.7	296.6	298.5	299.9	301.0	301.6	18.0	317	2410
2	202.8	272.3	300.6	304.4	306.4	307.8	308.7	309.8	309.6	27.2	825	1690
3	164.3	266.6	309.3	313.3	312.6	313.5	313.6	313.9	312.0	32.4	1260	1720
4	133.6	267.4	317.7	314.7	314.2	314.8	314.3	313.9	311.1	33.4	1350	2110
5	98.1	262.7	316.9	313.3	317.0	317.2	316.3	316.5	315.9	35.7	1590	2250
6	249.7	311.2	244.2	347.6	348.5	349.1	349.3	350.2	350.7	21.1	142	1600
7	212.0	311.2	351.5	353.9	354.0	354.6	354.7	355.2	355.8	26.6	240	1470
8	178.3	309.2	355.8	357.2	357.5	358.2	357.7	357.8	357.4	29.9	315	1500
9	139.6	302.4	358.4	359.6	360.4	361.2	360.6	360.3	358.5	32.5	383	1450
10	242.9	341.3	381.3	385.0	385.5	385.9	386.1	386.6	386.5	27.6	132	9530
11	175.3	335.9	385.4	388.7	388.5	388.8	387.7	387.6	385.3	29.1	149	1380
12	217.8	335.5	425.2	425.6	426.1	426.2	425.4	425.9	425.1	24.8	43.3	1220
13	98.2	311.8	359.0	359.7	360.5	361.3	360.2	359.4	356.1	33.5	412	1160
14	141.1	316.5	359.4	360.0	359.8	360.0	358.0	356.7	353.6	32.2	375	1270
15	195.6	308.6	350.6	355.2	355.9	355.5	354.1	353.6	352.0	28.2	275	1700
16	207.5	307.1	348.2	352.6	353.9	353.8	350.4	351.0	350.9	26.2	232	1990

TABLE III (cont.)  
1.02% by wt. Methanol

#	Bulk Temp.		Inside Wall Temperature							$\Delta T_i$	X	Y
	Inlet	Outlet	1	2	3	4	5	6	7			
1	234.4	277.5	292.9	295.7	297.9	299.5	300.9	302.5	303.5	20.0	415	1490
2	202.2	273.0	300.3	304.5	308.4	310.9	313.0	314.3	313.2	32.0	1220	948
3	161.8	266.7	308.2	314.3	316.9	317.2	316.9	316.0	313.1	36.2	1640	1080
4	130.1	267.0	317.8	315.5	316.5	317.4	316.4	314.7	310.3	36.4	1660	1390
5	89.3	256.3	318.3	318.0	319.4	320.5	320.3	319.6	315.8	39.5	2030	1440
6	249.0	319.4	343.5	347.7	351.3	354.0	355.7	356.0	354.3	28.2	277	686
7	213.5	318.9	354.8	360.3	359.4	359.0	358.1	357.1	356.1	32.5	383	761
8	178.2	316.2	361.2	361.2	361.3	361.8	361.2	360.3	357.7	34.0	425	904
9	136.4	303.9	362.3	363.1	363.3	364.1	363.7	362.7	359.7	36.3	496	973
10	240.7	343.6	377.4	383.9	388.3	387.3	385.9	385.1	383.4	29.9	160	632
11	173.0	340.4	391.4	390.9	391.3	391.3	390.5	390.0	387.2	33.0	120	834
12	218.1	382.9	429.7	429.4	429.6	428.8	427.7	426.8	424.3	28.6	60.1	706
13	89.7	297.6	356.8	360.0	362.8	363.7	363.3	362.0	357.9	35.9	483	799
14	132.8	307.6	361.4	362.6	364.4	364.8	363.7	361.7	358.0	37.0	518	751
15	197.7	311.9	355.6	360.7	361.8	362.3	362.1	361.9	360.3	34.5	440	873
16	213.0	313.8	352.6	358.4	362.0	361.7	361.5	361.3	359.1	34.2	431	887

TABLE III (cont.)  
2.04% by wt. Methanol

#	Bulk Temp.		Inside Wall Temperature							$\Delta T_i$	X	Y
	Inlet	Outlet	1	2	3	4	5	6	7			
1	233.1	275.3	291.1	293.9	296.0	297.8	299.4	300.3	299.8	18.0	340	1690
2	197.1	268.9	295.3	299.6	303.7	306.4	308.9	311.2	312.6	32.0	1230	882
3	157.6	261.1	303.9	310.0	315.6	318.2	318.6	317.5	314.6	37.6	1800	931
4	122.3	257.6	314.8	319.6	320.0	320.1	319.6	318.9	315.3	39.1	1980	1120
5	90.0	255.8	323.5	323.2	324.1	325.0	324.5	324.3	321.6	44.0	2650	1070
6	249.4	319.4	344.1	347.9	351.7	354.4	356.7	357.7	354.8	30.0	323	560
7	209.1	312.7	350.2	356.3	361.6	363.7	362.9	362.7	360.8	35.9	486	572
8	178.5	314.2	361.6	364.4	363.5	363.8	363.1	362.3	359.5	36.0	489	474
9	137.1	304.6	365.5	366.5	366.2	366.6	365.8	364.3	360.4	38.8	583	785
10	240.5	342.4	377.4	384.1	389.4	390.6	389.8	389.1	386.1	32.2	194	493
11	173.7	340.2	393.9	394.8	394.0	393.7	392.3	391.3	385.7	36.4	255	625
12	221.3	384.7	431.0	432.2	431.2	430.6	429.5	429.7	428.4	31.2	73.4	547
13	92.4	305.6	365.7	366.2	365.8	365.2	363.8	361.6	356.7	38.4	569	647
14	137.2	310.8	364.3	364.8	364.4	364.7	363.1	361.5	356.5	36.9	518	705
15	199.9	314.3	357.0	363.6	365.2	364.6	363.6	362.9	362.8	37.4	535	685
16	213.0	312.0	353.0	357.8	363.0	365.5	363.5	363.2	361.8	37.7	545	677



TABLE III (cont.)  
3.06% by wt. Methanol

#	Bulk Temp.		Inside Wall Temperature							$\Delta T_i$	X	Y
	Inlet	Outlet	1	2	3	4	5	6	7			
1	231.5	273.5	289.6	292.1	294.3	296.1	297.6	299.0	299.5	16.0	340	1688
2	197.5	268.0	297.0	301.0	304.8	307.4	309.9	312.3	312.9	32.0	1230	882
3	156.5	261.0	305.5	311.1	316.8	319.9	321.9	322.2	316.8	41.2	1800	931
4	128.1	264.1	320.0	320.1	319.7	320.4	319.6	317.4	312.0	39.4	1980	1120
5	93.7	260.2	326.4	327.0	326.9	325.8	326.4	325.3	317.5	46.0	2650	1070
6	246.3	316.3	341.4	345.5	349.0	351.8	354.2	356.2	356.0	28.4	323	560
7	205.9	309.5	348.4	354.1	359.5	362.5	363.8	363.9	362.0	36.1	486	572
8	173.6	308.0	358.4	365.2	366.4	366.2	365.6	364.3	360.9	38.6	489	744
9	137.8	304.4	366.7	368.9	368.3	367.6	365.9	363.7	359.5	41.1	583	785
10	240.7	344.3	379.1	385.0	390.7	393.7	392.3	391.0	389.1	35.3	194	493
11	172.0	337.0	392.9	395.6	395.6	395.5	394.1	392.8	390.8	37.2	255	625
12	210.7	372.9	423.3	430.5	433.4	431.7	431.1	431.2	429.0	32.4	73.4	547
13	89.7	301.8	365.0	367.1	367.5	366.4	364.7	362.3	357.7	39.7	569	647
14	129.3	302.5	360.6	368.1	370.9	370.1	368.0	365.4	360.6	42.3	518	705
15	195.9	309.7	355.0	361.5	366.4	366.4	365.8	364.9	362.2	39.0	535	685
16	209.1	309.4	349.9	355.9	361.2	364.6	366.0	365.4	362.5	38.2	545	677

TABLE 31(cont.)  
1.00% by wt. MEK

#	Bulk Temp.		Inside Wall Temperature							$\Delta T_1$	X	Y
	Inlet	Outlet	1	2	3	4	5	6	7			
1	228.0	270.7	286.2	288.7	291.0	292.9	294.5	296.1	297.6	13.5	162	3210
2	197.2	268.6	294.8	298.9	301.7	305.2	308.6	311.5	312.4	32.0	1160	877
3	159.0	263.2	301.4	302.2	308.5	313.7	317.9	319.2	316.5	38.2	1790	890
4	125.0	259.7	304.6	309.8	315.6	318.9	319.8	320.4	317.0	39.4	1930	1080
5	90.3	257.0	308.9	314.1	318.1	320.5	321.2	321.4	318.6	40.4	2060	1270
6	247.5	317.9	340.6	346.3	349.9	353.1	355.9	358.1	359.1	32.0	352	493
7	208.8	312.7	346.9	354.7	361.1	365.3	368.2	369.5	367.7	42.0	672	401
8	172.5	308.6	353.5	364.1	371.6	374.7	373.2	371.9	368.6	47.0	885	410
9	142.2	308.9	363.7	372.9	373.4	373.1	369.6	367.5	363.0	46.5	862	518
10	242.9	345.7	375.6	385.4	392.3	396.4	399.1	399.6	396.1	41.2	320	293
11	176.0	341.8	390.9	401.9	405.5	406.3	403.1	402.0	398.9	47.9	460	340
12	221.1	385.6	430.5	441.8	446.3	446.8	444.6	442.5	438.8	46.0	169	232
13	93.5	304.6	368.1	375.9	378.0	378.3	375.2	372.8	367.4	50.5	1060	347
14	130.8	304.5	362.2	373.1	377.4	379.0	377.0	375.6	371.0	51.2	1090	338
15	200.2	314.3	354.9	363.8	370.8	374.5	377.0	375.9	370.2	49.2	991	370
16	213.9	315.4	352.4	360.4	366.5	370.5	373.4	373.9	368.3	46.5	862	421

TABLE III (cont.)  
2.03% by wt. MEK

#	Bulk Temp.		Inside Wall Temperature							$\Delta T_i$	X	Y
	Inlet	Outlet	1	2	3	4	5	6	7			
1	223.5	266.3	281.9	284.5	287.0	288.9	290.5	291.8	293.3	10.0	80.4	5460
2	191.5	261.9	290.5	294.9	298.8	301.9	304.6	307.0	309.3	29.0	849	998
3	154.1	258.1	300.2	306.6	312.7	317.1	320.8	322.9	316.6	42.0	2090	660
4	118.1	253.9	309.5	317.8	325.3	328.5	327.8	324.9	320.7	47.5	2850	655
5	83.3	249.4	319.4	327.5	329.4	331.0	328.5	326.3	322.1	50.0	3260	721
6	244.1	314.3	336.2	341.6	346.6	349.7	352.6	355.1	357.0	30.0	281	513
7	206.0	309.1	342.2	350.4	358.1	362.8	367.0	369.4	365.5	42.0	621	369
8	170.9	305.6	348.2	359.2	369.3	374.1	375.7	373.7	369.2	47.9	856	361
9	136.9	303.5	356.5	370.5	379.8	380.7	375.4	373.2	367.9	53.5	1120	346
10	237.2	340.1	370.2	379.4	387.2	391.5	395.3	397.8	395.3	40.0	277	288
11	168.7	333.3	383.7	398.7	407.7	410.6	408.7	407.4	403.0	52.2	523	255
12	218.5	382.3	430.6	441.7	448.7	449.7	447.6	445.7	441.1	49.0	181	185
13	85.5	298.4	367.5	375.0	379.0	378.5	376.7	375.2	369.3	51.2	1010	309
14	127.4	300.4	360.9	370.4	376.8	378.6	376.1	375.3	369.9	51.0	999	313
15	194.1	308.9	353.8	361.1	367.2	371.6	374.6	374.6	369.5	48.0	860	357
16	208.9	309.7	350.6	357.0	362.8	366.6	369.9	371.6	366.9	44.0	695	433

TABLE III(cont.)  
3.00% by wt. MEK

#	Bulk Temp.		Inside Wall Temperature							$\Delta T_i$	X	Y
	Inlet	Outlet	1	2	3	4	5	6	7			
1	218.9	261.3	278.1	280.8	282.9	284.9	286.4	287.9	289.4	5.0	19.2	18700
2	186.7	258.0	286.7	290.3	294.3	297.7	300.6	302.9	305.0	25.0	565	1280
3	146.0	250.4	293.2	299.6	304.8	308.7	312.2	313.9	311.3	32.9	1080	1050
4	114.5	250.2	304.0	311.3	316.1	318.0	316.4	315.9	312.8	37.0	1430	1070
5	83.8	250.6	314.4	318.8	319.1	319.7	317.8	316.5	312.1	38.7	1600	1200
6	238.8	309.4	329.1	334.1	339.5	344.0	347.8	350.7	352.2	25.0	175	709
7	202.0	305.5	334.5	340.9	348.8	355.6	362.1	365.1	360.1	38.0	459	429
8	165.6	300.7	336.3	344.6	354.4	363.5	371.2	371.2	367.1	45.0	687	390
9	134.8	301.2	344.1	354.2	367.0	376.8	376.4	372.9	367.6	50.0	889	377
10	233.4	335.5	358.3	365.1	373.5	382.3	390.0	393.7	393.1	36.0	203	340
11	169.0	334.5	371.7	382.6	397.8	407.7	406.4	403.3	399.1	50.0	441	264
12	215.1	379.3	415.3	428.2	443.6	448.3	447.1	445.0	441.1	48.0	162	182
13	88.2	301.7	353.1	368.0	379.1	377.3	373.8	370.5	364.2	52.0	980	281
14	125.5	300.0	346.4	360.0	374.9	378.3	374.6	372.1	367.2	50.0	911	300
15	188.9	302.9	339.3	348.6	359.9	365.7	370.0	372.1	367.6	44.3	662	402
16	204.9	305.5	338.5	346.8	356.9	362.2	366.5	368.8	365.2	41.0	549	477

TABLE III (cont.)  
1.00% by wt. n-Butanol

#	Bulk Temp.		Inside Well Temperature							$\Delta T_i$	X	Y
	Inlet	Outlet	1	2	3	4	5	6	7			
1	232.3	272.0	289.3	291.7	293.8	295.7	297.3	298.6	299.8	15.0	208	2700
2	197.7	265.1	294.4	298.9	302.4	305.0	307.7	310.0	311.8	31.0	1110	964
3	158.8	259.0	302.8	308.3	313.4	317.3	318.3	318.5	317.1	38.0	1840	924
4	127.6	258.7	313.7	317.8	323.0	322.2	317.5	316.3	315.8	42.7	2470	931
5	87.1	247.7	315.7	313.8	315.7	316.7	317.0	316.5	316.5	36.0	1610	1690
6	248.2	316.7	343.4	347.8	351.3	353.9	356.3	358.1	358.0	30.3	321	561
7	214.9	319.9	356.2	361.6	361.5	360.8	361.1	360.1	359.4	34.2	427	652
8	177.6	312.1	362.0	364.4	362.3	362.3	362.8	362.1	361.5	36.6	502	732
9	148.3	316.1	366.2	362.9	361.3	361.4	361.0	360.1	358.3	39.0	585	802
10	245.7	348.3	382.5	384.2	384.3	385.5	386.5	385.9	385.2	28.1	136	699
11	182.9	348.1	390.7	389.8	388.8	389.2	389.7	388.9	387.9	32.0	184	850
12	227.5	393.5	428.0	426.9	427.0	427.0	426.9	425.9	425.4	27.0	51.8	767
13	98.6	310.6	368.6	367.8	363.9	363.0	362.6	362.0	360.1	41.0	660	568
14	141.5	318.2	368.7	367.3	363.4	363.0	362.3	360.7	357.9	41.0	660	568
15	194.7	308.2	354.4	360.9	364.7	364.7	364.9	364.5	363.9	37.1	519	710
16	206.7	307.0	349.6	355.7	360.6	364.3	364.4	364.2	364.1	37.0	515	716

TABLE III (cont.)  
2.07% by wt. n-Butanol

#	Bulk Temp.		Inside Wall Temperature							$\Delta T_i$	X	Y
	Inlet	Outlet	1	2	3	4	5	6	7			
1	227.0	268.6	287.1	289.5	291.8	293.7	295.2	296.7	298.1	13.0	150	3160
2	193.3	262.6	293.1	297.3	301.0	303.6	306.3	307.7	307.3	27.0	791	1120
3	154.1	257.2	303.3	309.2	314.4	317.5	319.4	317.5	313.2	38.4	1870	771
4	119.2	253.1	313.2	320.7	326.8	329.8	330.8	325.4	319.0	50.4	3740	544
5	82.3	246.8	323.9	330.9	332.4	333.1	329.5	325.8	322.3	52.5	4160	613
6	245.5	316.1	341.4	346.0	349.7	352.3	355.0	357.1	359.2	33.0	389	405
7	213.5	318.8	354.9	361.8	367.1	370.4	370.0	365.3	360.1	43.0	735	333
8	174.1	309.5	360.4	368.1	374.1	376.0	369.4	368.1	361.0	48.5	989	332
9	135.6	301.6	367.1	374.3	371.2	367.4	364.4	364.1	362.0	46.5	891	452
10	240.4	343.9	380.2	386.7	391.9	395.4	397.1	395.8	392.1	38.7	285	295
11	173.6	340.4	398.1	401.0	398.6	395.5	394.4	393.5	392.5	42.6	358	386
12	219.8	386.4	434.3	433.7	432.9	432.2	430.9	429.7	429.4	33.5	836	412
13	80.9	291.8	364.1	373.1	376.1	376.4	375.0	373.0	366.9	48.6	994	331
14	134.3	307.8	368.1	372.2	370.1	367.9	364.3	361.9	359.8	44.5	799	404
15	194.7	308.2	354.4	361.3	367.1	368.8	364.5	360.4	360.6	41.0	654	485
16	211.3	311.4	353.7	359.6	364.4	367.7	368.1	367.7	362.2	40.5	635	497

TABLE III (cont.)  
3.12% by wt. n-Butanol

#	Bulk Temp.		Inside Wall Temperature							$\Delta T_i$	X	Y
	Inlet	Outlet	1	2	3	4	5	6	7			
1	227.3	269.1	287.1	289.7	292.0	293.7	295.4	296.7	298.2	12.5	135	2950
2	197.1	266.6	296.8	300.7	304.3	307.0	310.0	312.2	314.9	35.0	1450	556
3	156.5	259.2	306.4	311.9	317.2	320.4	324.8	327.6	326.3	47.0	3060	428
4	115.9	250.5	312.9	319.6	325.1	328.2	325.9	321.1	321.5	47.2	3080	555
5	82.8	247.2	326.2	332.0	329.6	332.2	322.4	318.0	318.8	51.0	3790	570
6	244.1	312.7	340.6	344.6	348.1	351.2	353.8	356.2	358.2	31.0	330	404
7	204.5	307.4	348.9	354.7	359.6	363.6	367.4	366.0	361.6	39.6	591	353
8	173.5	309.1	361.4	368.2	374.3	376.5	365.7	361.8	355.5	49.0	998	284
9	140.2	306.8	372.1	378.8	367.0	363.6	359.1	358.3	356.7	51.0	1100	320
10	239.6	342.7	378.7	384.8	390.6	394.5	397.8	398.6	395.1	40.5	312	233
11	176.5	343.6	398.8	406.6	402.8	399.9	393.3	391.7	390.3	48.2	475	256
12	223.4	391.2	438.3	442.4	439.5	437.5	434.1	432.4	430.0	41.4	134	225
13	81.2	290.8	365.5	371.5	371.1	370.1	362.9	362.6	361.6	44.0	764	363
14	118.3	290.8	355.7	364.7	370.3	370.6	365.2	364.7	362.8	42.8	714	386
15	188.6	301.6	350.2	356.1	361.5	365.8	368.9	365.7	365.9	41.0	643	425
16	204.6	304.5	348.2	354.1	359.0	362.3	364.2	358.9	359.4	36.4	482	553

## CHAPTER VI

### ANALYSIS OF THE EXPERIMENTAL RESULTS

#### Temperature profile

The temperature profiles of some experimental runs for water and for the mixtures were shown in Figure 11.

In the case of water, the heating surface had nearly a constant temperature throughout the boiling region. This wall temperature, during nucleate boiling of water, was observed in this investigation to increase slightly as the subcooling  $\Delta T_2$  decreased for low heat flux values. At the higher values of the heat flux  $\bar{q}$ , the wall temperature was observed to decrease slightly as the subcooling decreased. This can be seen in Figure 30.

The wall temperature in the boiling region of the test section, in the case of the mixture runs, increased to a maximum and then decreased steadily along the boiling length of the tube. This decrease of the wall temperature can be seen in Figure 11 for the mixture runs. The temperature profiles of the experimental runs for water and some mixtures are also shown in Figure 31 where the temperature difference  $(T_w - T_B)$  is plotted against the bulk temperature of the fluid  $T_B$ . It is believed that this decrease of the wall temperature (i.e. the decrease of the superheat  $\Delta T_1$ ) along the boiling length of the tube is due to one or both of the following two reasons:



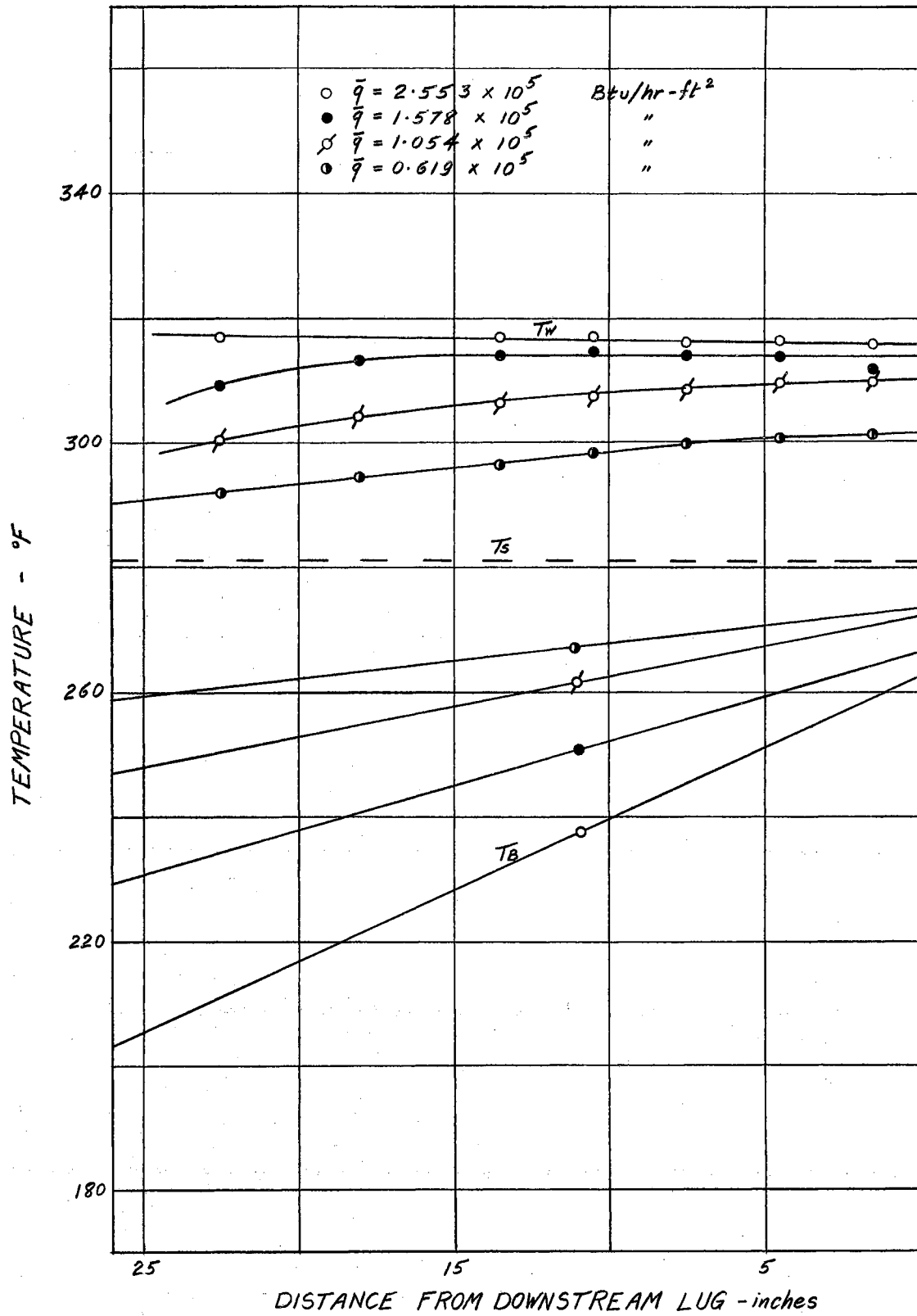


Figure 30. Temperature Profiles of Some Water Data

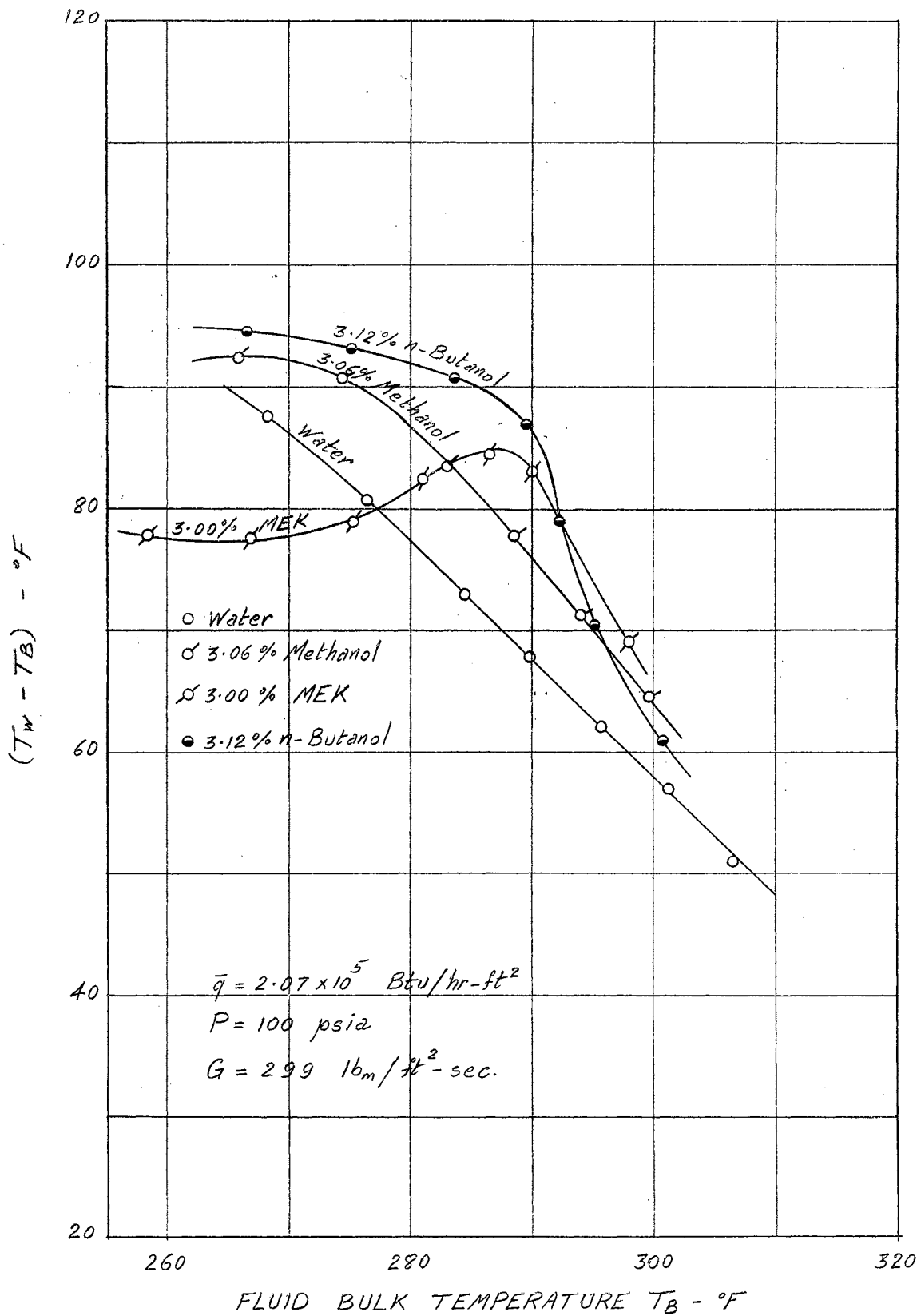


Figure 31. Temperature Profiles of Water and Some Mixtures

1. A possible depletion of the volatile component from the mixture at the wall as the flow progresses downstream. It was observed that the decrease in  $\Delta T_1$  along the boiling length for the mixtures is more pronounced on the average for the higher heat flux values.
2. A possible influence of the degree of subcooling on the bubble lifetime, on the average maximum bubble radius  $R_{\max}$ , and especially on the bubble population (bubbles/ft<sup>2</sup>-sec.). The heat flux during subcooled nucleate boiling of water is insensitive to the degree of subcooling and is usually expressed as a function only of the superheat  $\Delta T_1$ . In the case of mixtures, the subcooling may enter the picture resulting in a lower value of the superheat for lower values of the subcooling.

In the case of the mixtures, the maximum value of the wall temperature near the start of local boiling was used to evaluate the superheat  $\Delta T_1$ . The average value of the superheat in the case of the mixture runs is somewhat lower than the maximum value listed in Table III. If it is assumed that there is no depletion of the volatile component at the wall, and if this average value is used to compare the mixture superheat with that of pure water, then the curves shown in Figures 13 through 27 for the mixtures will be lower. This will have no effect on the conclusions drawn from the qualitative behavior of these mixtures as represented in Figures 13 through 27.

The decrease of the superheat  $\Delta T_1$  for all mixtures was found to be about 10 °F per foot length in the boiling region on the average.

#### Effect of Concentration of the Additive on the Superheat

Figures 13 through 24 show that for very low heat flux values (around

$0.62 \times 10^5$  Btu/hr-ft<sup>2</sup>) the superheat  $\Delta T_1$  decreased in general as the concentration of the additive in the water increased.

For the higher values of the heat flux and for the Methanol additives, the superheat  $\Delta T_1$  in general increased steadily as the concentration increased. In the case of the n-Butanol and MEK additives, the superheat first increased until the concentration of the additives reached about 2% by weight and then decreased. Figures 17 through 19 indicate that in the case of the MEK additives the superheat will actually show a decrease over that of pure water for concentrations higher than 3% by weight, and especially at low pressures.

#### Effect of Pressure on the Superheat

The relationship between the superheat and the system pressure for the water data of this investigation at a constant heat flux of  $2.57 \times 10^5$  Btu/ft<sup>2</sup>-hr, was found to agree very well with the relation given by Bonilla et al. (13) (21). This relationship is

$$\left[ \frac{d(\log \Delta T_1)}{d(\log P)} \right]_{\bar{q}} = \text{const.} = -\frac{1}{4}$$

The same relationship was found to hold for all Methanol mixtures as can be seen from Figures 32 which show the data of Figure 16 plotted on a log-log graph. This relationship did not hold for the n-Butanol and for the MEK mixtures.

It can be seen from Figure 32 that the straight line representing the water and the different Methanol mixtures are parallel. They have a slope of

$$\left[ \frac{d(\log \Delta T_1)}{d(\log P)} \right]_{\bar{q}} = \text{const.} = -0.22$$

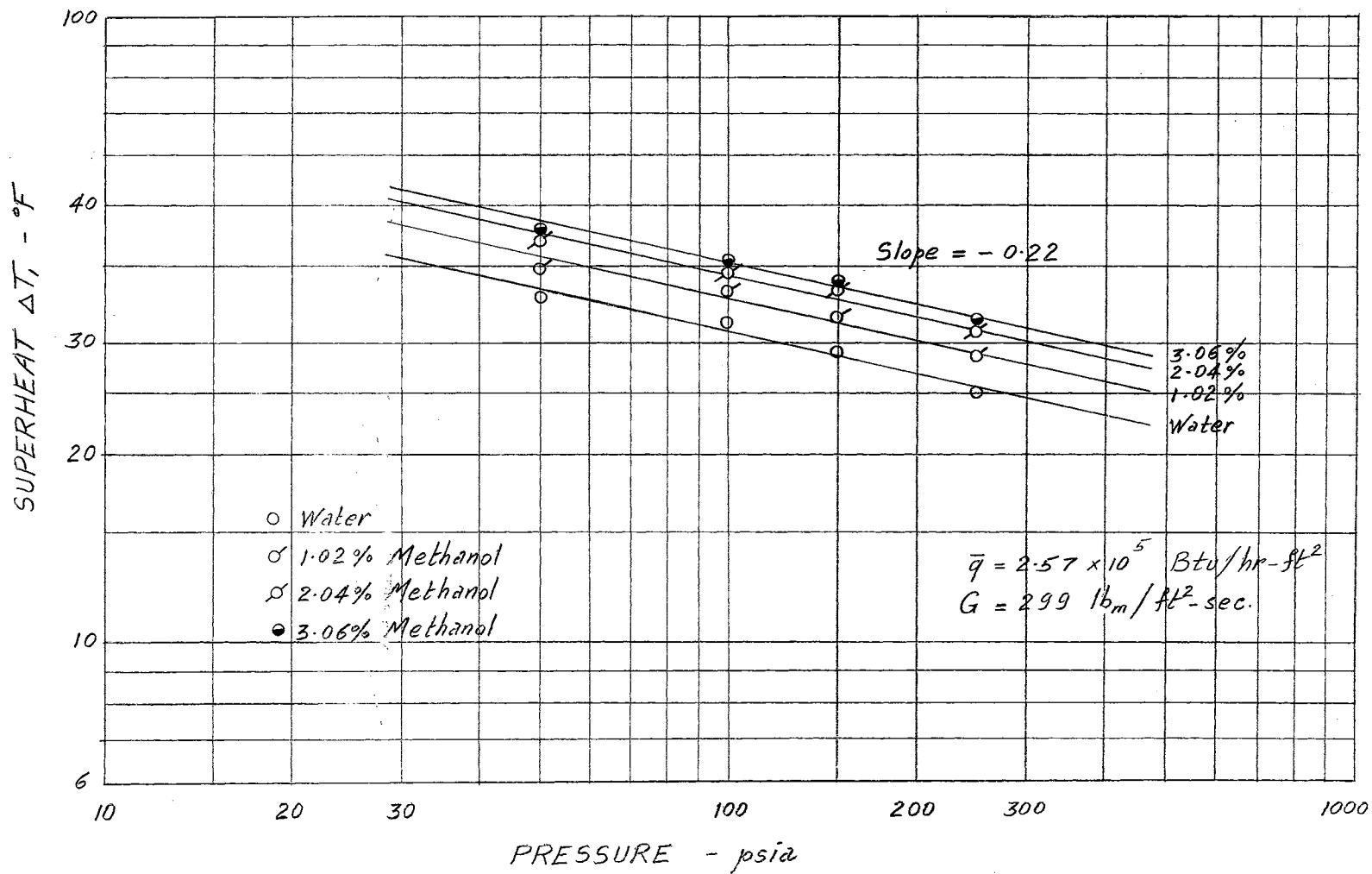


Figure 32. Pressure-Superheat Relationship for Water and Methanol Mixtures

For the MEK mixtures and for 1% and 3% n-Butanol mixtures, the superheat  $\Delta T_1$  increased first as the pressure was increased to about 100 psia, and then decreased for higher pressures. Figure 20 shows that the superheat in the case of the MEK mixtures increased as the concentration of the additive increased to about 2% by weight, and then decreased for the 3% by weight MEK mixture at the same heat flux.

This behavior of the MEK and n-Butanol mixtures at low pressures suggests that the interplay of bubble dynamics, bubble growth, and fluid-heating-surface combination for these mixtures is more complicated than for pure fluids, but none-the-less extremely interesting to study further by high speed photography.

#### Correlation of Data in the Fully Developed Nucleate Boiling Region

Correlation of the experimental data of this investigation in the fully developed nucleate boiling regions of water, the Methanol mixtures, and the n-Butanol mixtures were shown in Figures 28 and 29. The slope of the Forster-Greif line  $a a$  for the water data of this investigation and of Gunther and Kreith (30) at 1 atmosphere was found to agree very well with the value given by Forster and Greif, namely

$$n = \frac{1}{5}$$

The slope of the line  $a a$  in Figures 28 and 29, which is equal to the exponent  $n$  in Forster and Grief equation  $Nu \cdot Pr^{1/3} = C Re^n$  was found to be equal to 0.19. This value of the exponent  $n$  was found to agree also with the slopes of the lines representing the Forster-Greif correlation for the different mixtures of Methanol and n-Butanol.

The values of the constant  $C$  in the Forster-Greif equation, which

are equal to the intercepts of the lines in Figures 28 and 29 with the ordinate axis ( $\log Re = 0$  or  $Re = 1.0$ ), were measured from these two Figures and tabulated in Table IV for water and for the different n-Butanol and Methanol mixtures.

TABLE IV

Experimentally Determined Values of the Constant C in Forster-Greif Correlation for Water, Methanol, and n-Butanol Mixtures

Fluid	$C \times 10^3$
Water	6.0
1.02% Methanol	3.3
2.04% Methanol	2.5
3.06% Methanol	2.1
1.00% n-Butanol	3.5
2.07% n-Butanol	1.5
2.12% n-Butanol	0.9

#### The Relation Between the Heat Flux and the Superheat in the Transition Region

The transition region of the nucleate boiling is the portion of the heat transfer curve where the nucleate boiling mechanism starts, and where the convection heat transfer mechanism (eddy diffusion) is still operative to a greater or lesser extent.

In subcooled nucleate boiling, the heat flux  $\bar{q}$  is generally reported by different investigators to depend on the superheat  $\Delta T_1$  raised to a power between 2 and 4, i.e.

$$\bar{q} \propto \Delta T_1^m \quad (2 < m < 4)$$

Bonilla (39) reported that in forced convection boiling and for moderately high velocities "non-boiling heat transfer passes directly into saturated boiling without the appearance of local boiling," and this phenomena "can occur at low pressures, but has not been observed at high pressures."

The heat flux  $\bar{q}$  in saturated forced convection boiling is generally reported to depend on  $\Delta T_1^3$  if the velocity is low and on  $\Delta T_1^{1.0}$  if the velocity is high. This is to say that at high convective velocities in saturated boiling, the eddy diffusion mechanism of heat transfer will prevail and Colburn equation could be uses as a relationship between the heat flux  $\bar{q}$  and the superheat  $\Delta T_1$ . The Colburn line c - c and the heat transfer line of water at 50 psia shown in Figure 12 are for a mass velocity of 299 lb<sub>m</sub>/ft<sup>2</sup>-sec. (V = 5.2 ft/sec.). At higher velocities, it is expected that the Colburn line and the heat transfer line at low and moderate values of the heat flux may coincide. Therefore at low pressures and at higher flow velocities than were used in this investigation, it is expected that  $\bar{q}$  may be proportional to  $\Delta T_1$  indicating that saturated boiling rather than local boiling will take place. The Colburn equation could be applied also at moderate velocities and small values of the superheat  $\Delta T_1$  i.e. at the beginning of the transition region.

Near the end of the transition region, the heat flux  $\bar{q}$  varies strongly with the superheat  $\Delta T_1$  as can be seen in Figure 33, and in some cases the superheat actually decreased when the heat flux was increased. This over shooting of the heat transfer curve at the last part of the transition region has been observed with some data of other investigators.



Figure 34 is a reproduction of the nucleate pool boiling data of Haselden and Peters (32) for liquid nitrogen and oxygen. The dotted lines in Figure 34 which were fared between the experimental points were given by Haselden and Peters to represent the heat transfer line for boiling  $N_2$  and  $O_2$  on the outside of different size tubes. The experimental data of Haselden and Peters shown in Figure 34 are for Nitrogen boiling on 5/8 inch O. D. horizontal tube, and for Oxygen boiling on 1/2 inch O. D. horizontal tube. In joining these experimental points by a solid line as shown in Figure 34, this author ignored the two points on either side of the  $N_2$  line.

#### Effect of Flow Velocity on the Superheat

Figures 25 through 27 shows the effect of the fluid flow velocity (mass velocity) on the superheat for water and for the different mixtures studied in this investigation. For each mixture and for water all points except the point representing the data at  $299 \text{ lb}_m/\text{ft}^2\text{-sec.}$  were taken consecutively and therefore were relied upon to draw the curves in Figures 25 through 27. The point representing the data at  $299 \text{ lb}_m/\text{ft}^2\text{-sec.}$  for each mixture and for water was read about seven or eight hours before the other four points and was ignored in Figures 25 through 27.

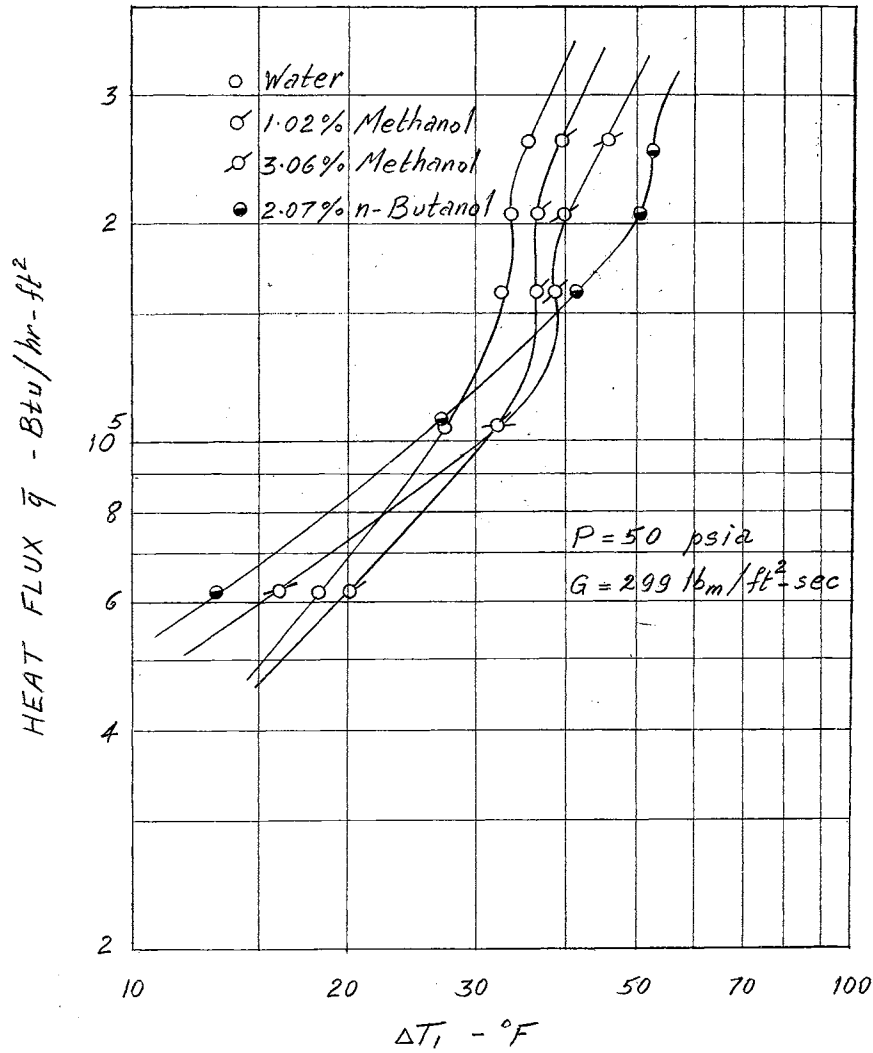


Figure 33. The Transition Region for Water and Some Mixtures

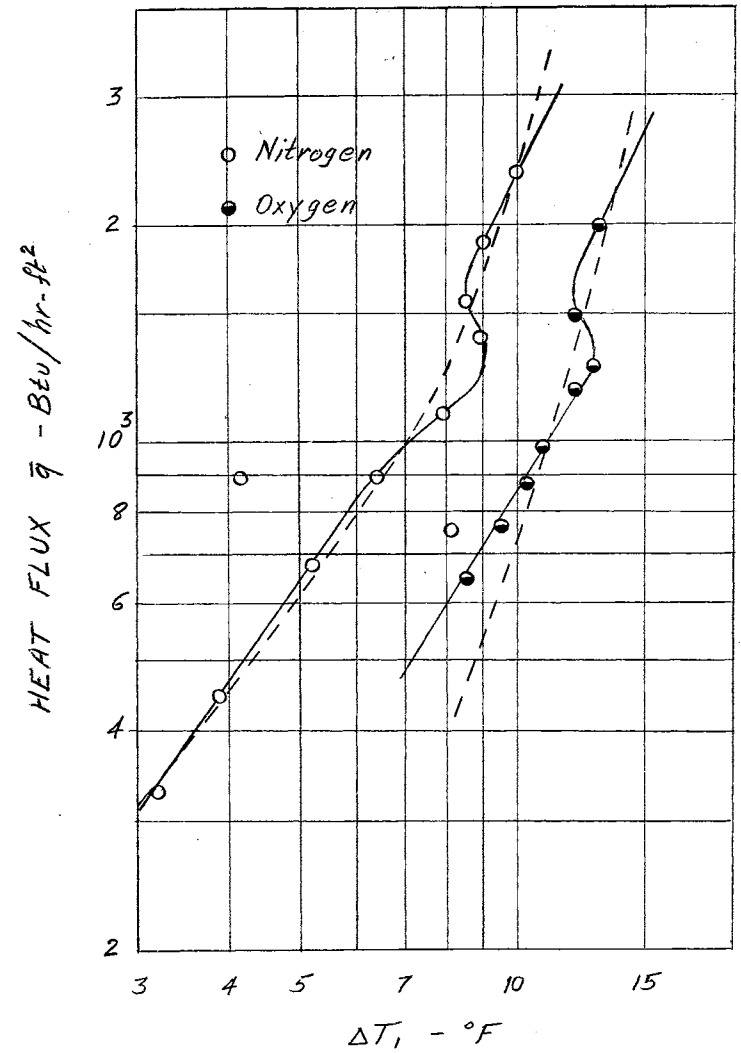


Figure 34. Haselden and Peters Data For  $N_2$  and  $O_2$

## CHAPTER VII

### ANALYSIS OF EXPERIMENTAL ERRORS

The experimental errors and losses which affect the accuracy of the experimental measurements of this investigation can be categorized as follows:

1. Errors in temperature measurements.
2. Errors in the power measurements.
3. Errors in reading the system pressure.
4. Errors due to heat losses.
5. Errors in the flow measurement.

The measurement of the outside wall temperature of the test section was estimated to be within  $\pm 1.50$  °F. The uncertainties in measuring this temperature comprise the following:

Error in the wire calibration	$\pm 0.25$ °F
Error from applying corrections in Figure (C-1) (Estimated)	$\pm 0.50$ °F
Error due to calculating the inside wall temperature	
From Kreith-Summerfield equation (A-6)	$\pm 0.50$ °F
Error due to fluctuation of wall temperature	$\pm 0.25$ °F
	<hr/>
	$\pm 1.50$ °F

All temperature measurements were read twice and the variation in these readings was within 1.0% of the highest value of the superheat.

The wattmeter used to measure the electrical power input to the test section allowed power measurements of an accuracy within a maximum error

of  $\pm 1.3\%$  at low power and an error of  $\pm 0.5\%$  at the higher levels of the power input.

Within the range of the system pressures used in this investigation, the system pressure measurements were believed to be read accurate to within  $\pm$  psi.

The smallest division of the system pressure gage was 1 psia and the calibration curve furnished by the manufacturer indicated zero correction for the range of pressures used in this investigation.

The heat losses from the test section to the surroundings, through the test-section insulation in the non-boiling region, were calculated and found very small and negligible. No heat loss to the surroundings occurred in the boiling region because of the addition of the thermal guard. Heat conduction in the test-section wall along its axis, was almost nil, and so were the heat losses from the electrical lugs.

The accuracy of the flow measurements, as estimated from the orifice calibration and from the readability of the flow manometer, was believed to be within a maximum error of  $\pm 2\%$  for the flow rate at which most of the experimental runs were conducted.

## CHAPTER VIII

### CONCLUSIONS AND RECOMMENDATIONS

From the analysis of the experimental data of this investigation it was concluded that

1. Whereas the superheat  $\Delta T_1$  for water remained virtually constant throughout the boiling length of the tube, the value of the superheat for water when it contained a volatile additive reached a maximum near the start of local boiling and then decreased steadily as the flow progressed downstream.
2. Generally, the additives studied in this investigation and at very low values of the heat flux, the superheat  $\Delta T_1$  near the start of local boiling decreased in comparison with that of pure water as the concentration of the additive in water was increased. At higher values of the heat flux, the superheat first increased to a maximum at a constant heat flux and then decreased as the concentration increased. This maximum value of  $\Delta T_1$  (at  $\bar{q} = \text{constant}$ ) was noticed to occur at higher values of the concentration as the heat flux level increased.
3. The relationship between the superheat  $\Delta T_1$  and the system pressure  $P$  for the experimental data of water and water-Methanol mixtures of this investigation agreed very well with the relation

$$\left[ \frac{d (\log \Delta T_1)}{d (\log P)} \right]_{\bar{q} = \text{const.}} = -\frac{1}{4}$$

For the water-MEK mixtures, and for the water-Butanol mixtures, the superheat  $\Delta T_1$  at constant  $\bar{q}$  was found to increase with the pressure, to reach a maximum at about 100 psia, and then to decrease.

The Forster-Greif correlation equation  $Nu \cdot Pr^{-1/3} = C Re^{1/5}$  correlated satisfactorily the experimental data of this investigation for the water, the water-methanol mixtures, and the water-Butanol mixtures in the fully developed nucleate boiling region.

From the analysis of the heat transfer curves in the transition region between the convective heat transfer and the nucleate boiling regions, it was concluded that there are two portions of this transition region which were found to have different characteristics. In the first portion, the heat flux  $\bar{q}$  had low values, was proportional to the superheat  $\Delta T_1$ , and followed a moderate exponential increase as the superheat increased. The second portion of the transition region occurred just before the fully developed nucleate boiling region. In this second portion the heat flux  $\bar{q}$  varied strongly with the superheat  $\Delta T_1$ , and in some cases, the heat flux actually increased when the superheat decreased.

As a result of this investigation, the following recommendations are made:

1. A photographic study of the bubble growth, and study of the parameters affecting the bubble population and the average maximum radius of the bubbles  $R_{max}$  for the MEK and the n-Butanol additives, should help explain their behavior in nucleate boiling.
2. A photographic study of the bubble population just before the start of the fully developed nucleate boiling region for water at small

and moderate pressures should help clarify the immediate relationship between the bubble growth and the characteristics of the heating-surface-fluid combinations.

3. An extension of the present study in the higher flux density region would be valuable especially near the burnout. If the apparatus used in this investigation is used for such a study, provisions must be made to increase the power to the test section.

## BIBLIOGRAPHY

1. Clark, J. A., W. M. Rohsenow, "Local Boiling Heat Transfer to Water at Low Re and High Pressures," ASME, Vol. 76, pp. 553, (1954).
2. Mumm, J. F., "Heat Transfer to Boiling Water Forced Through a Uniformly Heated Tube," ANL-5276, (November, 1954).
3. Jens, W. H., P. A. Lottes, "Analysis of Heat Transfer, Burnout, Pressure Drop, and Density Data for High-Pressure Water," ANL-4627, (May, 1951).
4. Rohsenow, W. M., J. A. Clark, "Heat Transfer and Pressure Drop Data for High Heat Flux Densities to Water at High Sub-Critical Pressures," 1951 Heat Transfer and Fluid Mechanics Institute, Stanford University, (June, 1951).
5. Kreith, F., M. Summerfield, "Heat Transfer to Water at High Flux Densities With and Without Surface Boiling," Transactions of ASME, Vol. 71, pp. 805-815.
6. Monroe, A. G., H. A. S. Bristow, J. E. Newell, "Heat Transfer to Boiling Liquids at Low Temperatures and Elevated Pressures," J. Applied Chem., Vol. 2, pp. 613-624, (November, 1952).
7. Forster, H. K., N. Zuber, "Growth of a Vapor Bubble in a Superheated Liquid," J. Applied Physics, Vol. 25, p. 474, (1954).
8. Wellman, E. J., "A Survey of the Thermodynamic and Physical Properties of Water," M. S. Thesis, Purdue University, (1950).
9. Rohsenow, W. M., "A Method of Correlating Heat Transfer Data for Surface Boiling of Liquids," Transactions of ASME, Vol. 74, pp. 969-976, (1952).
10. Forster, K., R. Greif, "Heat Transfer to a Boiling Liquid-Mechanism and Correlations," Transactions of ASME, J. Heat Transfer, Vol. 81, p. 43, (1959).
11. Van Wijk, W. R., A. S. Vos, S. J. D. Van Stralen, "Heat Transfer to Boiling Binary Liquid Mixtures," Chem. Engr. Science, Vol. 5, pp. 68-80, (April, 1956).
12. Vos, A. S., "Heat Transfer to Boiling Binary Liquid Mixtures," Ingenieur, Vol. 68, No. 17, C9-13, (1956).



13. Bonilla, C. F., C. H. Perry, "Heat Transmission to Boiling Binary Liquid Mixtures," Trans., Am. Inst. Chem. Engrs., Vol. 37, pp. 685-705, (1941).
14. Leppert, G., C. P. Costello, B. M. Hogland, "Boiling Heat Transfer to Water Containing a Volatile Additive," Transactions of ASME, p. 1395, (October, 1958).
15. Leppert, G., "Two-Phase Pressure Drop," unpublished Ph. D. dissertation, Illinois Institute of Technology, (1953).
16. Reynolds, J. B., "Local Boiling Pressure Drop," ANL-5178, (March, 1954).
17. Tanger, G. E., "Local Boiling Pressure Drop for Forced Convection of Water," unpublished Ph. D. thesis, Oklahoma State University, (1959).
18. McAdams, W. H., Heat Transmission, Third edition, McGraw-Hill Company, Inc., New York, 1954.
19. Ellison, M. E., "A Study of the Mechanism of Boiling Heat Transfer," Memo No. 20-88, Jet Propulsion Laboratory, California Institute of Technology, p. 72, (March, 1954).
20. Dergarabedian, P., "The Rate of Growth of Vapor Bubbles in Superheated Water," J. Applied Mechanics, Vol. 20, Transactions of ASME, Vol. 75, pp. 537-545, (1953).
21. Bonilla, C. F., Y. S. Bush, A. Stalder, N. S. Shaikhmahmud, A. Ramachandran, "Pool-Boiling Heat Transfer with Mercury," Reactor Heat Transfer Conference, New York, (November, 1956); also Report NYO-7638.
22. Griffith, P., "Bubble Growth Rates in Boiling," Transactions of ASME, Vol. 80, pp. 721-727, (1958).
23. Plesset, M. S., S. A. Zwick, "The Growth of Vapor Bubbles in Superheated Liquids," J. Applied Physics, Vol. 25, pp. 493-500, (1954).
24. Forster, H. K., N. Zuber, "Dynamics of Vapor Bubbles and Boiling Heat Transfer," A. I. Ch. E. Journal, Vol. 1, p. 531, (1955).
25. Siegel, R., C. Usiskin, "A Photographic Study of Boiling in the Absence of Gravity," J. Heat Transfer, Transactions of ASME, p. 230, (August, 1959).
26. Gunther, F. C., F. Kreith, "Photographic Study of Bubble Formation in Heat Transfer to Subcooled Water," Progress Report No. 4-120, Jet Propulsion Lab., California Institute of Technology, (March, 1950).

27. Cichelli, M. T., C. F. Bonilla, "Heat Transfer to Liquids Boiling Under Pressure," Trans. A.I.Ch.E., Vol. 41, pp. 755-787, (1945).
28. Piret, E. L., H. S. Isbin, "Natural-Circulation Evaporation," Chemical Engineering Progress, Vol. 50, pp. 305-311, (1954).
29. Addams, J. N., "Heat Transfer at High Rates to Water Boiling Outside Cylinders," D. Sc. Thesis, Chemical Engineering Department, Massachusetts Institute of Technology, (1948).
30. Gunther, F. C., F. Kreith, "Photographic Study of Bubble Formation in Heat Transfer to Subcooled Water," Heat Transfer and Fluid Mechanics Institute, Berkeley, Calif., published by The ASME, New York, N. Y., May, 1949, pp. 113-126.
31. Kreith, F., M. Summerfield, "Pressure Drop and Convection Heat Transfer with Surface Boiling at High Heat Flux; Data for Aniline, n-Butanol Alcohol," Transactions of ASME, Vol. 72, p. 869, (1950).
32. Haselden, G. G., J. I. Peters, "Heat Transfer to Boiling Liquid Oxygen and Liquid Nitrogen," Trans. Instn. Chem. Engrs., London, Vol. 27, p. 201, (1949).
33. Von Glahn, U. H., J. P. Lewis, "Nucleate and Film Boiling Studies With Liquid Hydrogen," Proc. Cryogenic Engr. Conf., K. D. Timmerhaus, ed., Univ. of Colorado, Boulder, (1959).
34. Levy, S., "Generalized Correlation of Boiling Heat Transfer," J. Heat Transfer, Transactions of ASME, pp. 37-42, (February, 1959).
35. Jakob, M., Heat Transfer, Vol. I, John Wiley & Sons, Inc., New York, 1953.
36. Keenan, J. H., F. G. Keyes, Thermodynamic Properties of Steam, John Wiley & Sons, Inc., New York, 1954.
37. Gunther, F. C., "Photographic Study of Surface Boiling Heat Transfer with Forced Convection," Transactions of ASME, Vol. 73, pp. 115-123, (1951).
38. Forster, H. K., "On the Conduction of Heat Into A Growing Vapor Bubble," J. Applied Physics, Vol. 25, pp. 1067, (1954).
39. Bonilla, C. F., Nuclear Engineering, McGraw Hill Co., Inc., p. 416, New York, 1957.
40. Reid, R. C., and T. K. Sherwood, The Properties of Gases and Liquids; Their Estimation and Correlation, McGraw Hill Co., New York, N. Y., (1958).
41. Methyl Ethyl ketone, Shell Chemical Corp., New York.

42. Handbook of Chemistry and Physics, 40th Ed., Chemical Rubber Publishing Co., Cleveland, Ohio, 1958-1959.
43. June, R. R., "Pressure Drop During Forced Convection Local Boiling of Water Containing an Organic Additive," unpublished Ph. D. thesis, Oklahoma State University, (1961).
44. Metals Handbook, 1948 Edition, The American Society for Metals, Cleveland, Ohio, p. 314.
45. Engineering Materials Handbook, 1st Ed., McGraw-Hill Co., New York, N. Y., (1956).
46. Robinson, C. S., and E. R. Gilliland, The Elements of Fractional Distillation, 4th Ed., McGraw-Hill Co., New York, N. Y., (1950).

**A P P E N D I C E S**

## APPENDIX A

### INSIDE WALL TEMPERATURE

The differential equation describing the temperature distribution inside the wall of an electrically heated tube follows and the solution of this differential equation, which was given by Kreith and Summerfield (5), is presented, together with a simplified solution, which was found to be very helpful in rough calculations.

#### 1. Derivation of the heat equation:

In the derivation of the heat conduction equation for the electrically heated tube, it was assumed that there was no temperature gradient along the length of the tube; that is, any heat conduction along the axis of the tube was neglected. It was also assumed that there was no change of temperature circumferentially. Therefore, the thermal conductivity and the electrical resistivity of the isotropic material of the tube are functions only of the radius  $r$ .

Consider an element of the tube at radius  $r$ , thickness  $dr$  and unit length, Figure (A-1).

The energy balance equation for this tube element is:

$$(-q_{in}) + q_g = (-q_{out}) \quad (A-1)$$

where  $q_g$  is the time rate of heat generation within the element.

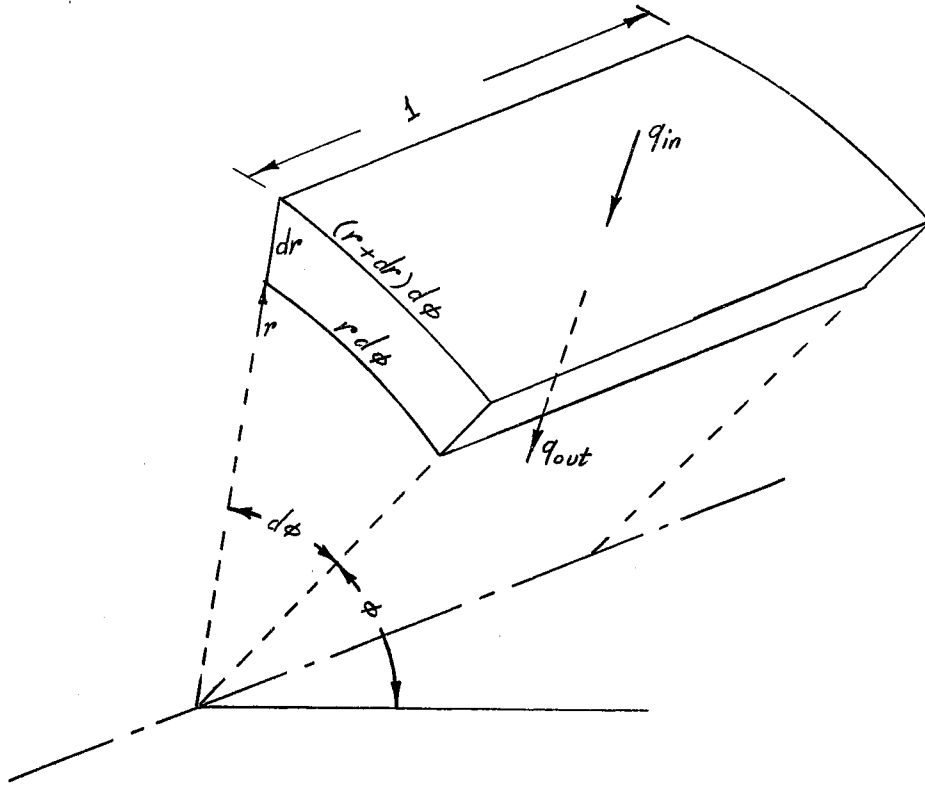


Figure A-1. Segment of Heated Tube

Let  $\dot{q}$  be the rate of energy dissipated electrically in the tube material per unit volume; therefore

$$\dot{q} = \frac{E^2}{J\rho}$$

and

$$q_g = \frac{E^2}{J\rho} r d\phi dr$$

where  $E$  = voltage drop per unit length of the tube (Volts/ft)  
 $\rho$  = volume resistivity of the tube wall material ( $\Omega/\text{ft}^3$ )

The volume resistivity in ( $\Omega/\text{ft}^3$ ) is equal numerically to the resistivity in ( $\Omega\text{-ft}$ ).

The time rate of heat inflow to the element is

$$q_{in} = -k \frac{dT}{dr} (r + dr) d\phi$$

$$= -k \frac{dT}{dr} r d\phi - k \frac{dT}{dr} dr d\phi$$

and the time rate of heat outflow from the element is

$$\begin{aligned} q_{out} &= -\left[k - \frac{dk}{dr} dr\right] \cdot \frac{d}{dr} \left[T - \frac{dT}{dr} dr\right] r d\phi \\ &= -k \frac{dT}{dr} r d\phi + k \frac{d^2 T}{dr^2} r dr d\phi + \frac{dk}{dr} \frac{dT}{dr} r dr d\phi \end{aligned}$$

Substituting these relations in the energy balance equation

(A-1) and dividing each term by  $rkdrd\phi$  gives

$$\frac{d^2 T}{dr^2} + \left[\frac{1}{r} + \frac{\beta k_1}{k} \frac{dT}{dr}\right] \frac{dT}{dr} + \frac{E^2}{Jk\rho} = 0 \quad (A-2)$$

where  $k = k_1(1 + \beta \theta)$ . [see Appendix (E)]

$$\text{and } \frac{dk}{dr} = \beta k_1$$

## 2. Solution of the heat equation:

The solution of the differential equation (A-2) is given for the case of an adiabatic outer wall of the tube;

$$\text{Let } \xi = r_0 - r, \quad \text{therefore } \frac{d\xi}{dr} = -1$$

$$\therefore \frac{dT}{dr} = -\frac{dT}{d\xi} \quad \text{and} \quad \frac{d^2 T}{dr^2} = \frac{d^2 T}{d\xi^2}$$

$$\therefore \Delta \xi = \Delta x$$

$$\text{where } \Delta x = r_0 - r$$

On changing the variables in equation (A-2), this equation becomes

$$\frac{d^2 T}{d\xi^2} - \left[\frac{1}{r_0 - \xi} - \frac{\beta k_1}{k} \frac{dT}{d\xi}\right] \frac{dT}{d\xi} + \frac{E^2}{Jk\rho} = 0 \quad (A-3)$$

The Taylor's series expansion of the temperature  $T$  at radius  $r$  about  $r = r_0$  or  $\xi = 0$  is

$$T = T_0 + T_0' \frac{\overline{\Delta x}}{1!} + T_0'' \frac{\overline{\Delta x}^2}{2!} + T_0''' \frac{\overline{\Delta x}^3}{3!} + T_0^{iv} \frac{\overline{\Delta x}^4}{4!} + \dots \quad (A-4)$$

where  $T' = \frac{dT}{d\xi}$

For the adiabatic outer wall, the boundary conditions are

$$T = T_0$$

$$\frac{dT}{dr} = \frac{dT}{d\xi} = T' = 0$$

Equation (A-3) could be rearranged in the form

$$T'' = \frac{T'}{r_0 - \xi} - \frac{\beta k_1}{k} T'^2 - \frac{E^2}{Jk\rho} \quad (A-5)$$

and  $T_0'' = -m$

where  $m = \frac{E^2}{J k_0 \rho_0}$

On differentiating equation (A-5) and substituting the boundary condition  $T'_0 = 0$ , the third and fourth derivatives become

$$T_0''' = -\frac{m}{r_0}$$

$$\text{and } T_0^{iv} = -m \left\{ \frac{3}{r_0^2} + \frac{m}{12} \left[ \frac{\alpha + 3\beta + 4\alpha\beta\theta}{(1+\alpha\theta)(1+\beta\theta)} \right] \right\}$$

Substituting in equation (A-4) and rearranging, the temperature  $T$  at radius  $r$  becomes

$$T = T_0 - \frac{m}{2} \left\{ \frac{\overline{\Delta x}^2}{r_0^2} + \frac{\overline{\Delta x}^3}{3r_0} + \left[ \frac{1}{4r_0^2} + \frac{m(\alpha + 3\beta + 4\alpha\beta\theta)}{12(1+\alpha\theta)(1+\beta\theta)} \right] \frac{\overline{\Delta x}^4}{r_0} + \dots \right\} \quad (A-6a)$$



At the inside wall and for the test section used in this investigation, this equation becomes

$$\Delta T_w = 10^{-6} M_0 \left\{ 33.91 + \left[ \frac{2.2515 + 1.1507 \times 10^{-4} \theta}{(1 + 5.16 \times 10^{-4} \theta)(1 + 3.373 \times 10^{-4} \theta)} \right] \right\} \times 10^{-6} M_0 \quad (A-6)$$

$$\text{where } M_0 = \frac{E^2}{K_0 \rho_0}$$

### 3. Simplified solution:

Assuming both the electrical resistivity and the thermal conductivity of the test section wall to be constant, equation (A-2) reduces to:

$$\frac{d^2 T}{dr^2} + \frac{1}{r} \frac{dT}{dr} + \frac{E^2}{Jk\rho} = 0$$

with a solution of

$$T = T_0 - \frac{m}{2} \left[ r_0^2 \ln(r_0/r) - \frac{r_0^2 - r_i^2}{2} \right]$$

$$\text{or } \Delta T_w = \frac{m}{2} \left[ r_0^2 \ln(r_0/r_i) - \frac{r_0^2 - r_i^2}{2} \right] \quad (A-7)$$

and for the system used in this investigation

$$\Delta T_w = 33.97 \times 10^{-6} M_0 \quad (A-8)$$

It was found that the mean electrical resistivity of the test section wall

$$\rho_m = (r_0^2 - r_w^2) / \int \frac{dr}{\rho_r}$$

is very nearly equal to the resistivity evaluated at the outside wall temperature  $\rho_0$ . By using this value of the resistivity, together with the thermal conductivity evaluated at the mean wall temperature

$$T_m = T_0 - \frac{\Delta T_w}{2}$$

almost identical results to the Kreith and Summerfield solution are found.

Table (A-I) shows the values of the temperature drop across the wall of

the test section at different levels of the voltage drop  $E$ , as calculated from equation (A-7) and from the Kreith and Summerfield solution.

TABLE (A-1)  
COMPARISON OF HEAT CONDUCTION EQUATION SOLUTIONS

# Run	$T_o$ °F	Current Amps	$E$ Volt/ft	$\Delta T_w$ (°F)	
				K. S. Equation	Simplified Equation
5-Water	371.1	1185	6.58	53.9	53.9
4-Water	358.4	1069	5.92	43.7	43.7
3-Water	347.0	937.5	5.15	33.4	33.4
2-Water	331.1	769	4.19	22.4	22.4
1-Water	313.1	593	3.2	13.2	13.2

This Equation (A-7) is recommended for rough calculations for thick-walled tubes and as a substitute for Kreith and Summerfield equation for thin-walled tubes.

## APPENDIX B

### PROPERTIES OF THE MIXTURES AND THE PURE COMPONENTS

In order to correlate and analyze the experimental data, it was necessary to determine the physical and transport properties of the mixtures used. The liquid properties needed were the density, the thermal conductivity, the specific heat, the viscosity, and the surface tension. The first and second derivatives of the vapor-pressure curves of the water and the mixtures, were also needed for the Forster-Greif correlation. In addition, the thermodynamic equilibria of the mixtures were calculated in order to determine the boiling points of the different mixtures at the system pressures used. The surface tension and the viscosity of the specific mixtures were measured experimentally at one temperature and then estimated at other temperatures.

The density, the thermal conductivity and the specific heat of saturated water are shown in Figures (B-1), (B-2), (B-3). The values of these properties for the water were also used for all the mixtures. The changes in these three properties of water due to the presence of small additives used in this investigation were calculated and found negligible and within the range of experimental uncertainties of determining these properties for water.

The vapor-pressure curves of the pure components used are shown in Figure (B-4). Table (B-1) lists the critical constants of the pure components.

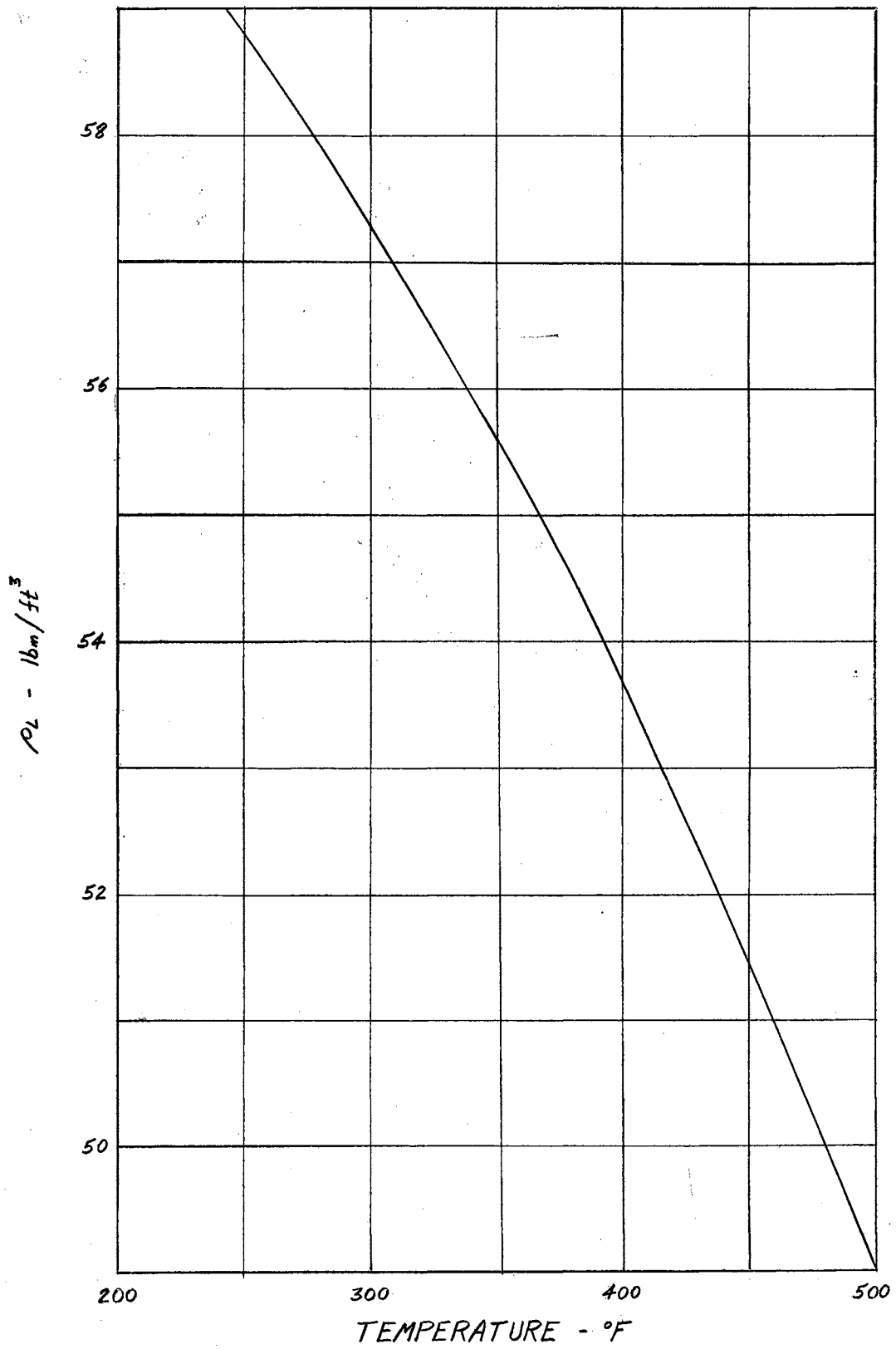


Figure (B-1). Density of Water

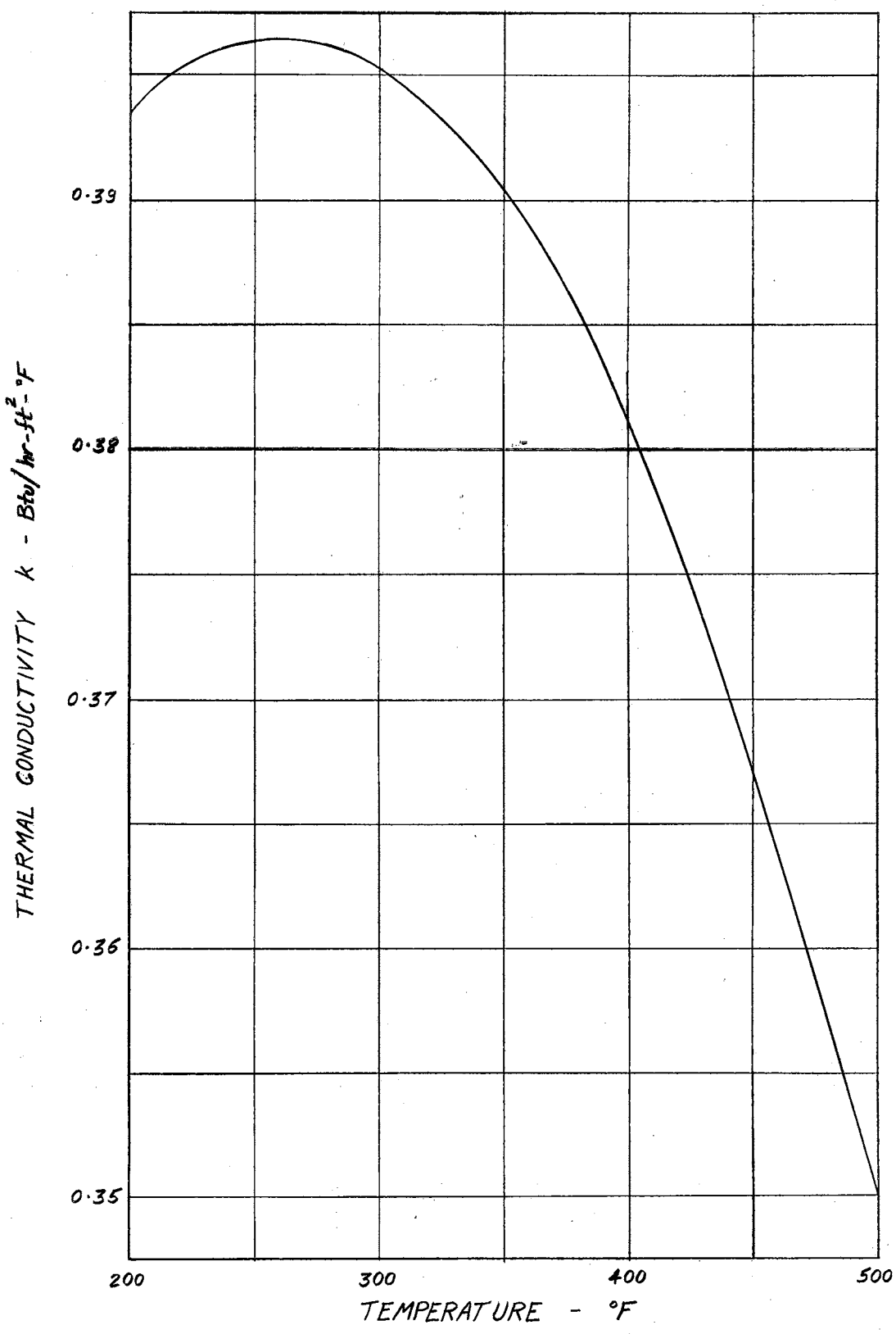


Figure (8-2). Thermal Conductivity of Water

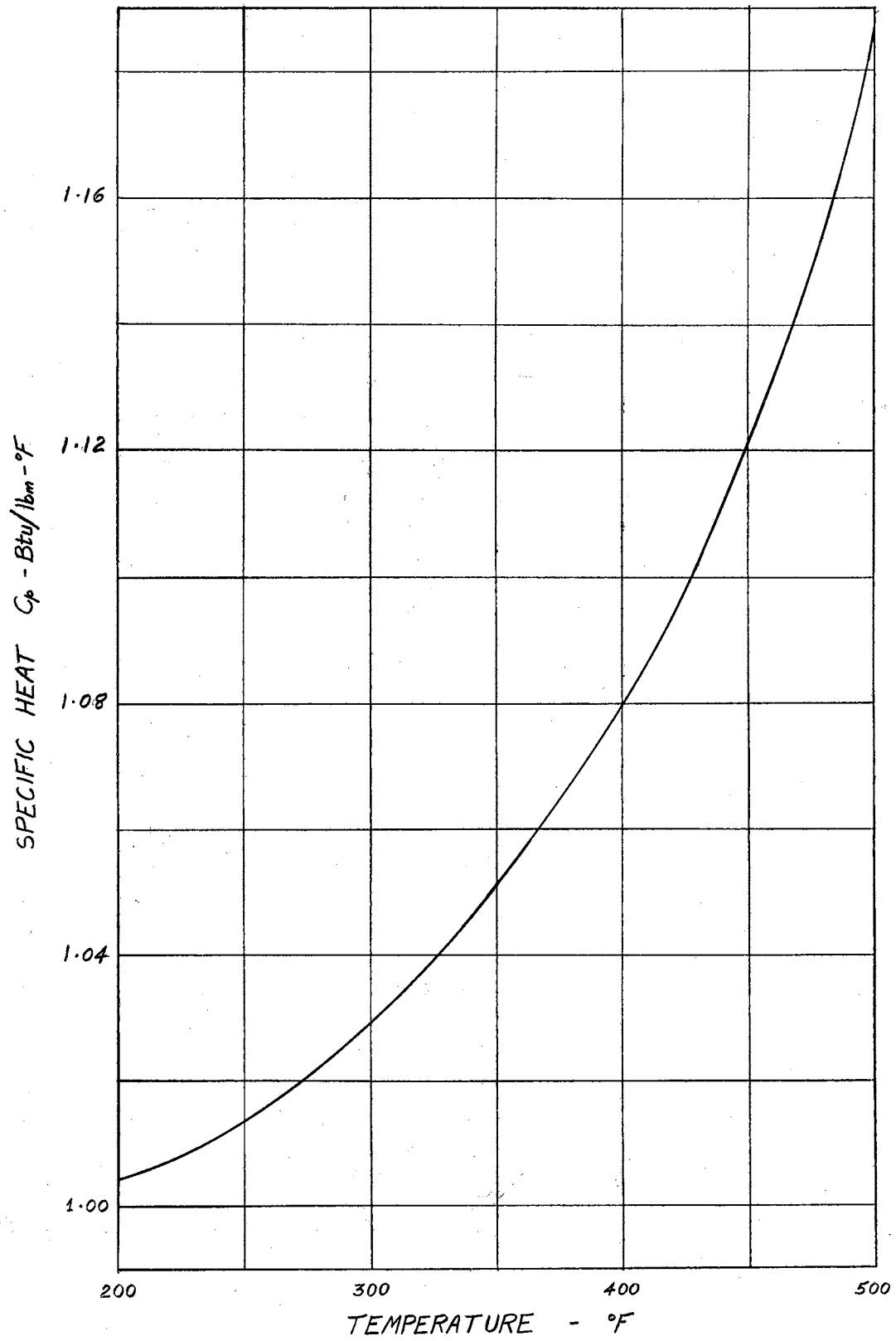


Figure (B-3). Specific Heat of Water

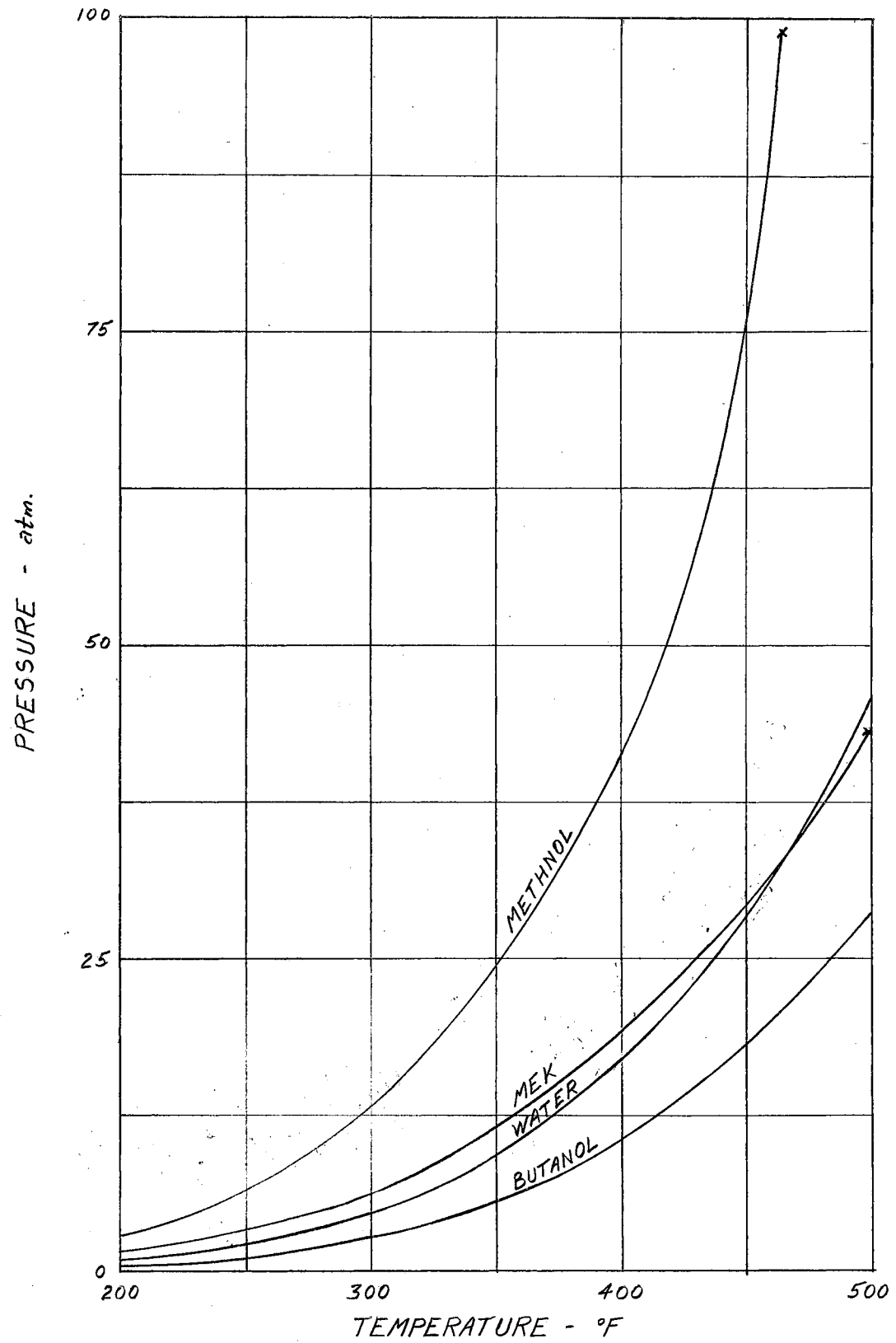


Figure B-4). Vapor Pressure of Pure Components

TABLE (B-I)  
CRITICAL CONSTANTS OF PURE COMPONENTS

	M	T <sub>c</sub> °F	P <sub>c</sub> atm.	lb <sub>m</sub> /ft <sup>3</sup>
H <sub>2</sub> O	18.02	705.4	218	19.9
Methanol	32.04	464	98.7	17.0
MEK	72.10	499.5	43.3	---
n-Butanol	74.08	548	48.4	---

Property values were taken from References (36), (40), (41), (42), (8).

#### Viscosity

In Figure (B-5), the fluidity  $\frac{1}{\mu}$  of the pure components is plotted as a function of the temperature.

The kinematic viscosity of the mixtures was measured experimentally at 140°F using an Ostwald viscosimeter with a capillary diameter of 0.4 mm. The viscosimeter was calibrated with distilled water, and the dynamic viscosity  $\mu$  was then calculated knowing the density  $\rho_L$  at 140°F. Table (B-II) lists the experimental values of the viscosity of the mixtures at 140°F.

To estimate the viscosity of the mixtures at other temperatures, use was made of the linear relation between the fluidity  $\frac{1}{\mu}$  and the temperature above 200°F as can be seen from Figure (B-5). The following equation was used to estimate the viscosity of the mixtures at a



TABLE (B-II)  
Experimentally Determined Mixture Properties

	Viscosity $\text{lb}_m/\text{hr.ft}^2$ at $140^\circ\text{F}$	$a^*$	Surface Tension ( $\text{lb}_f/\text{ft}$ ) at $810^\circ\text{F}$	$b^*$
Water	1.137	--	$4.91 \times 10^{-3}$	--
1.02% Methanol	1.165	0.021	$4.19 \times 10^{-3}$	0.853
2.04% Methanol	1.175	0.028	$4.09 \times 10^{-3}$	0.833
3.06% Methanol	1.205	0.050	$4.01 \times 10^{-3}$	0.816
1.00% MEK	1.162	0.019	$3.78 \times 10^{-3}$	0.770
2.03% MEK	1.180	0.033	$3.59 \times 10^{-3}$	0.730
3.00% MEK	1.203	0.048	$3.46 \times 10^{-3}$	0.704
1.00% MEK	1.165	0.021	$3.78 \times 10^{-3}$	0.768
2.07% Butanol	1.185	0.035	$3.23 \times 10^{-3}$	0.658
3.12% Butanol	1.223	0.062	$2.85 \times 10^{-3}$	0.580

\*See Equations (B-1) and (B-2)

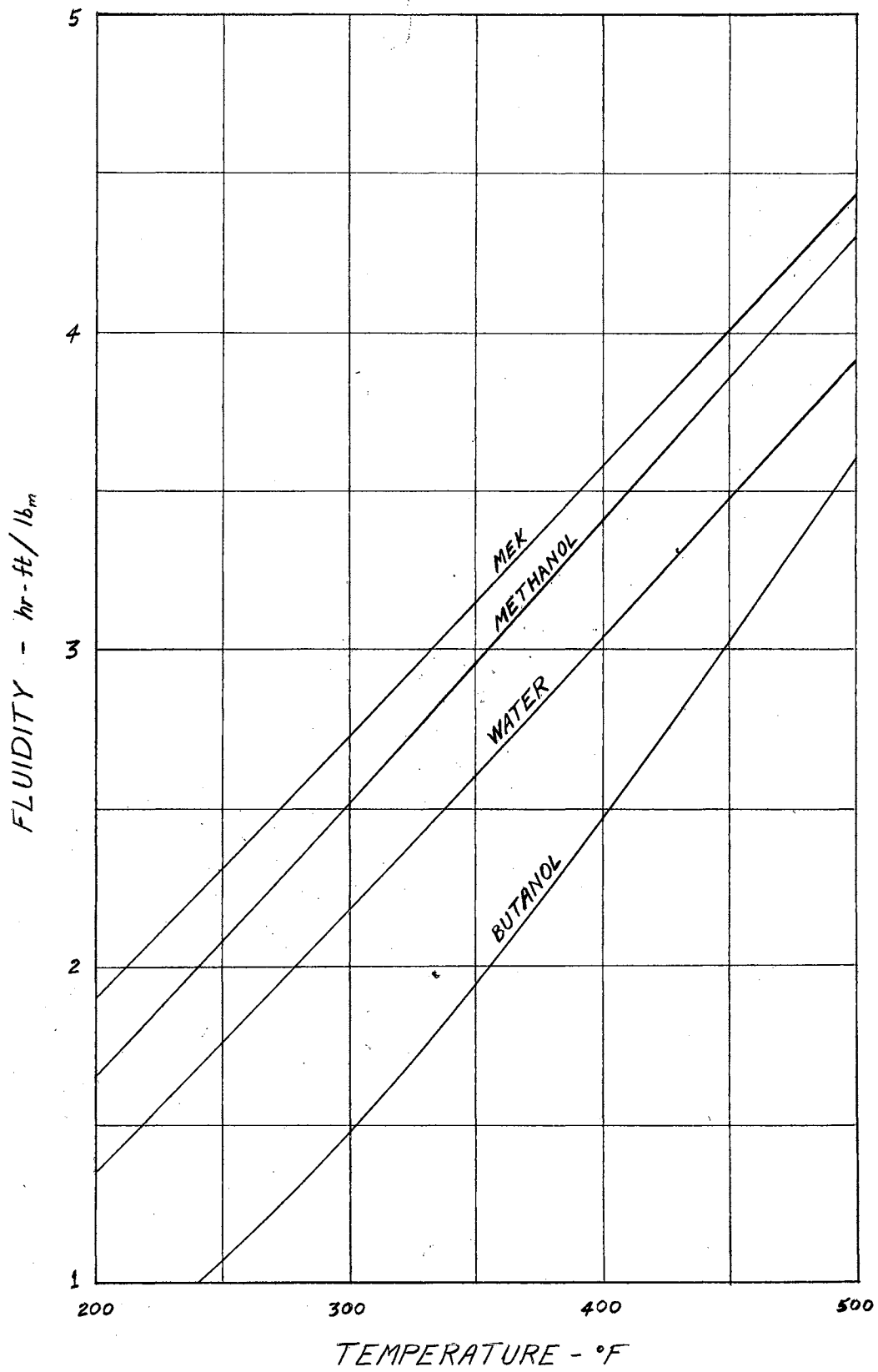


Figure (B-5). Fluidity of Pure Components

temperature T.

$$\left(\frac{1}{\mu}\right)_m = \left(\frac{1}{\mu}\right)_{H_2O} - \left[\left(\frac{1}{\mu}\right)_{H_2O} - \left(\frac{1}{\mu}\right)_m\right]_{T = 140^\circ F}$$

$$\text{or } \frac{\mu_m}{\mu_{H_2O}} = \frac{1}{1 - a \cdot \mu_{H_2O}} \quad (B-1)$$

where  $\mu_m$  is the viscosity of the mixture at a temperature T

,  $\mu_{H_2O}$  is the viscosity of the water at the same temperature T

$$a = \left[\left(\frac{1}{\mu}\right)_{H_2O} - \left(\frac{1}{\mu}\right)_m\right]_{T = 140^\circ F}$$

The values of the parameter a for the different mixtures used in Equation (B-1) are also listed in Table (B-II).

#### Surface Tension

Surface tension of the mixtures was determined experimentally at 80°F using a DuNouy Tensionometer. The tensionometer was calibrated with distilled water and the corrected values of the surface tension of the mixtures are listed in Table (B-II).

The surface tension of a fluid has a zero value at the critical temperature. Since the pseudo-critical temperatures of the mixtures are very close to the critical temperature of the water (due to the small mole fractions of the additives in the liquid mixtures), the following equation was used to estimate the surface tension of the mixtures at different temperatures:

$$\sigma_m = b \sigma_{H_2O} \quad (B-2)$$

where  $\sigma_m$  is the surface tension of the mixture at T

,  $\sigma_{H_2O}$  is the surface tension of water at T

$$b = \frac{\sigma_m}{\sigma_{\text{H}_2\text{O}}} / T = 80^\circ\text{F}$$

The values of the parameter  $b$  for the different mixtures are also listed in Table (B-II), and Figure (B-6) shows the surface Tension of the pure components.

#### Derivatives of the Vapor-Pressure Curve

Water:

The first derivative  $\frac{dP}{dT}$  for water was calculated at 4 pressures, using the Keenan and Keyes steam tables and the Clausius-Clapeyron relation

$$\frac{dP}{dT} = J \frac{S_V - S_L}{v_V - v_L} = \frac{J \cdot L}{T_s \cdot v_V} \quad (\text{B-3})$$

where  $S$  is the entropy, and the liquid volume was neglected in comparison with the saturated vapor volume.

The second derivative  $\frac{d^2P}{dT^2}$  was calculated at the same four pressures used in the experimental runs by the central difference method.

The values of these derivatives for water are listed in Table (B-III).

Mixtures:

The Hildebrand rule stipulates that the entropy of expansion of the various gases or of mixtures of gases has the same value when these gases have equal molar volumes.

Considering the vapor phases of both water and the mixtures, it can be shown that

$$\frac{\tilde{V}_m}{\tilde{V}_{\text{H}_2\text{O}}} = \frac{\gamma_m}{\gamma_{\text{H}_2\text{O}}} \frac{(T_s)_m}{(T_s)_{\text{H}_2\text{O}}} \quad (\text{B-4})$$

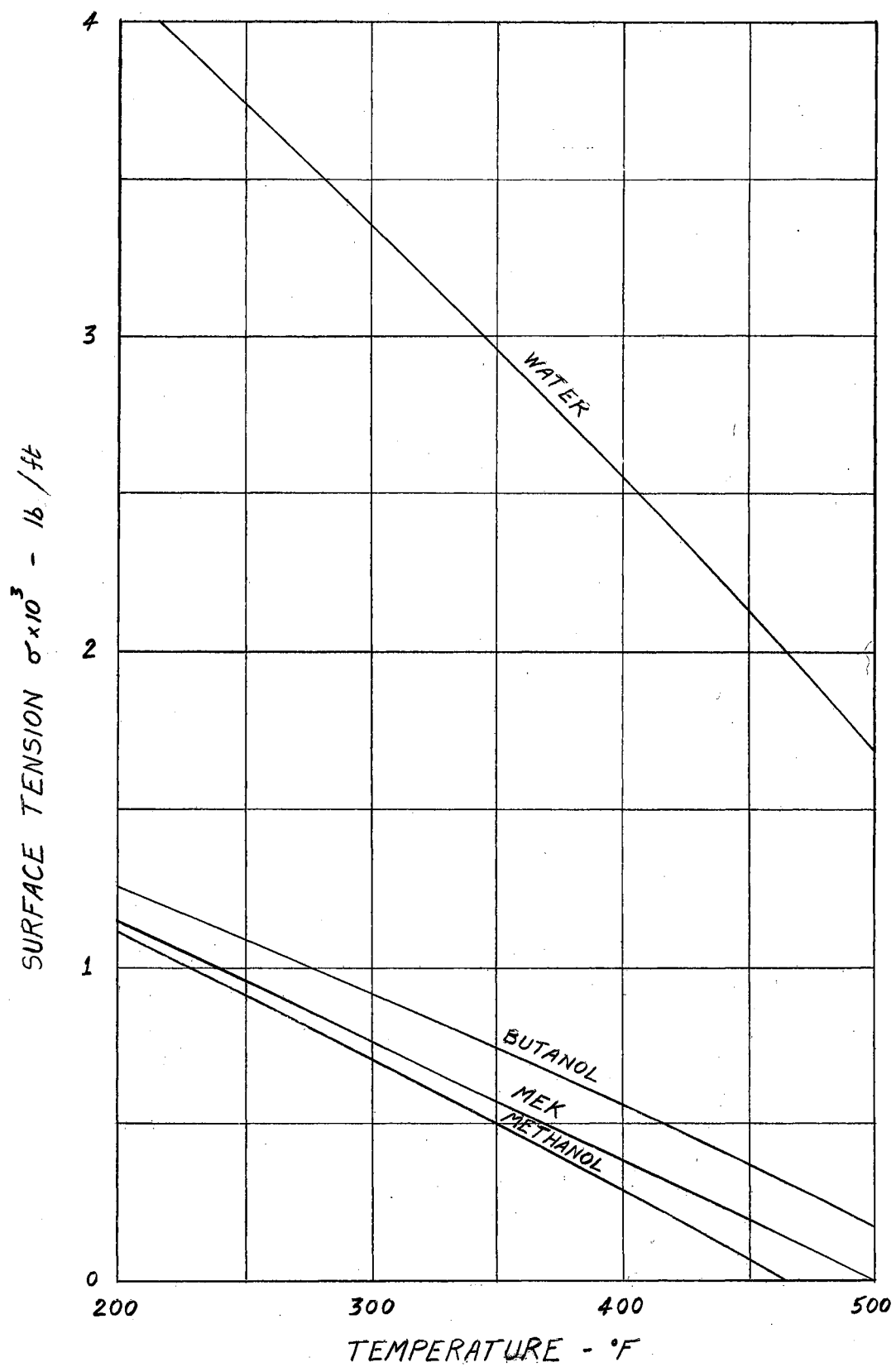


Figure (B-6). Surface Tension of Pure Components

TABLE (B-III)  
DERIVATIVES OF VAPOR-PRESSURE CURVE FOR WATER

Pressure psia	$(dP/dT)$ $\text{lb}_m/\text{ft}^2\text{-}^\circ\text{F}$	$(d^2P/dT^2)$ $\text{lb}_m/\text{ft}^2\text{-}^\circ\text{F}^2$
50	114.2	1.50
100	199.4	2.15
150	274.4	2.75
250	409.1	3.68

where  $\gamma$  is the compressibility factor defined by

$$\gamma = \frac{RT}{P\hat{V}}$$

and R is the universal gas constant in  $\text{ft}\text{-}\text{lb}_m/\text{}^\circ\text{F}\text{-(lb -mole)}$

$\hat{V}$  is the molar volume in  $\text{ft}^3/\text{(lb-mole)}$

Since the ratio  $\frac{(T_s)_m}{(T_s)_{\text{H}_2\text{O}}}$  in Equation (B-4) is almost unity as can

be seen from Table (B-IV), and the reduced pressures of the water and of the mixtures are very small and equal, it follows that

$$\hat{V}_m = \hat{V}_{\text{H}_2\text{O}}$$

and the Hildebrand rule can be utilized to write

$$S = \left(\frac{L}{T_s}\right)_m = \left(\frac{L}{T_s}\right)_{\text{H}_2\text{O}}$$

when the mixtures and the water are at the same pressure.

The Clausius-Clapeyron equation (B-3) can be put in the form

$$\frac{dP}{dT} = \frac{M J L}{T_s \hat{V}}$$

where  $M$  is the molecular weight of the gas or the mixture.

Therefore at the same pressure we have

$$\left(\frac{dP}{dT}\right)_m = \frac{M_m}{M_{H_2O}} \cdot \left(\frac{dP}{dT}\right)_{H_2O} \quad (B-5)$$

Table V-IV lists the values of the molecular weight ratios  $\frac{M_m}{M_{H_2O}}$  for the different mixtures.

#### Thermodynamic Equilibria of the Mixtures

The vapor-liquid equilibrium and saturation temperatures of the various mixtures at 50, 100, 150 and 250 psia were estimated by fugacity calculations using the vapor-pressure curves of the pure components shown in Figure (B-4) and the generalized fugacity chart. These calculations were done according to the method given in reference (47), page 44. Very small variations in the saturation temperature were found at the different pressures and the values at these different pressures were averaged and listed in Table (B-IV). This was due to the very small concentrations of the additives used.

TABLE (B-IV)  
Thermodynamic Equilibria of the Mixtures

	<sup>1</sup> x	<sup>2</sup> y	<sup>3</sup> T <sub>s</sub>	<sup>4</sup> $\frac{N_m}{MH_2O}$
1.02% Methanol	0.006	0.023	0.75	1.020
2.04% Methanol	0.011	0.035	1.40	1.032
3.06% Methanol	0.017	0.052	1.90	1.047
1.00% MEK	0.0025	0.01	0.4	1.025
2.03% MEK	0.0052	0.02	0.3	1.060
3.00% MEK	0.0077	0.03	0.2	1.090
1.00% Butanol	0.0025	0.001	0.0	1.002
2.04% Butanol	0.0051	0.002	0.0	1.004
3.12% Butanol	0.0078	0.003	0.0	1.007

<sup>1</sup>mole fraction of additive in the liquid phase

<sup>2</sup>mole fraction of additive in the vapor phase

<sup>3</sup>(T<sub>s</sub>)<sub>H<sub>2</sub>O</sub> - (T<sub>s</sub>)<sub>m</sub>

<sup>4</sup>see page 101



## APPENDIX C

### THERMOCOUPLE CALIBRATION

Iron constantan thermocouples, 30 gauge (0.010 inch wire diameter) were used to measure the temperature at all locations. All thermocouples were made of wire taken from the same spool. A junction of this wire was spot-welded and calibrated against the emf. temperature curve, which is represented accurately in the range of temperatures involved in this investigation by the linear relation

$$\text{emf.} = -1.33 + 3.09 \times 10^{-2}T$$

Besides measuring the saturation temperature of steam at a barometer reading of 29.11 inch Hg., the freezing points of tin and lead were also measured. Those two metals were chosen because their freezing points were in the temperature range within which the thermocouples were used.

An electrically heated furnace was used to melt the samples of tin and lead, which then were allowed to freeze. The thermocouple emf. was read during the freezing time using a Leeds and Northrup portable precision potentiometer, No. 8663. The ice point was used as the reference point. The thermocouple was connected to the potentiometer through the same multi-position selector switch used to connect the test-section thermocouples to this potentiometer.

Table (C-I) lists the measured emf.'s together with the actual values.

TABLE (C-I)  
THERMOCOUPLE WIRE CORRECTION

	Measured emf. (mv.)	Actual Temp. (°F)	Values emf. (mv.)	Correction emf. (mv.)
Steam Point	5.180	210.54	5.226	+ 0.046
Tin Freezing Point	12.497	449.42	12.553	+ 0.056
Lead Freezing Point	17.795	621.32	17.840	+ 0.045

Therefore a correction value of  $\frac{0.046 + 0.056 + 0.045}{3} = 0.049$  mv. was added to the emf. readings of all the thermocouples. This corresponds to a temperature correction of 1.60°F.

In addition to this correction which was applied to the emf. readings of all thermocouples, a second correction was necessary for the surface temperature thermocouples of the test section. Those thermocouples were calibrated in place against the inlet bulk temperature thermocouple as follows:

1. Distilled water was allowed to flow in the test section at a moderately low velocity and at different temperature levels which covered the range of temperatures used in this investigation.
2. Only the preheater was used to raise the flowing water bulk temperature, and the test section power was completely shut off.
3. The thermal guard power was increased until the emf. of the thermal guard thermocouples matched those of the test section thermocouples.
4. The emf.'s of the seven surface thermocouples were recorded at

different temperature levels and the difference between those emf.'s and that of the inlet bulk thermocouple was plotted versus the latter. Figure (C-1) shows the corrections that were added to the emf.'s of the seven surface thermocouples as a function of temperature, and Figure (C-2) shows the inside wall temperatures  $T_w$  at the seven locations of the surface thermocouples before and after adding these corrections.

It is believed that the irregular pattern of corrections for the different surface thermocouples shown in Figure (C-1) is due to the following:

1. Uneven heating of the ceramic tube which was heated by resistance wire coiled around its entire length. Poor contact of the resistance wire or the lack of it with the ceramic tube surface at some parts of the surface (when the wire expands as a result of heating it) will cause such uneven heating of the ceramic tube.
2. Nonisotropic material of the ceramic tube.
3. Differences in the wall thickness of the ceramic tube which was composed of three sections as can be seen from Figure 8.

The corrections for thermocouples #3 and #7 were exceptionally large because of end effects. It can be seen from Figures 6 and 8 that thermocouple #3 was located only half an inch from the gap between two sections of the ceramic tube. Thermocouple #7 was located an inch and a half from the end of the ceramic tube.

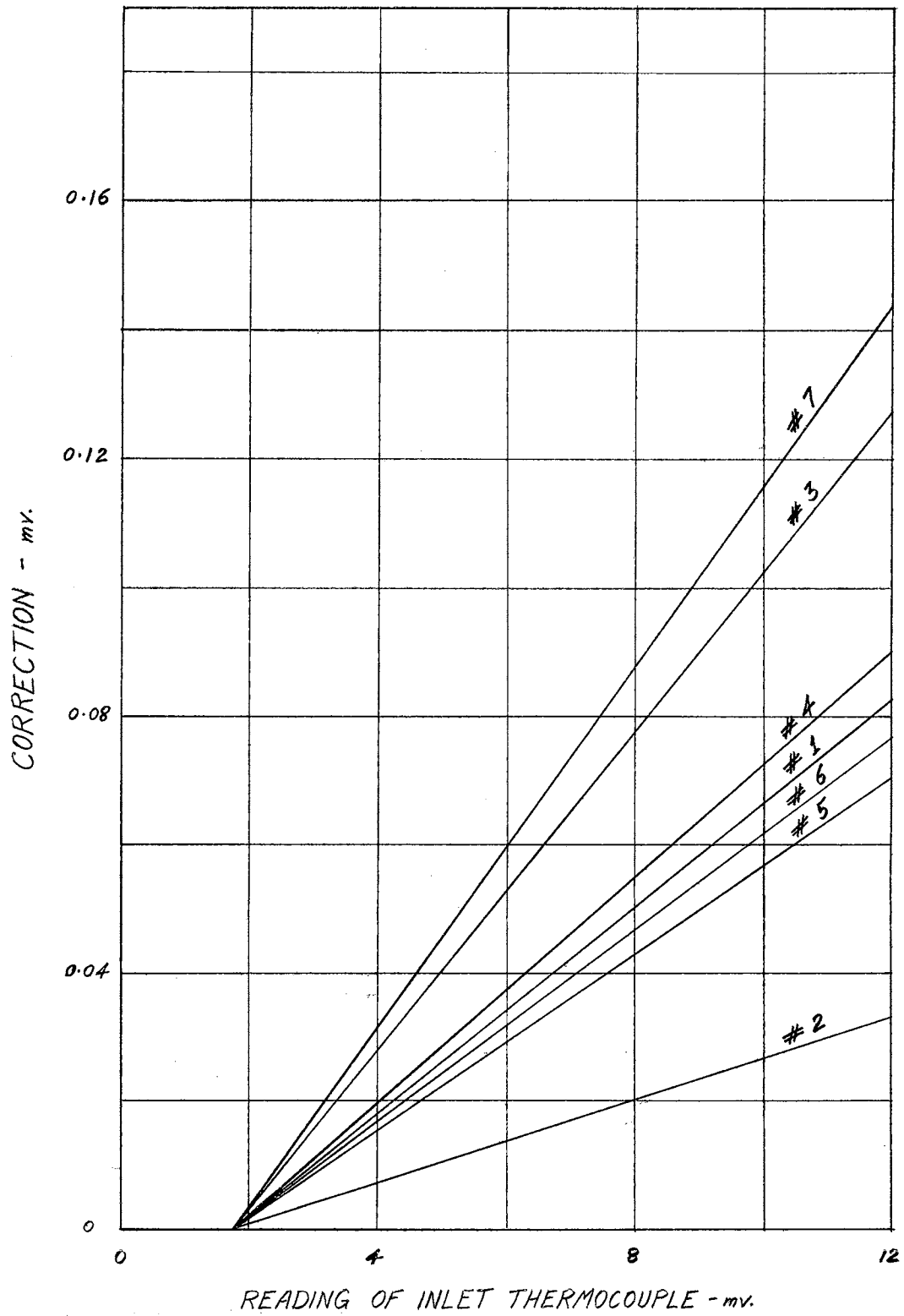


Figure (C-1). Corrections for Surface Thermocouples

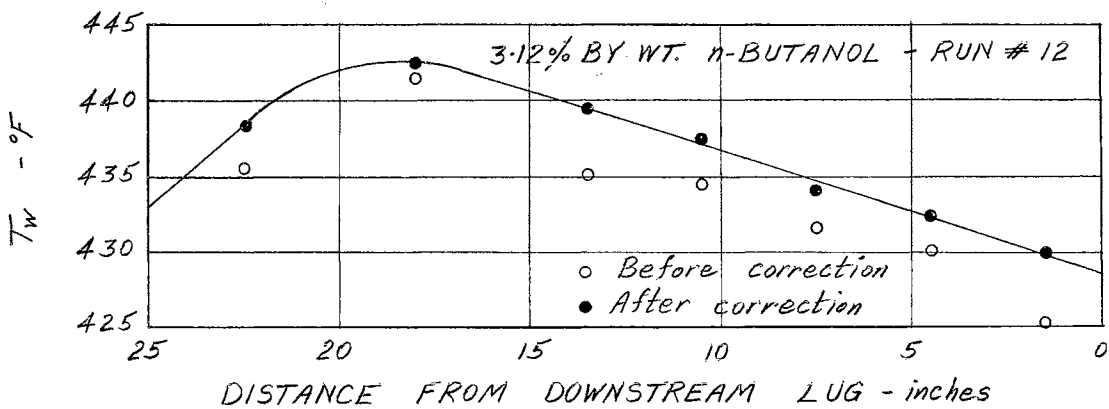
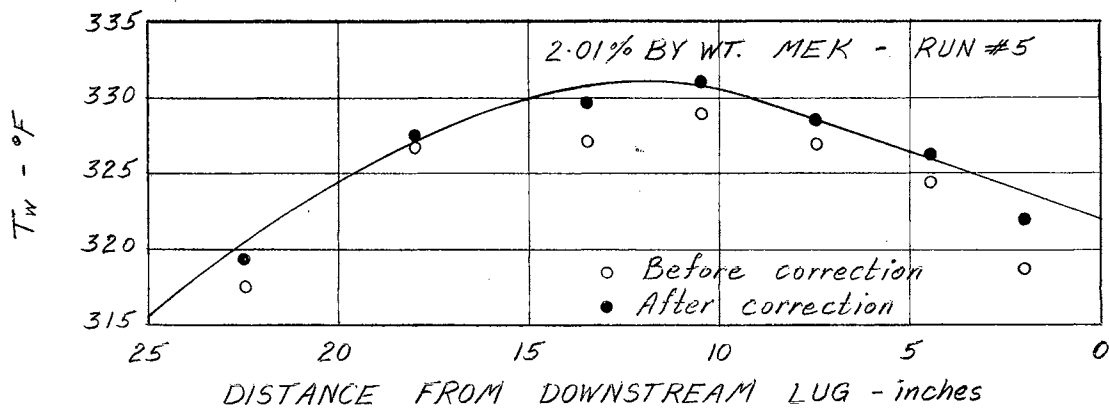
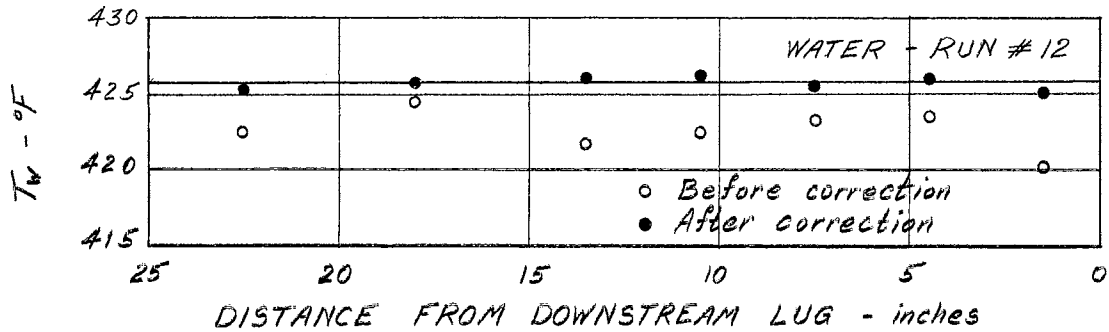
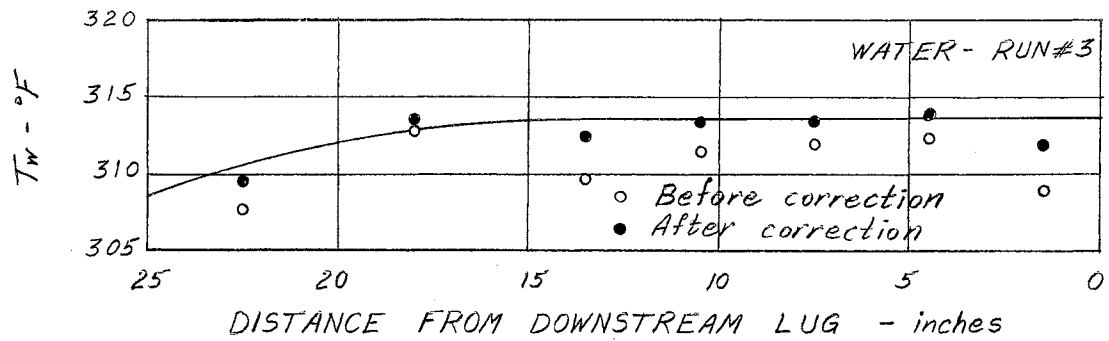


Figure (C-2). Temperature Profile Correction for some Runs

APPENDIX D

ORIFICE CALIBRATION

The loop was equipped with two orifice plates. Only the smaller orifice with a diameter of 0.353 inches was used in this investigation.

For the purpose of calibrating this orifice, 34 runs were made at different values of the system pressure and different values of the mass flow rate ranging between 180 lbm/ft<sup>2</sup>-sec and 900 lbm/ft<sup>2</sup>-sec. The following table shows a typical run.

TABLE (D-I)  
ORIFICE CALIBRATION DATA

# Run	P <sub>f</sub> inch				Time min.	Weight lbs.	t <sub>2</sub> °F	System Pressure psia
	1	2	3	Average				
3	27.10	26.90	27.00	27.00	3.014	48.65	71.0	100

where  $\Delta P_f$  = height of flow manometer fluid.

$t_2$  = water temperature at the orifice.

Figure (D-1) is a plot of the mass flow rate G and the pressure drop  $\Delta P_w$

where  $\Delta P_w = 0.75 \Delta P_f$

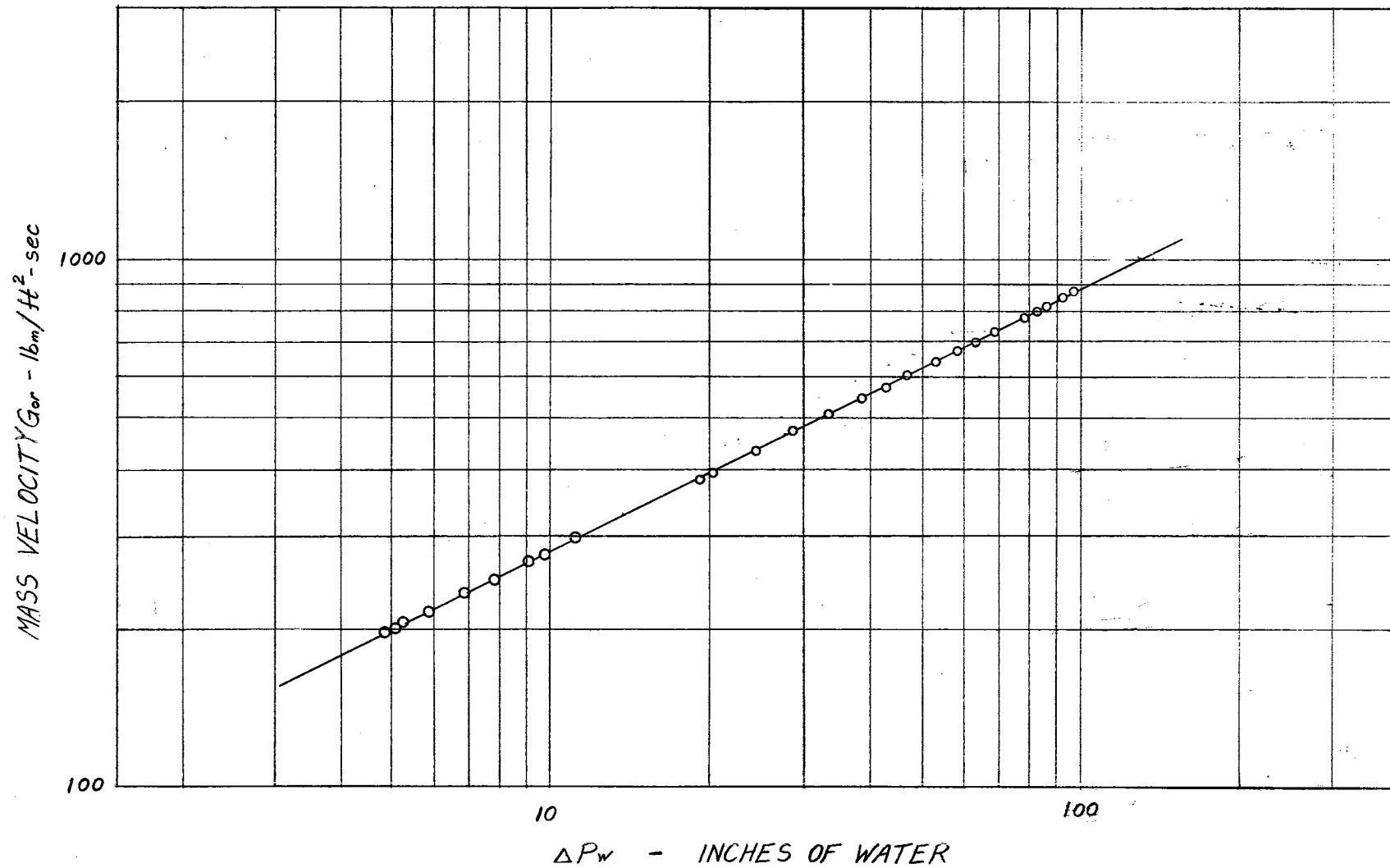


Figure (D-1). Orifice Calibration

## APPENDIX E

### PROPERTIES OF AISI STAINLESS STEEL TYPE 304

The AISI stainless steel type 304 has the following composition in percentages:

18-20 Cr; 8-12 Ni; 2-0 max. Mn; 1-0 max. Si; 0.08 C.

This type of steel possesses the highest corrosion resistance in the stainless-steel family. It has superior high temperature properties and offers the greatest resistance to scaling. The analysis balance of this steel is such that in the annealed condition it is non-magnetic.

The electrical resistivity and the thermal conductivity of the AISI stainless steel type 304 are given (45) each at two temperatures as

Temperature °F	$\rho \times 10^{-6}$ -ft	k Btu/hr-ft-°F
68	2.365	
212		9.40
932		12.40
1200	3.815	

In order to find values of the resistivity and the conductivity at intermediate temperatures, a quadratic equation of the type

$$y = a + bx + cx^3$$

was passed by each pair of points with the aid of the two slopes

$$\left. \frac{d\rho}{dT} \right|_{T=68^{\circ}\text{F}} = 1.575 \times 10^{-9} \quad \rho \text{ -ft}/^{\circ}\text{F}$$



and  $\left. \frac{dk}{dT} \right|_{T=212^{\circ}\text{F}} = 2.22 \times 10^{-3} \text{ Btu/hr-ft-}^{\circ}\text{F}/^{\circ}\text{F}$

These two slopes were arrived at by plotting the resistivity and conductivity curves of the stainless steel,

19-11 Cr; 8-14 Ni; 0-37 Mn; 0.68 Si; 0.08 C; 0.60 W,  
as given in the Metals Handbook (44), and comparing these curves with the corresponding two values for type 304 stainless steel.

The two quadratic equations are:

$$\rho = 2.265 \times 10^{-6} + 1.611 \times 10^{-9} T - 2.600 \times 10^{-13} T^2 \quad \Omega\text{-ft.}$$

and  $k = 9.050 + 1.074 \times 10^{-3} T + 2.710 \times 10^{-6} T^2 \quad \text{Btu/hr-ft-}^{\circ}\text{F}$

The Kreith and Summerfield solution requires the use of linear relations between the properties of steel and the temperature. Between 200°F and 500°F, which is the range of the outside wall temperatures  $T_o$  in this investigation, the electrical resistivity and the thermal conductivity are very nearly linear with the temperature and are represented

by  $\rho = \rho_1 (1 + \alpha \theta)$

and  $k = k_1 (1 + \beta \theta)$

where  $\alpha = 5.16 \times 10^{-4}/^{\circ}\text{F}$

$$\rho_1 = 2.717 \times 10^{-6} \quad \Omega\text{-ft.}$$

$$k_1 = 9.607 \text{ Btu/hr-ft}^{\circ}\text{F}$$

$$\theta = (T - 300)^{\circ}\text{F}$$

$$\beta = 3.373 \times 10^{-4}/^{\circ}\text{F}$$

## APPENDIX F

### REPRODUCIBILITY OF DATA

All previous experiments in nucleate boiling have established the fact that the heat flux is strongly dependent on the boiling-surface condition. Factors like scratching, pitting, aging or treating the surface with a non-wetting agent, have considerable effect on the relation between the heat flux and the superheat.

In the present experiment, the same test-section was used for all the experimental runs. Certain precautions and procedures have been undertaken to minimize, as far as possible, the effect of the changing surface condition on the reproducibility of the results.

To control the roughness of the test-section surface and its freedom from excessive deposits, which can easily change its characteristics, the following steps were taken:

1. Before performing any sequence of runs for one additive (48 runs), the surface was treated with a diluted solution of nitric acid for one hour, and then flushed thoroughly with distilled water.

2. The additives were then introduced and the mixtures were allowed to flow through the test section for a sufficient time before reading any data. This amount of time also allowed the additives to mix well with the distilled water.

3. All 48 runs of a particular sequence were read in the shortest amount of time possible (about 3 days). In order to do this, it was

necessary to keep the loop running continuously for about 16 hours daily.

4. The ion exchanger was kept operating 24 hours a day at all times when a test fluid was in the loop.

5. No atmospheric air was allowed to get in the test section while the loop was shut off. This was achieved by keeping the test section filled with the degassed system fluid.

One out of ten runs was reproduced at random. Reproduction runs were performed one day after the original runs were read, and except for Run #6 for water, all were read right after the loop was started and degassed. Table (F-1) lists the heat flux  $\bar{q}$ , the superheat  $\Delta T_1$ , and the time lapse before reproduction was performed. Figure (F-1) is a plot of the superheat in the reproduction runs as ordinate against the original superheat in the original runs.

Assuming that treating the heat transfer surface, as was discussed above, rendered the same surface to all experimental runs (except for the effect of entrenched gases in the surface), Figure (F-1) affords a means of determining the effect of the gradual desorption of gases from the surface of the tube (32) and (46).

Haselden and Peters (32) measured the increase of the superheat  $\Delta T_1$  as a function of time for the same heat flux. They also reported that "if the tube was removed from the liquid, warmed, and allowed to stand in air for several hours, the activity of the surface was partially restored."

In Figure (F-1) the dotted line which represents a weighed average of all the points (except the point for Run #6 for water), deviates by 5% from the solid  $45^\circ$  straight line. Since reproduction runs were taken at the beginning of a sequence of runs and immediately after the system

TABLE F-I  
Reproduction Data

	Run #	$\bar{q} \times 10^{-5}$ Btu/hr-ft <sup>2</sup>	$\Delta T_1$ (°F)		Time Lapse
			Data	Reproduction	
Water	1	0.620	18.0	20.5	2 weeks
Water	6	1.057	21.1	26.8	same day
Water	8	2.075	29.9	30.7	24 hrs.
Water	11	2.572	29.1	28.8	2 weeks
1.02% Methanol	3	1.584	36.2	34.0	24 hrs.
2.04% Methanol	3	1.584	37.7	38.1	24 hrs.
3.06% Methanol	15	2.075	39.0	36.6	24 hrs.
	16	2.075	38.2	35.8	24 hrs.
1.00% MEK	7	1.584	42.0	42.1	24 hrs.
2.03% MEK	4	2.075	47.5	48.2	24 hrs.
3.00% MEK	—	—	—	—	—
1.00% Butanol	6	1.057	30.3	29.2	24 hrs.
	11	2.572	32.0	30.3	24 hrs.
2.07% Butanol	5	2.572	52.5	47.4	24 hrs.
	10	1.584	38.7	37.4	24 hrs.
3.12% Butanol	8	2.075	41.0	39.0	24 hrs.
	15	2.075	49.0	44.6	48 hrs.

was degassed, the above mentioned deviation of the dotted line in Figure (F-1) represents the effect of entrenched gases in the tube surface after a running time of one-half hour, which was the time necessary for the steady state to be achieved.

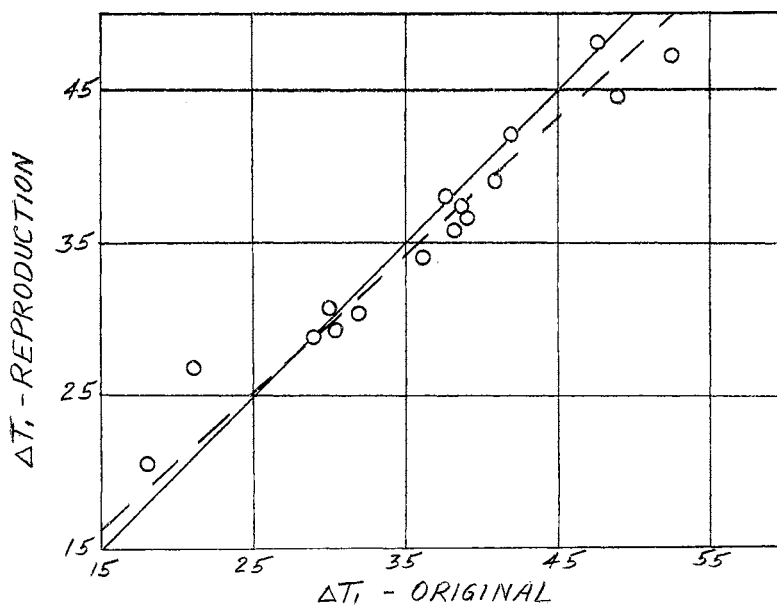


Figure (F-1). Reproduction

## APPENDIX G

### DEGASSING EXPERIMENT

Water at room temperature and at atmospheric pressure dissolves an amount of atmospheric gases equal to 2% of its volume. The content of oxygen in these dissolved gases is about 67% by volume, and the balance is mostly nitrogen. This illustrates the harmful corrosive effect of water on ferrous materials when the water is saturated with dissolved gases.

In addition to this corrosive effect, the presence of dissolved gasses in fluids during local boiling decreases considerably the superheat for the same amount of heat dissipation. This will make it extremely difficult to compare experimental results of different investigators unless the amount of dissolved gases is specified in each case. Therefore, it was necessary to degas the system fluid each time the heat transfer loop was started.

In order to determine the amount of degassing effected, the system fluid was circulated in the loop at a convenient pressure and at a temperature just below the saturation temperature corresponding to that pressure. The gases collecting in the condenser were allowed to pass through the valve located on top of the condenser. The construction and location of this valve was such that it would pass gas but not liquid. These gases then were collected and measured at equal intervals of time, and the result is shown in Figure (G-1).

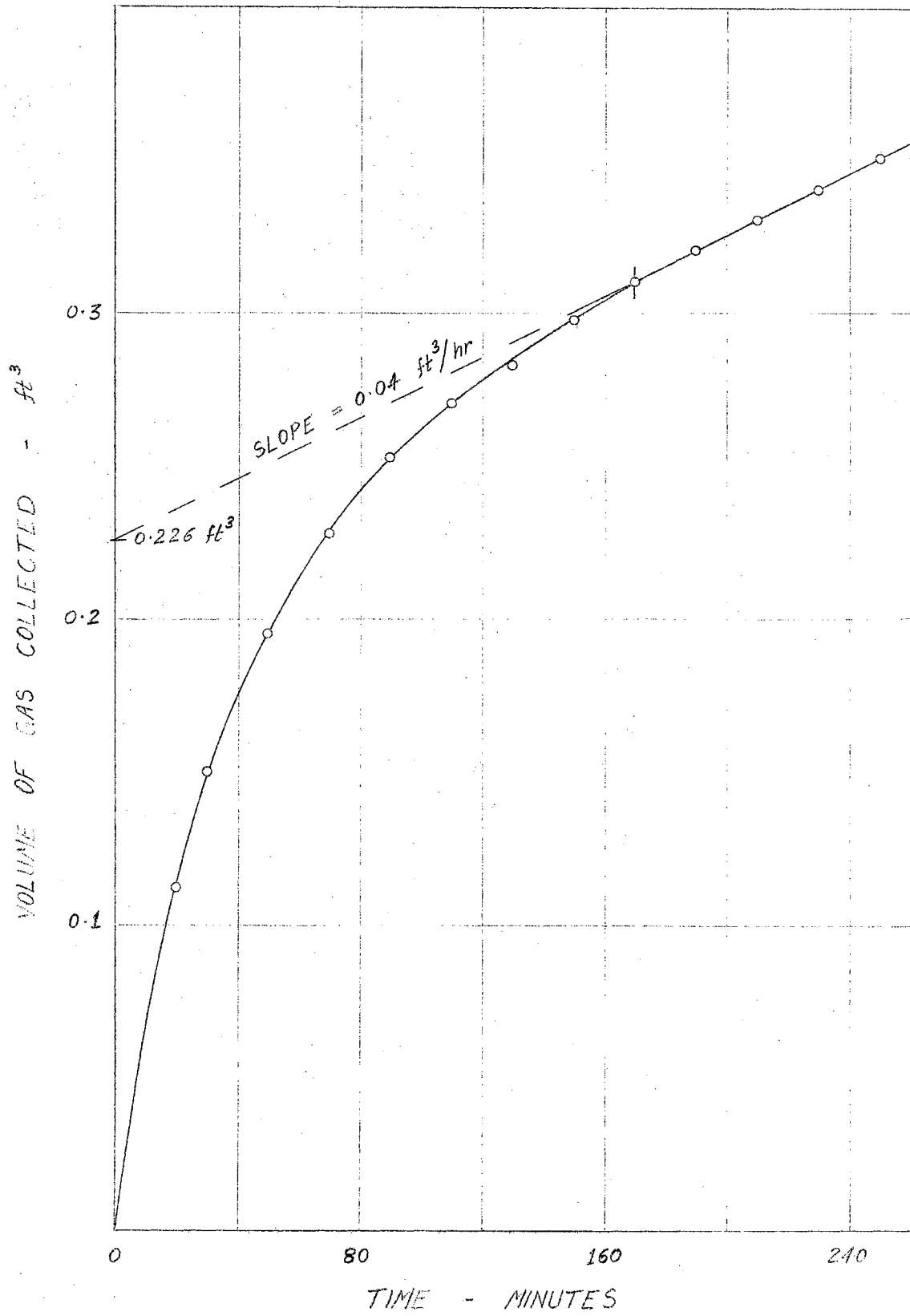


Figure (G-1). Degassing Experiment

It can be seen from Figure (G-1) that about two hours were needed to degas the system fluid. Beyond this amount of time, the slope of the curve became constant and was equal to the rate at which atmospheric gases were absorbed by the system fluid.

The extension of the constant slope portion of the curve in Figure (G-1) intersects the ordinate at a value of 0.226 ft<sup>3</sup>. This was the volume of gas given off by the water in the loop. Since the loop contained about 810 lbs. of water, then the amount of gas originally dissolved was

$$\frac{810}{62.4} \times \frac{2}{100} = 0.260 \text{ ft}^3$$

and the amount of degassing was

$$\frac{0.226}{0.260} = 0.87$$

Therefore degassing of the system fluid removed about 87% of its dissolved gases.



A P P E N D I X H

MOYNO PUMP CHARACTERISTICS

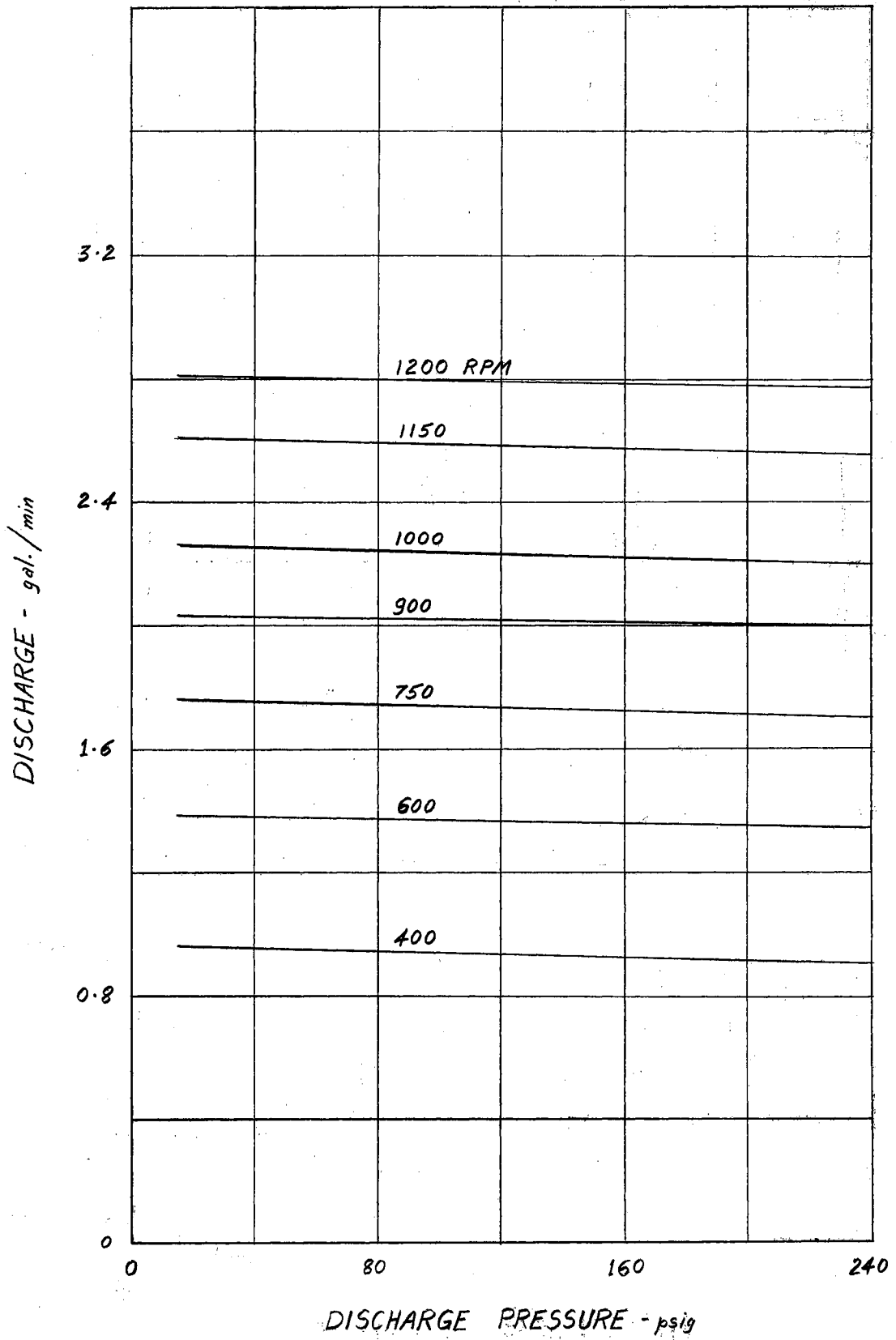


Figure (H-1). Moyno Pump Characteristics

## APPENDIX I

### NOMENCLATURE

#### Symbols

A	Area ( $\text{ft}^2$ )
C	Constant in Forster-Greif Correlation Equation
c	Specific heat of the liquid at constant pressure ( $\text{Btu}/\text{lb}_m\text{-}^\circ\text{F}$ )
D	Diameter (ft)
E	Voltage drop/unit length of the tube ( $\text{Volts}/\text{ft}$ )
G	Mass velocity ( $\text{lb}_m/\text{ft}^2\text{-sec.}$ )
g	Gravitational acceleration ( $\text{ft}/\text{hr}^2$ )
$g_c$	Conversion factor ( $4.17 \times 10^8 \text{ lb}_m\text{-ft}/\text{lb}_f\text{-hr}^2$ )
I	Test-section current (Amps)
J	Mechanical equivalent of heat ( $778.26 \text{ ft-lb}/\text{Btu}$ )
k	Thermal conductivity ( $\text{Btu}/\text{hr-ft-}^\circ\text{F}$ )
L	Latent heat of vaporization ( $\text{Btu}/\text{lb}_m$ ); Also, length (ft)
n	Exponent in Forster-Greif Correlation Equation
P	Pressure (psia) or ( $\text{lb}_m/\text{ft}^2$ ); Also, Power (watt)
$\Delta P$	Excess pressure (see Text) ( $\text{lb}_m/\text{ft}^2$ )
q	Time rate of heat flow ( $\text{Btu}/\text{hr}$ )
$\bar{q}$	Heat flux ( $\text{Btu}/\text{hr-ft}^2$ )
R	Radius of bubble (ft); Also, electrical resistance (Ohm)
r	Radius of tube (ft)

T	Temperature ( $^{\circ}\text{F}$ )
$\Delta T_1$	Superheat = $T_W - T_S$ ( $^{\circ}\text{F}$ )
$\Delta T_2$	Subcooling = $T_S - T_B$ ( $^{\circ}\text{F}$ )
$\overline{\Delta x}$	Test-section wall thickness = $r_o - r_i$ (ft)

#### Greek Letters

$\alpha$	Temperature coefficient of electrical resistivity ( $^{\circ}\text{F}^{-1}$ )
$\beta$	Temperature coefficient of thermal conductivity ( $^{\circ}\text{F}^{-1}$ )
$\theta$	Temperature difference = $T - 300$ ( $^{\circ}\text{F}$ )
$\mu$	Viscosity of the liquid ( $\text{lb}_m/\text{hr-ft}$ )
$\rho$	Density ( $\text{lb}_m/\text{ft}^3$ ); Also, electrical resistivity ( $\text{Ohm-ft}$ )
$\sigma$	Surface tension of the liquid-vapor interface ( $\text{lb}/\text{ft}$ )
$\tau$	Period of growth-collapse of a bubble (sec.)

#### Subscripts

l	Value at $300^{\circ}\text{F}$
B	Liquid bulk
b	Boiling
nb	Non-boiling
c	Critical value
f	Fluid (manometer)
$\text{H}_2\text{O}$	Water
i	Value at inside wall of the tube
L	Liquid
m	Mixture
o	Value at the outside wall of the tube
s	Saturation

v Vapor

w Value at the wall or at the heating surface; Also, water.

#### Dimensionless Numbers

Nu Nusselt modulus in boiling, and defined by Equation (IV-5)

Re Reynolds modulus in boiling, and defined by Equation (IV-3)

Pr Prandtl number defined by Equation (IV-2)

X Re

Y  $\text{Nu} \cdot \text{Pr}^{-1/3}$

## VITA

Mahmoud Hood Sabet

Candidate for the Degree of

Doctor of Philosophy

**Thesis:** FORCED CONVECTION NUCLEATE BOILING DATA FOR LOW HEAT FLUX DENSITIES TO WATER CONTAINING A VOLATILE ADDITIVE

**Major Field:** Mechanical Engineering

### Biographical:

**Personal Data:** The author was born in Suez, Egypt, April 11, 1925.

**Undergraduate Study:** The author graduated from the School of Mechanical Engineering of Alexandria University, Egypt, in May, 1949, where he received the Bachelor of Science degree in Mechanical Engineering.

**Graduate Study:** The author received the Master of Science degree in Mechanical Engineering from the School of Mechanical Engineering, Alexandria University, Egypt, in August, 1953. He entered the Graduate School of the University of Rhode Island in September 1955 and received the Master of Science Degree in Mechanical Engineering from that institution in May, 1957. He completed the requirements for the degree of Doctor of Philosophy in Mechanical Engineering at the Oklahoma State University in May, 1962.

**Professional Experience:** The author was teaching at the School of Mechanical Engineering of Alexandria University, Egypt, from November, 1949 to September, 1954. He was employed by Charles Maguire & Engineers, Providence, Rhode Island as an engineer during the summer of 1956. He taught courses or assisted in courses in Thermodynamics, heat transfer, physics, steam and gas laboratory, and drafting during his graduate study at the University of Rhode Island and the Oklahoma State University. In October, 1960 he was employed by The Boeing Company as a Research Engineer.